CONJUGATED POLYMER AND OLIGOMER BASED NANOSENSORS

WANG YUSONG

(M. Eng.)

A THESIS SUBMITTED

FOR THE DEGREE OF DOCTOR OF PHILOSOPHY

DEPARTMENT OF CHEMICAL AND BIOMOLECULAR ENGINEERING

NATIONAL UNIVERSITY OF SINGAPORE

2009

ACKNOWLEDGEMENTS

I would like to express my greatest appreciation to my supervisor, Dr. Liu Bin, for her support and guidance throughout the course of this research project. Her continuous guidance, constructive criticisms and insightful comments have helped me in getting my thesis in the present form. More importantly, her rigorous research methodology, objectivity and enthusiasm in scientific discovery will be a model for my future life and career.

I wish to express my heartfelt thanks to all my colleagues in the research group, in particular, Ms Dishari Shudipto Konika, Mr. Pu Kanyi, Dr. Cai Liping, Dr. Wang Chun, Dr. Zhu Rui, Dr. Liu Xizhe, Dr. Wang Jing, Dr. Fang Zhen, Mr. Li Kai, Mr. Wang Long, Mr. Zhang Wei, Ms Zhan Ruoyu, Ms Wang Yanyan. I thank them for their valuable suggestions and stimulating discussions. I also thank all friends including: Dr. Zhang Yu, Mr. Xu Zhiyong, Dr. Xu Jing, Dr. Chang Yu, Dr. Wang Likui, Dr. Qing Weijie, Dr. Khew Shih Tak, Mr. Hu Zhongqiao, and other senior and peer students, who provide candid suggestions and research assistances while completing this project.

I am indebted to the technical staff in the department of ChBE, especially Mr. Boey Kok Hong, Ms Lee Chai Keen, Mr. Chia Phai Ann, Mdm Li Xiang, Mr. Shang Zhenhua, Dr. Yuan Zeliang, Mr. Toh Keng Chee, and Mr. Han Guangjun. Their superb technical support and services are essential for the completion of this study.

Special acknowledgements are also given to National University of Singapore for her financial support.

Lastly, and most importantly, I would like to show my deepest gratitude to my family. Without their love, support, encouragement and understanding, this work could not have been completed successfully. To them I dedicate this thesis.

TABLE OF CONTENTS

SUMMARY

Highly sensitive and selective chemo/biodetection is a continuous demand in quantitative studies for biomedical research. In response to this demand, great efforts have been paid to develop convenient and effective detection systems compared with conventional radioactive/fluorescent dye assays. This Ph.D. study aims to develop fluorescent nanosensors based on conjugated polymer (CP)/oligomer and apply the developed platforms to highly sensitive and selective chemo/bioassays. The first major efforts were dedicated to silica nanoparticle (NP)-supported chemo/biosensing using CP/oligomer as a signal amplifier to enhance detection sensitivity and selectivity. Besides these, metal-enhanced fluorescence (MEF) of CP was explored and applied to DNA assays for further enhancement of sensing capability.

The initial study was to develop a strategy for silica NP-supported DNA assay with large signal amplification and high selectivity using CP as an optical signal amplifier. Single-stranded DNA (ssDNA) immobilized silica NPs (~100 nm in diameter) were first prepared through a seed-mediated growth followed by triazine bioconjugation, and then used as nanoprobes to capture target DNA. The CP (PFP-2F) was used to amplify the signal of fluorescein (Fl) labelled target DNA through fluorescence resonance energy transfer (FRET). The optimized detection system amplified fluorescence signal over 110-fold in real time, and allowed the detection of 10 pM target DNA as well as two-base mismatch discrimination. The assay was then developed for label-free single-nucleotide polymorphism (SNP) discrimination using ethidium bromide (EB) as the signal reporter.

A conjugated oligomer (tetrahedrafluorene) was selected as a signal amplifier for DNA intercalated EB in this study. The developed assay provided approximately 35-fold signal amplification with SNP selectivity. Thirdly, by modifying the NP-immobilized DNA probe, the assay is further extended from biosensing to chemical sensing for Hg^{2+}. A sigmoidal working curve of Hg^{2+} was obtained with a detection limit of 0.1 μM, while a linear one was achieved with a detection limit of 5 nM via CP (PFP-2F) signal amplification. The use of CP (PFP-2F) significantly enhances the detection selectivity and reduces false-positive signals. The above first major efforts successfully demonstrated that homogeneous CP/oligomer-based FRET assay could be potentially transferred to NP-supported format with an improved sensing performance.

In addition, metal-enhanced fluorescence (MEF) of CP (PFBT) was successfully demonstrated by exploiting substrates with underlying Ag NP array, and applied to DNA assay. Silver NPs (~75 nm in average with extinction maximum at ~440 nm) were first synthesized to prepare Ag NP arrays as PFBT support. That PFBT has two nearly equally intense absorption bands make it possible to identify the significant contribution of field enhancement to the overall distance-dependent MEF on Ag NP array surface. In addition, the Ag NP array amplified PFBT emission is further utilized to develop a sensing surface that in the presence of PNA probes provides selective detection of ssDNA with signal intensities that are higher than those obtained by use of PFBT alone. These findings open up new opportunities to improve the detection sensitivity of CP-based bioassays. Further tuning MEF substrate preparation and optimizing bioassay conditions could lead to more efficient DNA detection with high sensitivity and selectivity.

LIST OF TABLE

LIST OF FIGURES

LIST OF SCHEMES

LIST OF ABBREVIATIONS

APTES	3-Aminopropyltriethoxysilane
AQ-B^-	Anthraquinone-2,6-disulfonate with biotin
AFM	Atomic force microscope
CCP	Cationic conjugated polymer
CP	Conjugated polymer
C*	Chromophore
dsDNA	Double-stranded DNA
DNA-SH	Thiolated ssDNA
D-B^-	Dye-biotin conjugate
EB	Ethidium bromide
F	fluorophore
F*	excited fluorophore
FE-SEM	Field-emission scanning electron microscope
FETs	Field-effect transistors
Fl	Fluorescein
Fl-DNA	Fluorescein labeled DNA
FRET	Fluorescence resonance energy transfer
HOMO	Highest occupied molecular orbital
ICP-MS	Inductively coupled plasma mass spectroscopy
LbL	Layer-by-layer
LED	Light-emitting diode

LECs	Light-emitting electrochemical cells
LSPR	Local surface plasmon resonance
LUMO	Lowest unoccupied molecular orbital
MMP	Magnetic microparticle
MSO	Mercury-specific oligonuleotide
MEF	Metal-enhanced fluorescence
MV^{2+}	Methyl viologen
MB	Molecular beacon
NP	Nanoparticle
PNA	Peptide nucleic acid
PBS	Phosphate buffer saline solution
PBST	Phosphate buffer saline solution with Tween-20 surfactant
PCT	Photoinduced charge transfer
PL	Photoluminescence
PDGF	Platelet-derived growth factor
PDDA	Poly(diallyldimethyl ammonium chloride)
PPE	Poly(para-phenylene ethynylene)
PPV	Poly(para-phenylene vinylene)
PSS	Poly(sodium 4-styrenesulfonate)
PT	Poly(thiophene)
PFP-2F	Poly[9,9'-bis(6''-N,N,N-trimethylammonium)-hexyl)fluorene-co-alt-2,5-difluoro-1,4-phenylene) dibromide]
PFBT	Poly[9,9-bis(9-N,N,N-trimethylammonium)ethoxy)ethoxy)ethyl)fluorene-alt-(4,7-(2,1,3-benzothiadiazole)dibromide)]

PF	Polyfluorene
PLED	Polymer light-emitting diodes
QD	Quantum dot
QTL	Quencher-tether-ligand
RU	Repeat unit
SELEX	Selective evolution of ligands by exponential enrichment
SNP	Single-nucleotide polymorphisms
ssDNA	Single-stranded DNA
SERS	Surface-enhanced Raman scattering
TEOS	Tetraethoxysilane
TR	Texas Red
T-Hg^{2+}-T	Thymine-mercury(II)-thymine
TEM	Transmission electron microscopy
Tetrahedralfluorene	Tetrakis[4-(2-(9,9,9',9'-tetrakis(*N*,*N*,*N*-trimethylammoniumhexyl)-7,2'-bifluorenyl))-phenyl]methane hexadecanebromide

CHAPTER 1

INTRODUCTION

1.1 Background

Sensors such as chemical and biological sensors are devices that can deliver information on the presence of specific target in the concerned samples or environment [1-8]. They play a critical role in a wide range of applications such as clinical diagnostics, environmental monitoring, and antiterrorism, and provide important information for medical research, human health, and safety of our living space. Chemical and biological sensing (chemo/biosensing) can be divided into optical detection and the non-optical such as electronical [2], electrochemical [3], and magnetic detection [4]. Compared with non-optical sensors, the optical sensors have several advantages such as the possibility of remote monitoring, immunity to electromagnetic interference, and safe operation for explosive environments [5-7].

Optical chemo/biosensing employs optical transduction techniques to yield analyte information. The most widely used techniques in optical sensors are fluorescence and absorption. Fluorescence chemo/biosensing is intrinsically more sensitive than absorption-based sensing techniques, and used more frequently [6,8]. In general, fluorescent sensors may be divided into direct fluorescence sensors and reagent-mediated

fluorescence sensors. Direct fluorescence sensors detect the analyte via the intrinsic fluorescent property of the analyte, while reagent-mediated fluorescence sensors monitor the optical response of an intermediate agent (e.g. analyte-sensitive dye molecules) as the probe to detect the analyte [8].

In the field of fluorescence chemo/biosensing, the optical principle has not changed greatly over the years. However, the sensing transduction platforms have changed significantly, which results in improved sensing performances [8]. Effective chemo/biosensing requires high sensitivity, selectivity, and ease of operation. These demands have driven the evolution of fluorescence chemo/biosensing platform from the use of traditional sensing materials (such as dye molecules) to numerous new ones with novel molecular structures (e.g. molecular beacon [9]) and nanostructues (e.g. quantum dot [10,11]).

Traditional sensing materials such as the conventional radioactive agent [12] and organic fluorescent dye are investigated broadly [12,13]. However, long-term exposure to radioactive agent is known to induce cancer or other diseases for human being, and many organic fluorescent dyes have not been fully tested in terms of safety issue, which pose a potential threat to human health. On the other hand, new sensing materials constructed at the molecular and nanostructure scale have recently emerged in academic literatures. The molecular approach to develop novel sensing materials is effective in many cases such as the development of peptide nucleic acid (PNA)[14], molecular beacon (MB) [9], aptamer [15,16], and autofluorescent protein [17]. Nevertheless, more often, application of these probes in chemo/bioassay faces some challenges such as requirements of complex labelling and

additional instrumentation, which incite higher levels of complexity and cost. Meanwhile, sensing materials with nanostructure features have been quickly developed, e.g. quantum dot (QD)-based probe [10,11] and Au nanoparticle (NP)-based probe [18]. These nanoprobe-based detection systems can be highly specific and extremely sensitive when combined with appropriate signal transduction and amplification mechanisms, e.g. QD-encoded sensor [19], Au NP nanosensor with surface-enhanced Raman scattering (SERS) [20], dye-doped silica NP nanosensor [21], and metal-enhanced fluorescence (MEF) nanosensor [22-24]. These nanosensors are promising but have not been fully developed. For instance, the toxicity remains an issue for QD-based sensors. The limitation of the above detection systems poses a challenge for their practical implementation in research and medical/environmental application.

An alternative is to use fluorescent conjugated polymers for chemo/biosensing with improved performances [25,26]. Conjugated polymers (CPs) are macromolecules that contain π-delocalized backbones. Their large absorption cross section and delocalized electronic structure allow efficient light-harvesting and rapid intra- and interchain exciton migration. This results in huge fluorescent signal amplification upon molecular-recognition events, and imparts the CP-based sensor high sensitivity, which offers a key advantage over small molecule counterparts [25-30]. In addition, compared with other methods employed to enhance fluorescent detection sensitivity, such as the use of superquenchers-labelled molecular beacon [38] and dye-doped silica NP probe [21], CP-based chemo/biosensing systems do not require complicated probe labelling or tailored instrumentations and should be adaptable to many standard fluorescent assays. On the

other hand, as the analogs of CPs but with fewer repeat units, most conjugated oligomers exhibit similar properties as their polymeric counterparts. These properties and advantages enable CP/oligomer based chemo/biosensors to have a variety of applications such as ion detection [26] and nucleic acid detection [26-28]. Nevertheless, chemo/biosensing based on CPs/oligomers still faces some challenges. For instance, more often, CPs/oligomers-based sensing is conducted in homogeneous solution. This can be complicated by non-specific interactions and result in poor detection selectivity [25,26]. Besides selectivity concern, sensitivity matters. To get higher fluorophore signal intensity, MEF has been reported for a variety of small fluorophores [22-24], but few on large flurophores such as CP. The introduction of CP MEF in conjunction of CP signal amplification would potentially enormously enhance the reporter signals for higher detection sensitivity. Combining these considerations, new types of chemo/biosensing based on CPs/oligomers are highly desirable as so to circumvent the above problems and improve sensing performance.

1.2 Objectives and scope of this study

This study aims to develop fluorescent nanosensors based on conjugated polymer and oligomer, and apply the developed platforms to highly sensitive and selective chemo/bioassays. The scope of the research includes developing silica nanoparticle (NP)-supported detection strategies using conjugated polymers/oligomers as optical signal amplifiers, and applying these strategies to sensitive and selective detection of DNA and mercury(II). Meanwhile, by exploiting silver NP arrays as supporting substrates, metal-

enhanced fluorescence (MEF) of conjugated polymer is explored and applied to DNA assay. More specifically, the objectives and activities of this study are:

1. To develop a silica NP-supported detection strategy using cationic CPs (PFP-2F, poly[9,9'-bis(6''-*N*,*N*,*N*-trimethylammonium)-hexyl)fluorene-*co*-*alt*-2,5-difluoro-1,4-phenylene) dibromide]) as fluorescence signal amplifiers, and apply this strategy to sensitive and selective DNA detection. DNA immobilized silica NPs (~100 nm in diameter) were first prepared after a seed-mediated growth and triazine bioconjugation. The obtained DNA-NP bioconjugates were then used as nanoprobes to capture fluorescein (Fl)-labelled DNA (Fl-DNA). Addition of PFP-2F generated an amplified signal of Fl-DNA while introduction of salt wash facilitated detection selectivity improvement. Experimental conditions were optimized, such as Fl-DNA surface coverage on silica NP and its effect on PFP-2F amplification.

2. To conduct label-free single-nucleotide polymorphism (SNP) discrimination using DNA-NP nanoprobes and conjugated oligomers (tetrahedralfluorene, tetrakis[4-(2-(9,9,9',9'-tetrakis(N,N,N-trimethylammoniumhexyl)-7,2'-bifluorenyl))-phenyl]methane hexadecanebromide) as signal amplifiers. Ethidium bromide (EB) was used as signal reporter on the hybridized DNA-NP surface, and the tetrahedrafluorene was selected to amplify DNA-intercalated EB emission. Salt-wash was used to assist detection selectivity improvement. Experiments for the detection were optimized, such as EB intercalation on hybridized DNA-NP surface and the subsequent tetrahedralfluorene complexation.

3. To develop highly sensitive and selective mercury(II) assay using DNA-NP nanoprobes and cationic PFP-2F as the optical signal amplifier. Mercury-specific DNA was first immobilized onto the silica NP surface. Employing a CP-assisted and silica NP-supported detection strategy, the amplified fluorescence turn-on assay for mercury(II) was conducted. Thermal washing was used to facilitate discrimination of mercury(II) from non-specific ions. Various parameters in this assay were studied, such as metal ion concentration and the ratio of Hg^{2+} to the Hg^{2+}-specific DNA duplex.

4. To investigate the feasibility of metal-enhanced fluorescence (MEF) of fluorescent CP (PFBT, poly[9,9-bis(9-*N*,*N*,*N*-trimethylammonium)ethoxy)ethoxy)ethyl)fluorene-*alt*-(4,7-(2,1,3-benzothiadiazole)dibromide)]) film, and apply the developed MEF substrate to DNA detection. Silver NPs (~75 nm in average) were prepared and self-assembled onto glass slides to form silver NP arrays. Through layer-by-layer (LbL) assembly, varied proximity of the PFBT from the Ag NP array surface was fine tuned using none-fluorescent poly(diallyldimethyl ammonium chloride) (PDDA) and poly(sodium 4-styrenesulfonate) (PSS) as spacers. Various parameters affecting PFBT fluorescence in the above system were studied, such as spacer distance and excitation wavelength. The developed Ag NP array-PFBT substrates were further employed for DNA detection using Cy5-labelled peptide nucleic acid as the probe.

The original contributions of this research include two parts: 1) development of probe-immobilized silica NP as a unique platform to enhance CP-based homogeneous solution sensing performance, particularly on detection selectivity and signal amplification for higher sensitivity. First, as a solid-state sensing platform, silica NP can help us minimize

non-specific interactions through separation by centrifugation of the NP probe-target complex out of interfering medium. This produces a favorable environment for CP-based assay in terms of selectivity improvement. Furthermore, we first explored fluorescence resonance energy transfer (FRET) signal amplification by CP on silica NP surface, which expands our understanding of CP fluorescence behavior in NP-confined space toward large FRET signal amplification for higher detection sensitivity. On top of that, this study successfully demonstrated that homogeneous CP/oligomer-based assay could be potentially transferred to NP-supported format with an improved sensing performance, with the practical applications including the detection of DNA SNP and mercury(II) assay. 2) Demonstration of metal enhanced fluorescence (MEF) of CP on silver NP array surface, which deepens the understanding of CP photophysics when interfacing plasmonic Ag nanostructure. Furthermore, the developed MEF-PFBT substrate was successfully applied to the DNA assay with an improved performance, which represents the first report on the application of MEF-CP substrate. These findings open up new opportunities to improve the detection sensitivity of CP-based bioassays. In addition, the silver NP array enhanced excitation and fluorescence of conjugated polymers should find other applications in organic electronic devices besides the demonstrated biosensing.

CHAPTER 2

LITERATURE REVIEW

In this chapter, a literature survey of deoxyribonucleic acid (DNA), nanoparticles, and conjugated polymer and oligomer based sensors is presented. The function and structure of DNA and its detection are described firstly. Then, the NP-based optical detection of DNA is discussed. Finally, recent advance of chemo/bioassays based on fluorescent conjugated polymers and oligomers is reviewed.

2.1 Deoxyribonucleic acid (DNA) and its detection

Deoxyribonucleic acid (DNA) is a nucleic acid that contains the genetic instructions for the development and function of living organism [31-33]. It is composed of four types of bases including Adenine (A), Guanine (G), Thymine (T), and Cytosine (C) (structure shown in Figure 2.1), which are held together by a backbone made of sugars and phosphate groups while the sequence of these four bases encode genetic information [32-33]. Meanwhile, DNA is very important for protein synthesis, and it is the direct connection between genetic features and protein expression [31-33]. Due to its role in gene carrier and protein synthesis, the detection and analysis of DNA is of vital importance. The efforts in the research on DNA will help us better understand the gene mutation, diseases at the molecular level, and finally find personalized medicine.

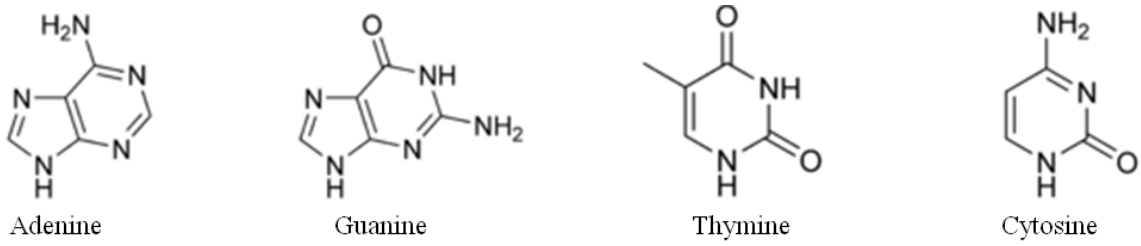

Figure 2.1 Chemical structures of the nucleobases including Adenine (A), Guanine (G), Thymine (T), and Cytosine (C) [33].

Moreover, DNA possesses the unique structure of double helix (see Figure 2.2), which make them stable in the biological system. The mechanism of the double helix formation, which is called base paring, can be used to develop versatile molecular probes (e.g. PNA, MB) for DNA detection or heavy metal ion detection [31], and even assembly nanostructure materials for novel application [34].

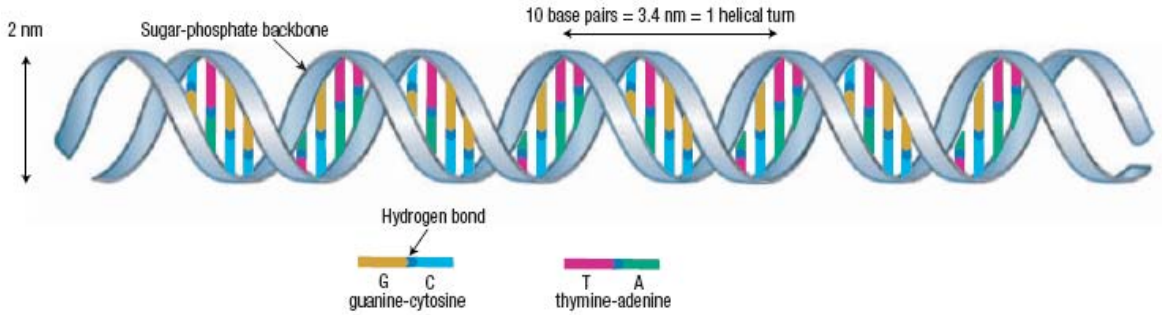

Figure 2.2 Double-helical DNA: a linear molecule formed by Watson–Crick base-pairing (G-C and A-T), 2 nm in thickness, and ~0.34 nm per base pair in the DNA fragment structure [35].

Traditional sensing materials for DNA detection include conventional radioactive agent [12] and organic fluorescent dye [13]. However, long-term exposure to radioactive agent is known to induce cancer or other diseases for human being. Meanwhile, many organic fluorescent dyes have not been fully tested either in animals or human being, which pose a potential threat to human health.

In the meanwhile, chemo/biosensing materials constructed at the molecular level have recently emerged in the literature. This type of probes is typically represented by peptide nucleic acid (PNA), molecular beacon (MB) [9], and aptamer [15,16].

Peptide nucleic acid (PNA) is a DNA analogue, which has the structure similar to DNA molecule. In contrast to the sugar-phosphate backbone of DNA, PNA backbone is composed of repeating N-(2-aminoethyl)-glycine units, where the nucleobases are linked to the backbone by methylene carbonyl bonds (see Figure 2.3) [14,36]. In terms of chemo/biosensing, PNA have several advantages such as: 1. stronger binding between PNA/DNA strands than that between DNA/DNA strands due to the lack of electrostatic repulsion; 2. greater specificity to complementary DNA; 3. stability over a wide pH range. Nevertheless, PNA is more expensive relative to traditional DNA in current market.

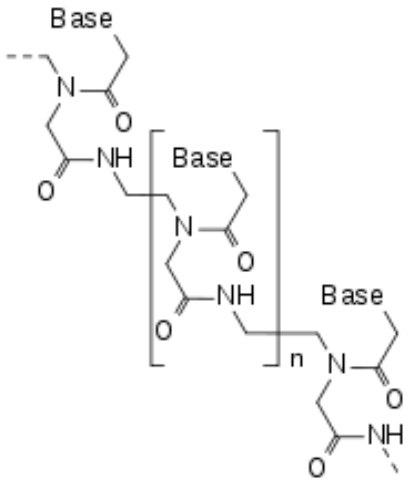

Figure 2.3 Schematic illustration of peptide nucleic acid (PNA) structure [36].

Molecular beacon (MB) is another type of the molecular probe since the first report in 1996 [9]. The principle of MB-based detection is shown in Figure 2.4 [37]. At the beginning, a stem–loop MB structure holds the fluorophore and the quencher in close proximity to

one another, resulting in weak fluorescence signal. Upon binding with target molecules, the fluorophore in the MB will be separated from the quencher, resulting in an enhanced fluorescence [37]. However, this molecular sensing material introduces a high fluorescence background and affects the accuracy in signal readout. Concerning this point, superquenchers-labelled molecular beacon was further developed [38], which can reduce the background signal to some extent.

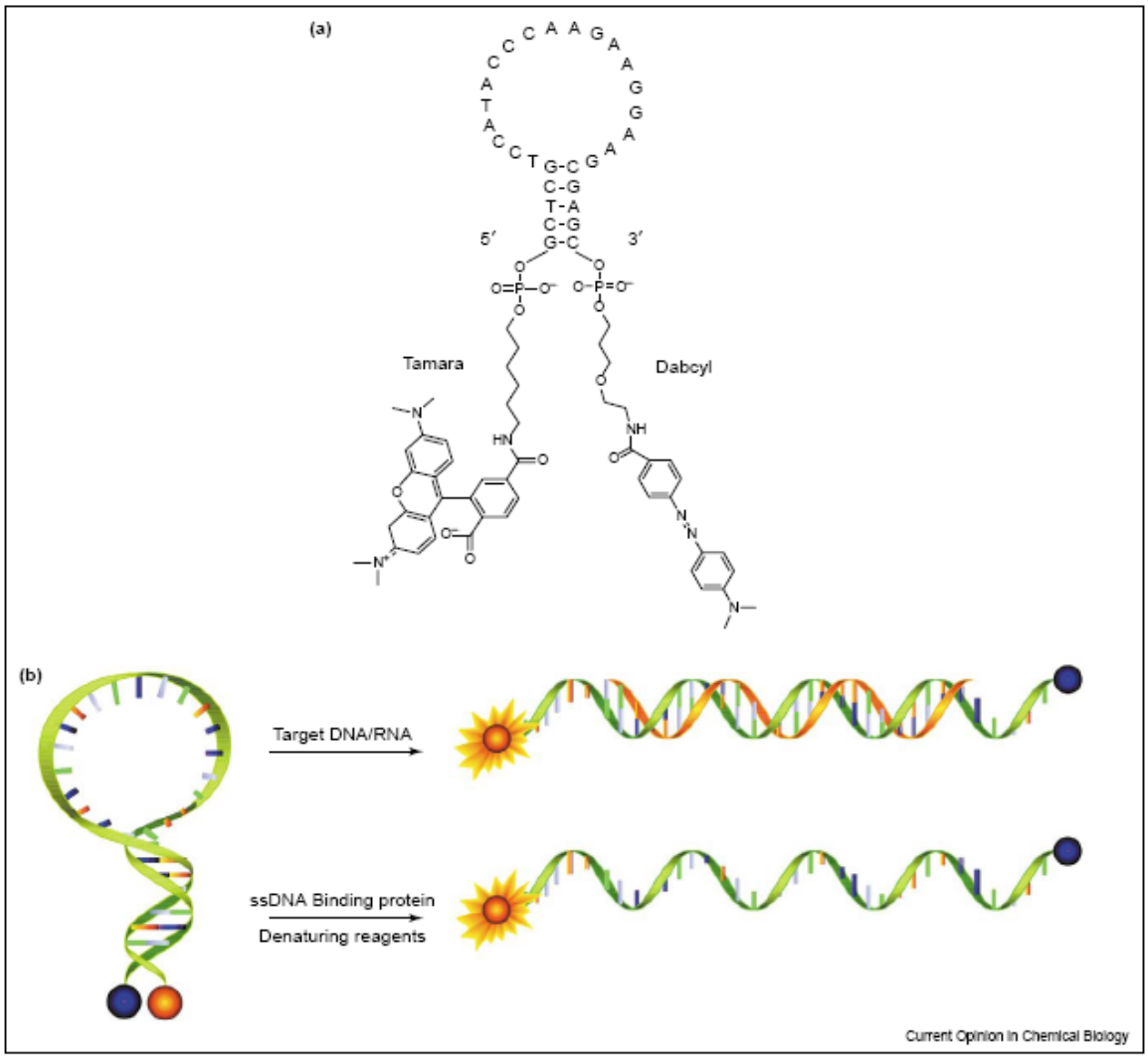

Figure 2.4 Structural characteristics of molecular beacon probes: (a) A typical molecular beacon DNA probe; (b) Molecular beacon working principle [37].

More recently, another kind of molecular probe, aptamer from SELEX (selective evolution of ligands by exponential enrichment) has been developed [15,16]. Aptamers are DNA or RNA molecule which has been artificially manipulated to allow binding with other specific molecular targets, such as a protein. A typical detection using this molecular probe is reported by Yang et.al.[39]. The aptamer-based assay scheme is shown in Figure 2.5. A specific binding of aptamer to its target protein, platelet-derived growth factor (PDGF), changes the aptamer conformation. This brings the two labelled pyrene molecules into close proximity to form an excimer, resulting in a change of fluorescence wavelength from ~400 nm (pyrene monomer) to 485 nm (pyrene excimer). In this report, the authors further coupled the light-switching detection with time-resolved measurements, which minimized background signal from the probe and the multiple species in the biological environment. This developed strategy enables a detection of picomolar target in a few seconds, and avoids a sample clean-up process.

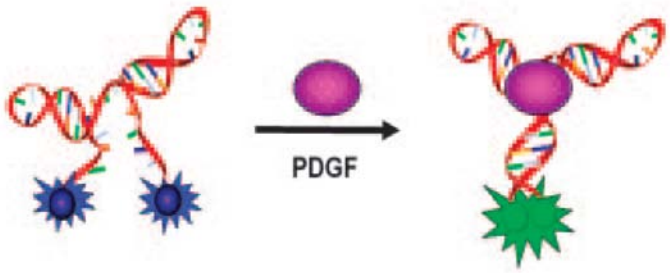

Figure 2.5 Schematic illustration of an aptamer-based detection for the target protein, platelet-derived growth factor (PDGF) [39].

The above developed molecular probes (e.g. PNA, molecular beacon and aptamer) bear some intrinsic advantages compared with traditional DNA, and procure proper positions in chemo/bioassay. However, more often, application of these probes in chemo/bioassay

faces some challenges such as expensive cost, requirement of complex labelling [38] or additional instrumentation [39].

2.2 Nanoparticle (NP)-based optical DNA detection

On the other hand, chemo/bioassays based on nanoparticles, or nanosensors, have recently appeared in literature with significant volumes and shown promising application in biological research and medicine. This type of NP-based optical sensor can be highly specific and extremely sensitive when combined with appropriate signal transduction and amplification mechanisms. In the following section, we review some novel NP-based optical DNA detection, mainly focusing on QD-encoded sensor [19], Au NP nanosensor [20], dye-doped silica NP nanosensor [40], magnetic assisted biobar-code nanosensor [41], and MEF nanosensor for DNA detection [22,23].

QD-encoded sensor for DNA detection

Semiconductor nanocrystal quantum dots (QD) as sensitive biological labels are potential candidates for replacing conventional fluorescent markers in bioassays [10,11,42,43]. This type of nanoprobes has several advantages such as: 1. broad excitation spectra; 2. intensely bright, narrow, and size-tunable fluorescence emission spectra, spanning from ultraviolet to near infrared (NIR); 3.and high resistance against photobleaching [19,42-44]. To apply this new type of probes to DNA assays, Nie and co-workers developed QD-tagged beads for multiplex DNA detection [19]. In this study, different-sized QDs (zinc sulfide–capped cadmium selenide nanocrystals) were encapsulated into polystyrene beads at precisely

controlled ratios, producing variable emission signals. As shown from DNA assay in Figure 2.6, the optical properties enable triple-color QD encoded beads suitable for wavelength-and-intensity multiplexing. Note that the combination of 10 intensity levels and 6 colors could theoretically code one million different DNA sequences. The DNA hybridization results show that the coding and target signals can be simultaneously read at the single-bead level.

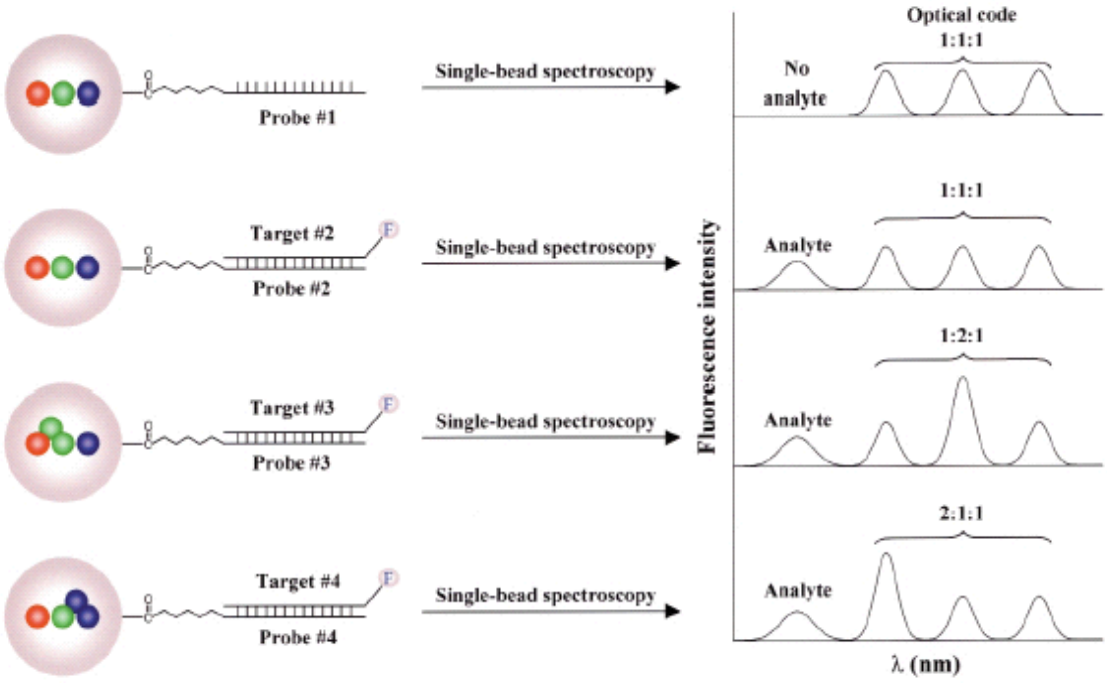

Figure 2.6 Schematic illustration of DNA hybridization assays using QD-tagged beads. Probe oligos (No. 1–4) were conjugated to the beads by crosslinking, and target oligos (No. 1–4) were detected with a blue fluorescent dye such as Cascade Blue. After hybridization, nonspecific molecules and excess reagents were removed by washing. For multiplexed assays, the oligo lengths and sequences were optimized so that all probes had similar melting temperatures (T_m = 66°–99°C) and hybridization kinetics (30 min) [19].

Au NP nanosensor with surface-enhanced Raman scattering (SERS)

Another important NP-based detection is the Au NP nanosensor [18,20,45]. Mirkin and coworker developed a series of bioassay methods derived from gold NP, e.g. Raman

optical detection [20], electrical and electrochemical detection [45]. Figure 2.7 shows a typical DNA detection using surface enhance Raman scattering based on Au NP [20]. In this study, 13-nm-diameter Au particles were functionalized with Raman dye-labelled oligonucleotides and used as the DNA probes. Followed a sandwich-structured DNA recognition, Raman spectroscopic fingerprint of the target was identified after Ag enhancing by scanning Raman spectroscopy. This chip-based format enables multiplexed detection of oligonucleotide, and provides high sensitivity with a detection limit of 20 femtomolar [2] besides high selectivity.

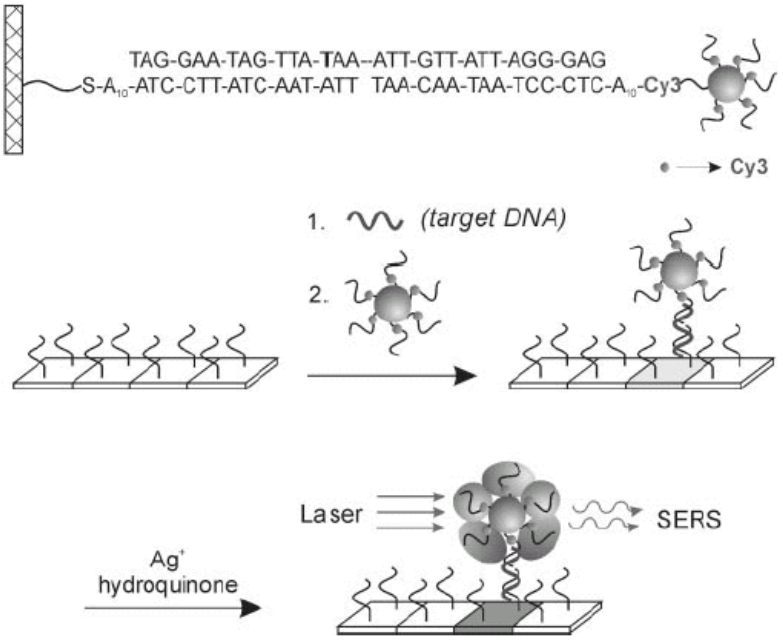

Figure 2.7 Gold NP functionalized with oligonucleotides and Raman labels, coupled with surface-enhanced Raman scattering (SERS) spectroscopy, for performing multiplexed detection of oligonucleotide targets [20].

Magnetic assisted biobar-code nanosensor

Based on the above detection platform, Mirkin and coworkers recently reported a 'bio-bar-code amplification' for DNA detection with high sensitivity [41]. This assay relies on two-component DNA-modified gold NPs and single-component DNA-modified magnetic

microparticles (MMPs), and a chip-based detection of bar-code DNA. As shown in Figure 2.8B, target DNA is first recognized by a sandwich recognition using DNA-funtionalized MMP and gold NP probes. After magnetic separation and dehybridization, free bar-code DNA was collected and applied to a chip-based DNA detection system. This developed detection platform provides high selectivity and a sensitivity with very low detection limit down to 500 zeptomolar without the need for enzymatic amplification. In addition, this system has an excellent dynamic range and is ideal for multiplexing.

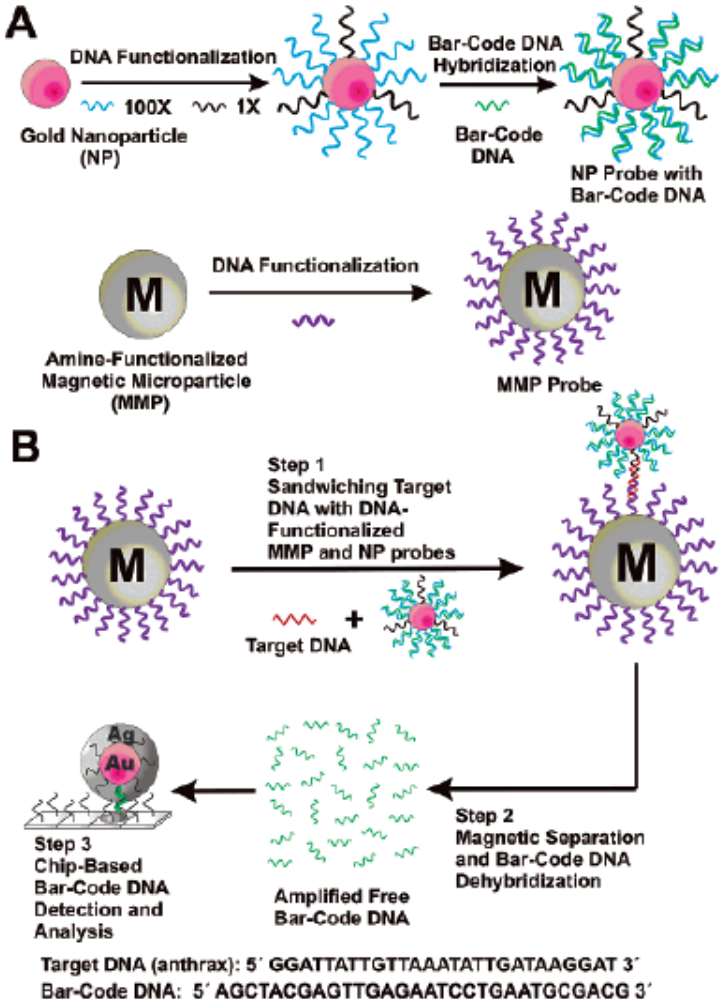

Figure 2.8 The magnetic microparticle (MMP)-assisted biobar-code DNA assay. (A) Nanoparticle and MMP probe preparation. (B) Nanoparticle-based DNA amplification scheme for anthrax DNA detection with 500 zeptomolar detection limit [41].

Dye-doped Silica NP nanosensor

Fluorescent dye doped silica NPs have been used for chip-based sandwich DNA detection [40]. As shown in Figure 2.9, the captured DNA is first immobilized onto a glass surface and hybridized with unlabelled target DNA complementary to both capture DNA and probe DNA sequences. After addition of probe DNA modified dye-doped silica NPs, each pre-captured target DNA hybridizes with each probe DNA, which thus fixes corresponding dye-doped NP to the surface, and brings many dye molecules for signaling. Through monitoring fluorescence intensity or counting fluorescent spots from the surface-bound dye-doped NPs, DNA target molecules have been detected down to subpicomolar levels. In addition, discrimination of DNA single-base mismatch has also been demonstrated [40].

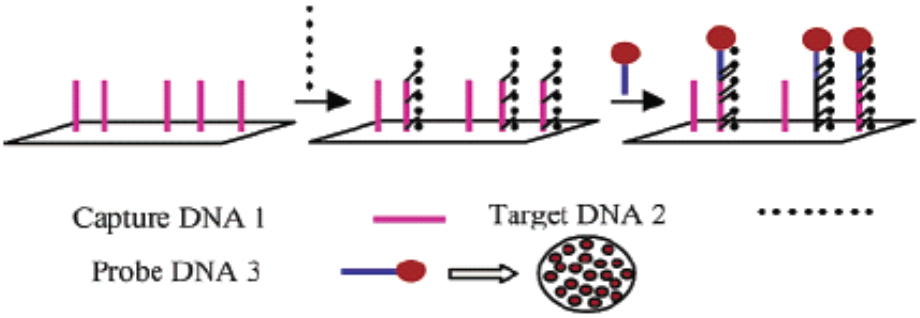

Figure 2.9 Schematic illustration of a sandwich DNA assay based on bioconjugated silica nanoparticles [40].

MEF nanosensor for DNA detection.

Metal-enhanced fluorescence (MEF), constructed on metallic nanostructures, is a relatively new technique that can be used to increase the sensitivity of fluorescent sensors [22-24]. MEF reflects the interactions of the excited-state fluorophores with surface plasmon electrons in the metallic nanostructures such as silver [46,47], gold [48,49], and alumina [50],

which in turn produces different effects on the fluorophores [22-24]. The overall fluorescence enhancement or quenching for a given system depends on the relative contributions among excitation rate enhancement, emission enhancement (radiative decay enhancement) and quenching (nonradiative decay enhancement) [22-24,51,52]. These contribution factors are sensitive to various parameters such as the spectral properties of both fluorophores and metal nanoparticles (NPs) [53], the distance between fluorophores and metal NPs [54,55], and the orientation of fluorophores relative to metal NPs [55].

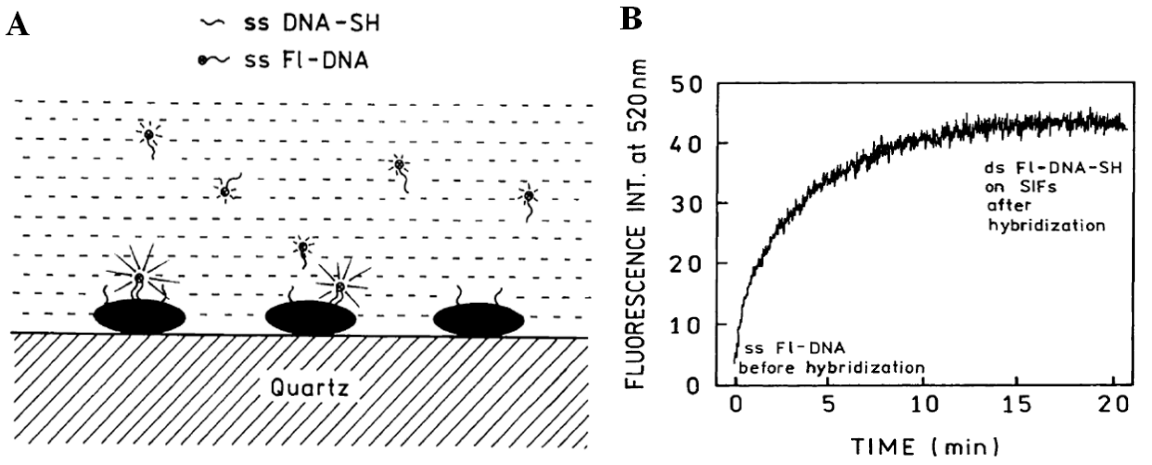

Figure 2.10 (A) Schematic illustration of the DNA oligomers bound to silver particles; (B) The time-dependent hybridization of ss Fl-DNA to ss DNA-SH [56].

One successful example using MEF for DNA detection is the report from Malicka and coworkers in 2003 [56]. As shown in Figure 2.10 (A), the thiolated ssDNA (DNA-SH) as the capture probe was first immobilize onto the silver particles surface in this study. A fluorometer was then used to monitor the real-time hybridization in the sample cell upon the addition of fluorescein labelled ssDNA (Fl-DNA), in a similar amount to that of silver-bound capture ssDNA. The fluorescence intensity increases immediately upon mixing as shown in Figure 2.10 (B). After ~20 min, the fluorescence signal approaches to

a plateau with ~12-fold enhancement relative the beginning. In the control experiments, ssDNA-SH was hybridized with ss Fl-DNA first, which is followed by deposition on silver particles. This results in a similar 12-fold increase in intensity upon immobilization on silver particles, relative to that of an equivalent amount of ds Fl-DNA-SH in solution. The authors ascribe this fluorescence enhancement to the localization of ss Fl-DNA near to the silver particles by hybridization with the capture DNA.

Employing a similar approach, Ginger and coworkers investigate the fluorescence from dyes near to silver nanoprisms [53]. With the aid of the single-particle darkfield scattering and fluorescence microscopy, the MEF with single nanopaticle resolution was studied after coupling the dyes to DNA functionalized metal nanoprisms as shown in Figure 2.11 The results show that, for dyes with ~5.5 nm thick DNA layers from silver surface, the brightest fluorescence is usually obtained near NPs with local surface plasmon resonance (LSPR) peaks that are only slightly blue shifted from the dye emission peak. This finding provides important information for those studies applying metal-enhanced fluorescence in biosensing.

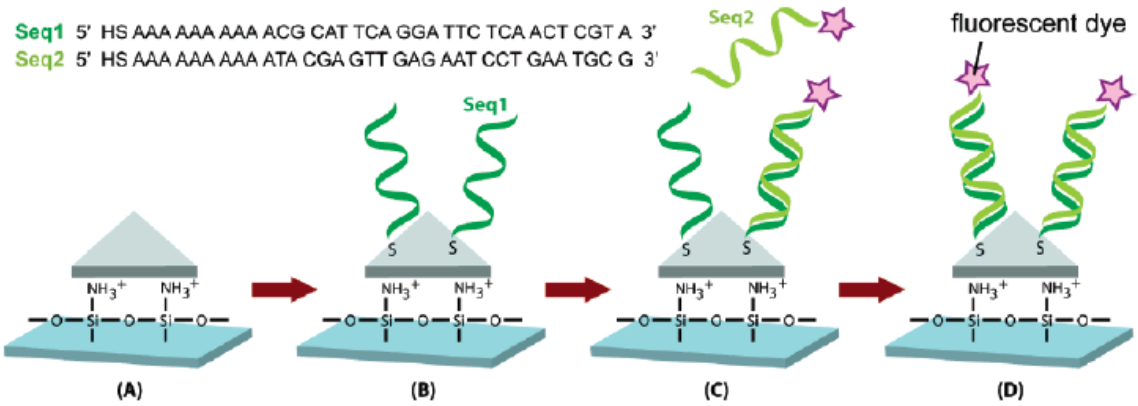

Figure 2.11 Schematic illustration of creating dye-functionalized silver nanoprisms using DNA as a structural linker [53].

Besides the above NP-based optical DNA detection, other NP-based methods/mechanisms have also been developed, such as integration of nanosensor into established platform [57] as well as a combinational setup [58,59]. With further exploration and understanding of nanomaterials, NP-based optical DNA assay will make a fast and great progress.

2.3 Conjugated polymer and oligomer based optical chemo/bioassays

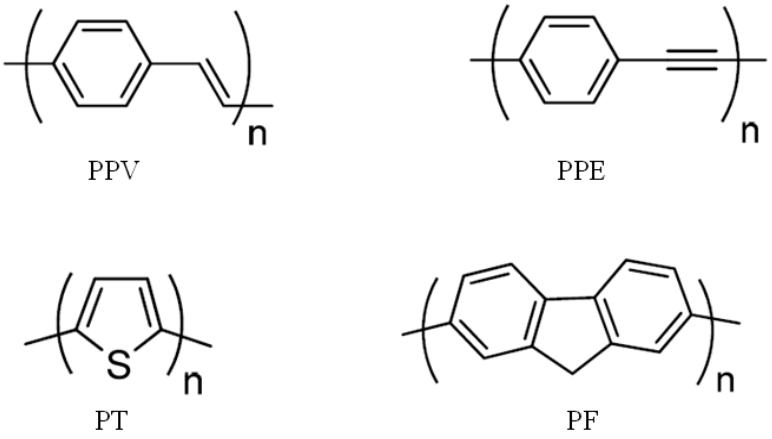

Figure 2.12 Backbone structures of some common conjugated polymers in chemo/bioassays.

Conjugated polymers are macromolecules that contain π-delocalized backbones. Traditional polymeric materials are most regarded as insulators [60,61]. However, the discovery of conducting polymers has bridged traditional insulating polymers with those of conducting or semiconducting materials [62,63]. The new materials are attractive for their favorable electronic properties, exceptional optical characteristics, and the processability of polymers [61-63]. These unique properties stimulated intense research interests from both

industrial and academic fields, and a wide range of applications using conjugated polymers has been explored, such as polymer light-emitting diodes (PLED) [64,65], field-effect transistors (FETs) [66,67], light-emitting electrochemical cells (LECs) [68,69], plastic lasers [70], solar cells [71], and chemo/biosensors [25,26].

The interest of applying CPs to chemo/biosensing partly comes from CP unique molecular structure suitable for highly sensitive detection [25,26]. Figure 2.12 shows the backbone structures of some commonly used CPs in chemo/biosensing, including poly(*para*-phenylene vinylene) (PPV) [64], poly(*para*-phenylene ethynylene) (PPE) [72], poly(thiophene) (PT) [73], and polyfluorene (PF) [74]. These conjugated polymers have large absorption cross section and delocalized electronic structures, which allow efficient optical response and rapid intra- and interchain exciton migration. This results in huge signal amplification upon molecular recognition events, and imparts the CP-based sensor higher detection sensitivity relative to small molecule counterparts [25-30]. In addition, compared with other methods employed to enhance detection sensitivity, such as the use of superquenchers-labelled molecular beacon [38] and dye-doped silica NP probe [21,40], CP-based chemo/biosensing systems do not require complicated probe labelling or tailored instrumentations and should be adaptable to many standard assays. On the other hand, as the analogs of CPs but with fewer repeat units, most conjugated oligomers exhibit similar properties as their polymeric counterparts. These properties and advantages enable CP/oligomer based chemo/biosensors to have a variety of applications such as ion detection [26] and nucleic acid detection [26-28]. Based on the type of detection signal,

CP/oligomer based chemo/biosensing can be divided into optical detection [26,28] and non-optical one such as electrochemical detection [75].

Conjugated polymer and oligomer based optical detection typically includes colorimetric and fluorescent methods [26]. In a colorimetric assay, color change occurs in the presence of target, which may preclude the need for analytical instruments but is restricted by the detection sensitivity. In contrast, the fluorescent detection is intrinsically more sensitive than the colorimetric one and has been widely used. For most of conjugated polymer and oligomer based fluorescent sensors, the fluorescence can be either enhanced (turn-on approach) or quenched (turn-off approach) in the event of target recognition [26]. The turn-on or turn-off approaches can be realized through several mechanisms such as superquenching mechanism, fluorescence resonance energy transfer (FRET) and conformation change mechanism [27,28,76]. Note that these different mechanisms are not exclusive to each other, and some developed detection systems actually employ more than one of them in a single assay [26,27]. In this review part, we will first describe the sensing mechanisms including superquenching, FRET and conformation change mechanism, and then discuss the sensing formats including homogeneous, heterogeneous, and particle-supported formats. Lastly, conjugated polymer and oligomer based optical detection of different analytes will be addressed.

2.3.1 Sensing mechanisms of conjugated polymer (CP) based chemo/bioassays

This section reviews some chemo/biosensing mechanisms based on fluorescent conjugated polymers/oligomers, mainly focusing on superquenching mechanism, fluorescence resonance energy transfer mechanism, and conformation change mechanism.

Superquenching mechanism

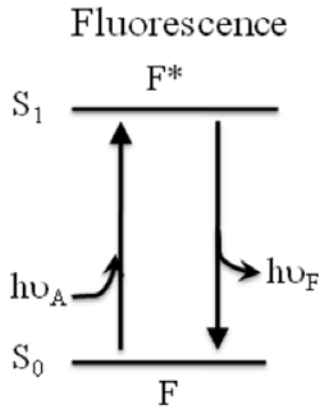

Figure 2.13 Generation of fluorescence using a simplified Jablonski diagram [247].

For conjugated polymer/oligomer based chemo/biosensing, fluorescence quenching refers to any process which decreases the fluorescence intensity/lifetime of a given substance, and the specie that causes the quenching process is called a quencher. Figure 2.13 shows fluorescence generation through a simplified Jablonski diagram [247]. Upon absorption of photons, a fluorophore (F) is excited to singlet excited electronic state (S1) and form an excited fluorophore (F*). The fluorescence is generated when F* relaxes to ground electronic state (S0) via photon emission. However, F* could return to the ground state by various competing pathways such as fluorescence quenching through interaction of F/F* with a quencher. These interactions include excited-state interaction, molecular

rearrangement, energy transfer, charge transfer, ground-state complex formation and dynamic collision, which follow non-radiative pathways against photon emission [247]. Superquenching may happen for CP, and this is attributed to a combination of two effects: strong association between the oppositely charged polyelectrolyte and quencher, and the rapid exciton migration along the polymer chain until quenching occurs at a 'trap site' [76].

Superquenching was first reported for CP-based biosensor by Whitten and coworkers in 1999 [77]. In a typical assay, a quencher-tether-ligand (QTL) conjugate is synthesized by connecting a quencher to a ligand. The superquenching behavior of CP is modulated by addition of analytes capable of binding the ligands. Figure 2.15 shows the detection scheme for specific biotin–avidin binding event using water-soluble polyanionic CP 1 (structure shown in Figure 2.14). At the beginning, methyl viologen (MV^{2+}) was linked to the biotin (B) molecule to form a QTL probe, which quenches the fluorescence of CP 1 by a charge transfer through electrostatic interactions. Upon addition of avidin into the solution of the polymer and quencher, the fluorescence turn-on response of the solution occurs. This fluorescence recovery is attributed to binding of the QTL probe by avidin, which pulls away the QTL from the CP 1 and prevents the close association of quencher with polymer. Using the method developed by Whitten and coworkers, the detection limit of the avidin protein reached a nanomolar level. This superquenching-based CP sensing design has subsequently led to the sensitive detection of a variety of targets such as DNA, antibodies and enzymes [76]. However, further studies on the same systems by Bazan and coworkers have suggested that the fluorescence increase is partially due to the formation

of the avidin-CP 1 complex by non-specific interaction, which shields the CP 1 from the quencher [78].

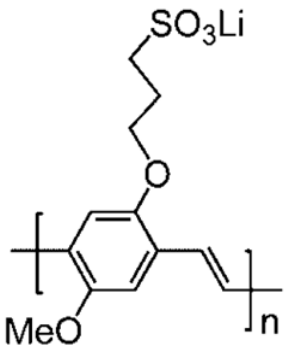

1

Figure 2.14 Molecular structure of CP 1 in superquenching-based avidin assay [77].

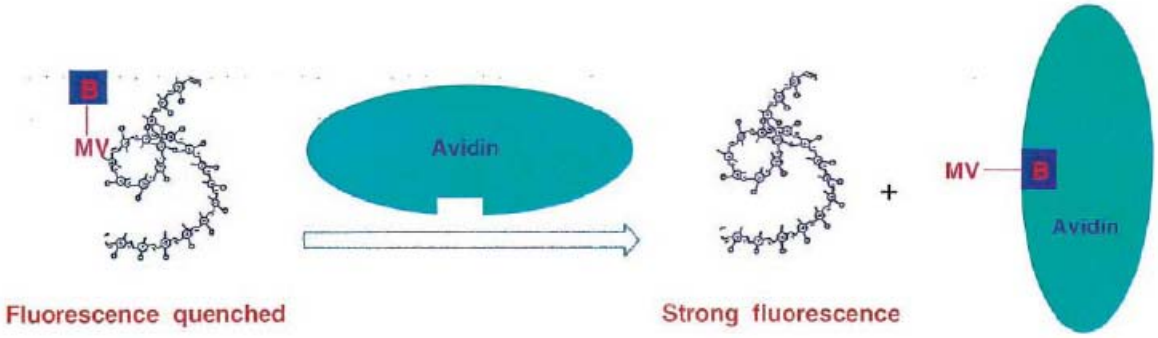

Figure 2.15 Schematic illustration of avidin detection using CP 1 based on superquenching mechanism [77].

Fluorescence resonance energy transfer mechanism

Förster resonance energy transfer (FRET), also known as fluorescence resonance energy transfer, describes the long-range dipole-dipole interaction between the electronic excited states of two chromophores in which the excitation of a donor chromophore results in emission from the acceptor chromophore [26]. CPs are excellent donor candidates for FRET.

Their large absorption cross section and π-delocalized structure allow efficient light-harvesting and rapid intra- and interchain fluorescence resonance energy transfer. This generates huge signal amplification of the acceptor chromophore upon molecular-recognition events, and imparts the CP-based sensor higher sensitivity relative to that based on small molecule [25,28-30].

The efficiency of FRET using CP follows Förster theory, a quantitative theory developed by Theodor Förster which assumes the energy transfer occurs through dipole-dipole interactions of donor and acceptor. According to Förster theory [79], for donor and acceptor separated by a distance (r_{DA}), the rate of FRET (k_{FRET}) could be simplified as the following relationship:

$$k_{FRET} \propto \frac{1}{r_{DA}^{6}} \kappa^2 J(\lambda) \qquad (1)$$

Where,

κ is the orientation factor, and κ^2 is usually assumed to be equal to 2/3;

$J(\lambda)$ is the overlap integral, expresses the spectral overlap of the donor emission and the acceptor absorption, and has the unit of $M^{-1}\cdot cm^{-1}\cdot nm^4$ when λ has the unit of nm;

r_{DA} is the distance between donor and acceptor, and can has the unit of Å;

k_{FRET} is the FRET rate, and can has the unit of s^{-1}.

Therefore, the FRET efficiency is dependent on the distance between the CP and acceptor, orientation of the acceptor relative to the CP, as well as the spectral overlap between the emission of the CP and the absorption of the acceptor. Modulation of various parameters

shown in Förster equation by different experimental conditions provides a viable means for signal generation.

On the other hand, FRET can be competed by photoinduced charge transfer (PCT), a charge transfer which occurs when certain photoactive materials interact with light. Figure 2.16 show a simplified illustration of two situations (FRET and PCT) that may occur upon donor excitation. When the highest occupied molecular orbital (HOMO) and lowest unoccupied molecular orbital (LUMO) energy levels of the acceptor are located within the donor's orbital energy levels as in Situation A (Figure 2.16), excitation of the donor leads to FRET energy transfer from the donor to the acceptor, resulting in photon emission from the acceptor with sufficiently large quantum yield. However, if the acceptor's energy levels are not within the orbital energies of the donor as in Situation B (Figure 2.16), donor excitation would lead to PCT to the acceptor. This charge transfer process is detrimental to FRET assay, and leads to the decrease of the acceptor chromophore's signal output [80].

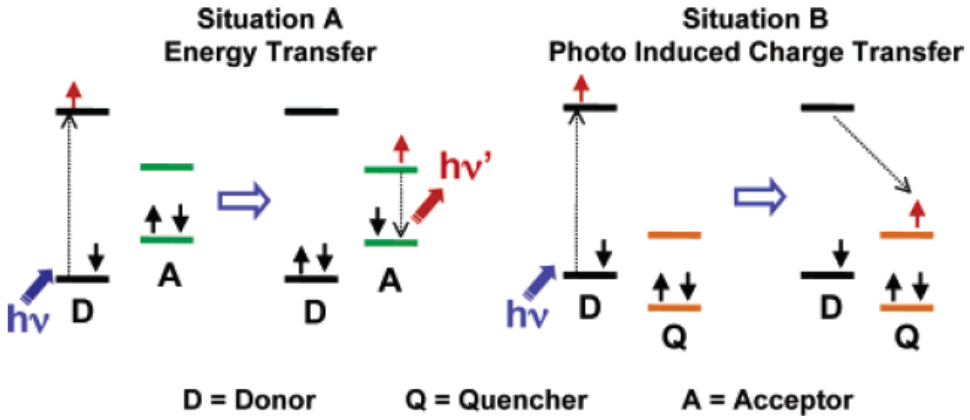

Figure 2.16 Effect of relative orbital energy levels on fluorescence resonance energy transfer (FRET) vs. photoinduced charge transfer (PCT) preferences [80].

To get better FRET efficiency, besides the concern on Förster theory, careful attention needs to be paid to the orbital energy levels, the molecular structure of the CP, and fluorescence quenching of the donor/acceptor within the FRET pair complex [81,82]. More detail will be discussed in a subsequent application section based on this mechanism.

As a typical example of FRET using CP, we describe the DNA assay scheme pioneered by Bazan and coworker in 2002 [83]. The developed assay contains three components, namely, a cationic poly(fluorene-co-phenylene) (CP 2, structure shown in Figure 2.17), a probe peptide nucleic acid (PNA) labelled at the 5' end with a chromophore (C*, fluorescein), and the target DNA strand. At the initial status, the neural PNA -C* displays no electrostatic interaction with the CP 2, and the average distance between them is too large for effective FRET. As shown in Figure 2.18, introduction to the PNA-C*/CP 2 solution of a complementary DNA, yields the PNA-C*/ssDNA duplex which features a negative charge and favorable electrostatic interaction with CP 2. This results in a decreased distance between DNA-PNA-C* and CP 2, allows for FRET from the CP 2 to the signaling C*. On the contrary, when a non-complementary ssDNA is added, complexation between CP 2 and the probe PNA-C* does not occur, and no electrostatic binding between CP 2 and PNA-C*. This results in large average distance between CP 2 and the signaling C*, and leads to less effective FRET. Using this FRET-based DNA assay, differentiation of complementary and noncomplementary ssDNA and a detection limit of 10 picomolar [58] has been demonstrated. This FRET-based CP sensing design has subsequently led to the sensitive detection of a variety of targets such as RNA [84], protein [85-87], potassium ion [88].

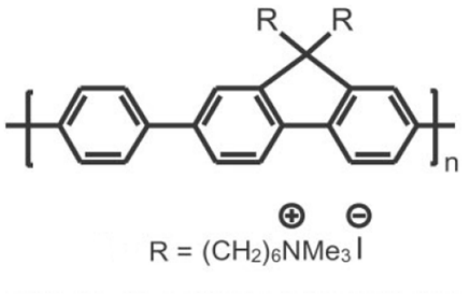

2

Figure 2.17 Molecular structure of CP 2 in FRET-based DNA assay [83].

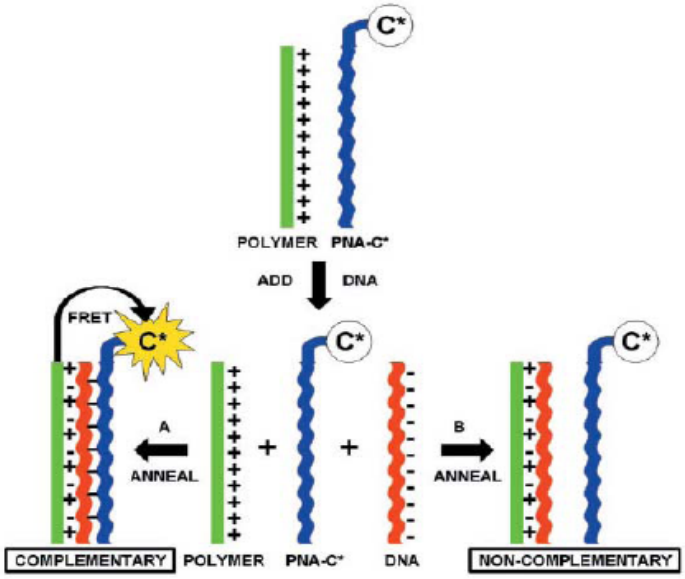

Figure 2.18 Schematic illustration of the PNA-C*/CP 2 assay to detect a complementary ssDNA sequence based on FRET mechanism [83].

Conformation change mechanism

The conformation change of the CP upon complexation with different analytes results in the changes of CP optical properties such as the absorbance and fluorescence [27,89]. Based on this mechanism, several DNA or protein biosensors with high sensitivity have been developed using cationic poly(thiophene) derivatives [27]. In compared with the superquenching or FRET-based sensing, conformation change-based sensing provides the advantage that it does not require either probe or analyte labeling.

As an example of conformation change-based assay using CP, we describe the first report about DNA detection by Leclerc and coworkers in 2002 by applying a cationic PT derivative (CP 3, structure shown in Figure 2.19) [89]. In this assay as shown Figure 2.20, the CP 3 adopts a random-coil conformation and exhibits a relatively short absorption wavelength (yellow aqueous solution, λ = 397 nm). Upon complexation with 20-base segment of ssDNA driven by electrostatic interactions, the equivalent CP 3 adopts a highly conjugated and planar conformation, and exhibits a relatively red-shifted absorption wavelength (red aqueous solution, λ = 527 nm) within 5 min of incubation. After the addition of a ssDNA complementary to the capture strand, the CP 3/dsDNA triplex forms, which enable the CP 3 to return the random-coil conformation and exhibits a relatively short absorption wavelength (yellow aqueous solution, λ = 421 nm). This optical response during DNA hybridization can be monitored by absorption spectroscopy or just observed by 'naked-eye'.

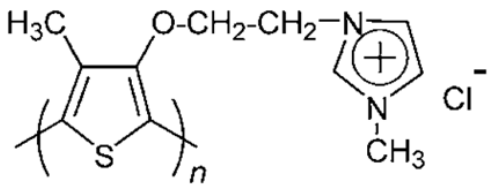

3

Figure 2.19 Molecular structure of CP 3 in conformation change-based DNA assay [89].

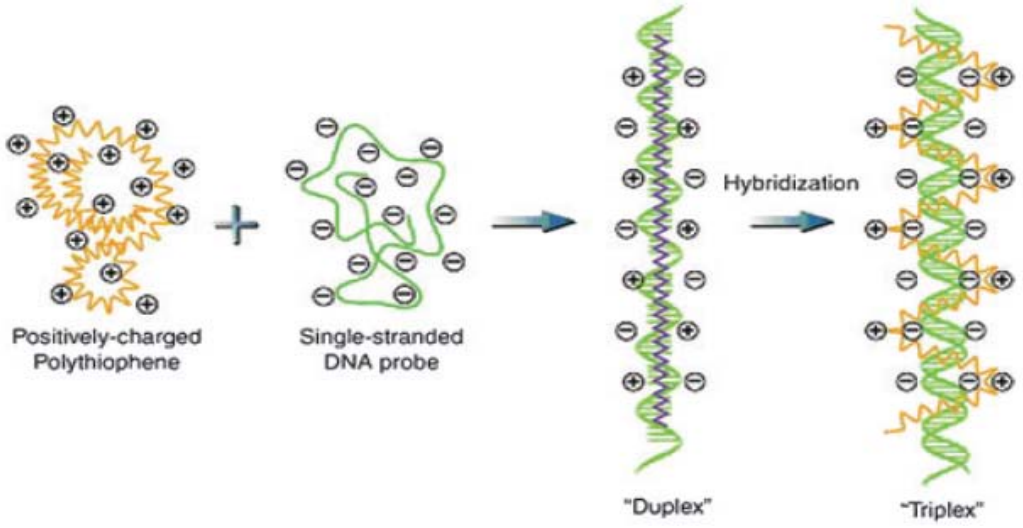

Figure 2.20 Schematic illustration of the formation of a planar CP 3/ssDNA duplex and a helical CP 3/dsDNA triplex for DNA detection based on conformation change mechanism [89].

2.3.2 Sensing formats of conjugated polymer based chemo/bioassays

This section reviews some chemo/biosensing formats based on fluorescent conjugated polymers/oligomers, mainly focusing on homogeneous assays in solution, heterogeneous assays with a solid support, and CP-based solution assays supported by micro/nanoparticles.

Homogeneous assays in solution

More often, CP-based chemo/bioassays are conducted in homogeneous assays in solution. Compared with the assay format with a solid support, the major advantages of homogeneous assays in solution may include: 1) higher reaction/recognition activity; 2) ease of the operation [28]. A typical example is the superquenching based detection for the avidin protein, which has already given in previous section, ‘Superquenching

mechanism'. However, homogeneous assays in solution based on CP superquenching can be complicated by other events that modulate the CP fluorescence, e.g. non-specific interactions with macromolecules such as proteins [76].

Heterogeneous assays with a solid support

The use of solid support for CP-based chemo/bioassays affords a means of controlling susceptibility to nonspecific interactions and opens the way to the development of practical sensing[76].

One successful example is the report using cationic conjugated polymers (CCPs) from Bazan and coworkers [90]. The authors adopted a solid-state optical detection when the PNA immobilized surface becomes negatively charged upon single-stranded DNA (ssDNA) hybridization, leading to an electrostatic interaction with the CCP (CP 4, structure shown in Figure 2.21). After employing the heterogeneous assay as shown in Figure 2.22, more than one order of magnitude amplification was achieved in emission from a Cy5-labelled ssDNA (shown as ssDNA-C* in Figure 2.22). In addition, optical properties of CP 4 in solid state offer the additional label-free detection capability (Figure 2.23), which may significantly simplify DNA detection methods currently requiring labelled probes or targets. Importantly, this bioassay could be easily incorporated into current fluorescence equipment or process, which should provide operational convenience and simplification as well as reduced costs in testing instrumentation.

4

Figure 2.21 Molecular structure of CP 4 in heterogeneous assay with a solid support [90].

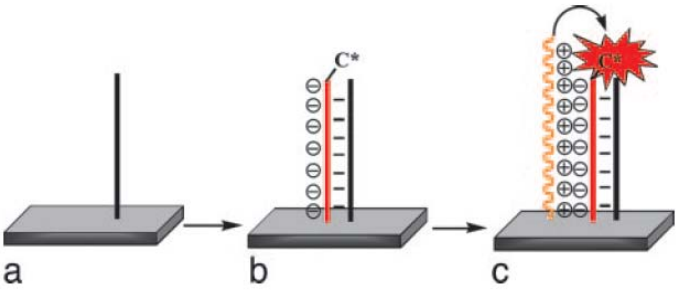

Figure 2.22. DNA assay through FRET on PNA microarray: hybridization of PNA (a) with ssDNA-C* resulting in an increase of negative charge at the surface (b), and electrostatic interactions resulting in CP 4 adsorption and leading to C* signal amplification through FRET (c) [90].

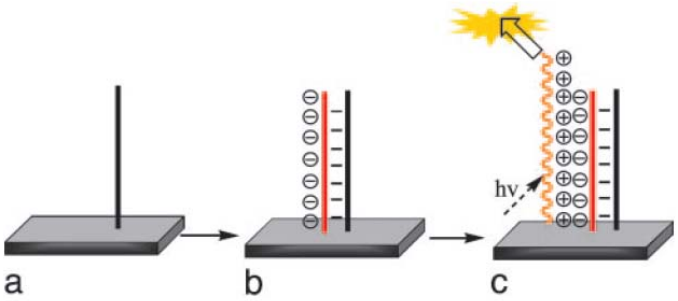

Figure 2.23 Label-free DNA assay on PNA microarray: hybridization of PNA (a) with ssDNA resulting in an increase of negative charge at the surface (b), and electrostatic interactions resulting in adsorption of the CP 4 (c) [90].

Similar strategies were developed for the electrochemical detection of DNA and protein by Leclerc and coworkers [86,92,93], and the detection of the vapor of dinitrotoluene by Whitten and coworkers [77]. Kim and coworkers also developed a strategy to prepare CP-

DNA hybrid chip via a light-directed on-chip oligonucleotide synthesis [94]. Such approaches of incorporating CCPs into solid platforms provide the new option for high-throughput genomics analysis and genetics diagnostics. However, there is a possibility of CP aggregation induced by the solid surface, which leads to CP fluorescence quenching [76]. In addition, recognition/reaction activity in a planar solid surface is poorer than that in the homogeneous solution. Finally, compared with homogeneous solution assays, heterogeneous solid-state assays often need a prolonged processing and supplementary facilities.

Particle-supported format

Considering the above disadvantages of homogeneous solution and heterogeneous solid detection formats, CP-based solution assays supported by micro/nanoparticles have been developed. This intermediate format between solution and solid ones is generally most practical for biosensing [76].

Whitten and coworkers reported that several fluorescent polyelectrolytes can be readily transferred from aqueous solutions to solid supports without substantial quenching of their fluorescence [95]. In this study, CP 5 (see Figure 2.24) can be coated onto commercial cationic polystyrene beads. Polystyrene-supported 5 is quenched by the conjugate of anthraquinone-2,6-disulfonate with biotin ($AQ\text{-}B^-$, $K_{sv} \approx 10^5\ M^{-1}$, structure shown in Figure 2.25), and addition of avidin results in a regeneration of the polymer fluorescence. Addition of avidin to unquenched polystyrene-supported 5 results in no detectable change in emission, and there is no fluorescence recovery when avidin is added to suspensions of

polystyrene-supported 5 that have been quenched by AQ^{2-}. The fluorescence of polystyrene-supported 5 is also quenched by the anionic dye-biotin conjugate ($D\text{-}B^-$, structure shown in Figure 2.25).

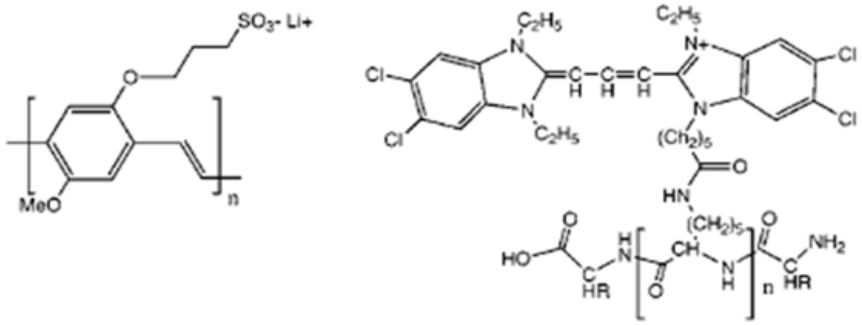

5 **6**

Figure 2.24 Molecular structures of the CP 5 and 6 in particle-supported assay format [95].

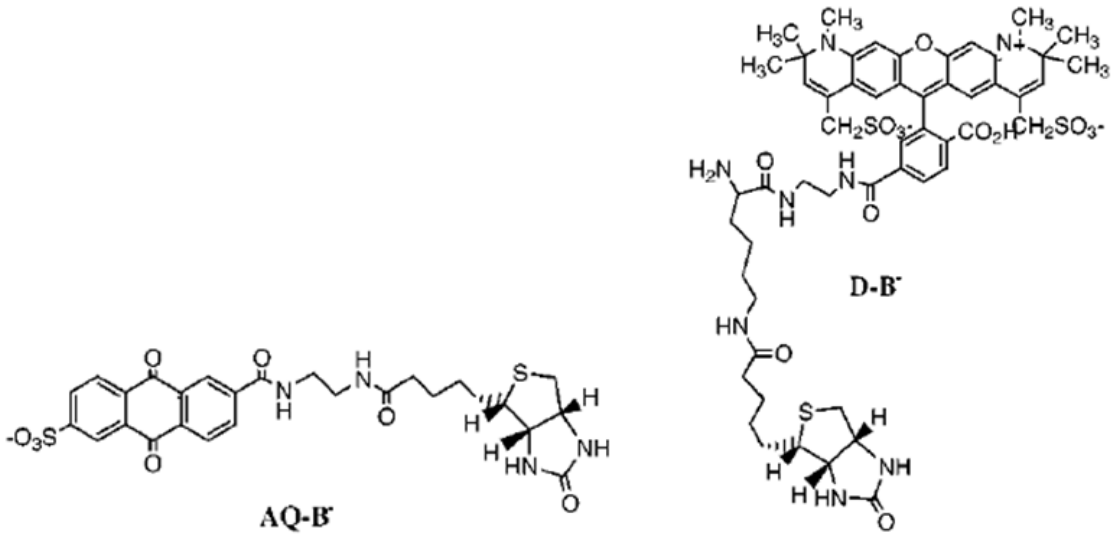

Figure 2.25 Molecular structures of biotin-tethered quencher: $AQ\text{-}B^-$ and $D\text{-}B^-$ [95].

The author further used a combined format to retain the polymer individual behavior. This was done by coating 6 (structure shown in Figure 2.24) onto Laponite clay followed by addition of 5 in aqueous solution, which leads to a mixture showing independent

behavior of the two polymers both with respect to their fluorescence and quenching. The fluorescence of this mixture with no quenchers added is the simple sum of the fluorescence of each polymer individually: no energy transfer quenching is observed. Addition of methyl viologen (MV^{2+}) quenches only 5, while addition of AQ^{2-} to the mixture results in the selective quenching of 6. This result indicates that supported formats may allow simultaneous sensing of different antigens by several different polymers in the same suspension [95].

Recently, particle-supported detection using conjugated polymers has also been reported in other schemes. For instance, Swager and coworkers have coated poly(phenylene ethynylene) films onto silica microspheres and used for sensitive detection of nitroaromatic quenchers [96]. In addition, Schanze and coworker have covalently grafted CP onto microsphere surface, and used the particle-supported format for ion detection [97].

2.3.3 Applications of conjugated polymer and oligomer based optical sensors

This section reviews some optical sensor application of fluorescent conjugated polymers/oligomers, mainly focusing on the detection of mercury(II) and DNA.

2.3.3.1 Detection of mercury(II)

Selective and sensitive determination of heavy metal ions such as mercury(II) is of vital importance due to its application in environmental pollutant treatment. Fluorescent conjugated polymers/oligomers can be used for heavy metal ion detection [26]. Most of these detection methods were conducted in organic solution. Taking the mercury(II) detection for example, Fan et al. reported a PPETE conjugated polymer functionalized

with N,N,N'-trimethylethylenediamino groups and used it for a turn-on Hg^{2+} detection in organic solution [98]. Tang et al. also gave a report on a polythiophene containing thymine moieties for Hg^{2+} detection [99]. Although good performance with high sensitivity and selectivity was achieved in the above studies, this type of detection employed neutral CP and its operation was restricted in organic medium.

In response to the restriction of detection in organic medium, water-soluble CP-based assays have been developed for heavy metal ion detection [26]. For instance, Bunz and coworker developed a mercury(II) assay in aqueous solution using an anionic conjugated polymer (CP 7, structure shown in Figure 2.26), and a papain protein which contained Hg^{2+}-responsive sulfhydryl groups [100]. The assay was based on formation of an electrostatic complex between the CP 7 and papain. The CP 7-papain complex displays the selective fluorescence quenching response only to Hg^{2+} over 9 other control metal ions (i.e., Zn^{2+}, Cd^{2+},Pb^{2+}, Fe^{2+}, Ni^{2+}, Co^{2+}, Cu^{2+}, Ca^{2+} and Mg^{2+}).An agglutination mechanism was proposed to explain the selective assay as show in Figure 2.27. It is known that papain contained Hg^{2+}-responsive sulfhydryl groups. Upon the formation of the CP 7-papain complex, positively charged papain molecules are held together by the negatively charged CP 7 chains, forming a supramolecular structure which is more sensitive towards agglutination than its parts alone. Consequently, after adding Hg^{2+} to the CP 7-papain complex solution, the CP-papain complex will precipitate by cross-linking of the papain molecules through Hg^{2+}, and a non-fluorescent solution were observed. However, the above sensor worked only in the turn-off mode, and small environmental perturbation might affect the detection specificity.

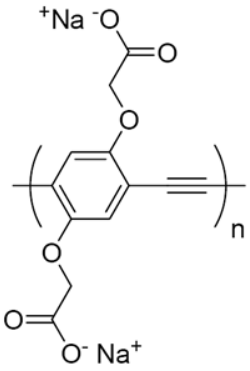

7

Figure 2.26 Molecular structure of CP 7 for Hg^{2+} assay in aqueous medium [100].

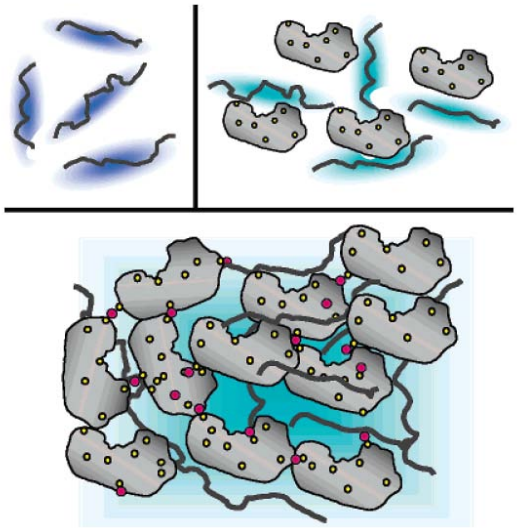

Figure 2.27 Qualitative interpretation of the Hg^{2+}-induced agglutination of the CP 7-papain complex. Top left: CP 7 alone. Top right: electrostatic complex of CP 7 and papain. Bottom: the addition of Hg^{2+} to CP 7-papain complex leads to its precipitation by cross-linking of the papain molecules through Hg^{2+} [100].

Instead of turn-off detection, turn-on assay in aqueous solution was reported by Liu et al. [101]. The authors made use of a cationic conjugated polymer (CP 8, molecular structure shown in Figure 2.28) and a mercury-specific oligonuleotide (MSO) to detect Hg^{2+} in aqueous solution. This MSO has the sequence of 5'-CATTTCTTTCTTCCCCTTGTTTGTTTCA -3' and is mercury-specific. As shown in

the Figure 2.29, in the absence of Hg^{2+} ions, CP 8 and the random coil-like MSO probe readily formed an electrostatic complex in aqueous solution, which rigidified CP 8 to form a planar conformation with a red color. In the presence of Hg^{2+} ions, the MSO probe readily formed a stem-loop structure through the specific thymine-mercury(II)-thymine (T–Hg^{2+}-T) binding, resulting in twisting of the conjugated backbone of CP 8. Consequently, the MSO–CP 8 complex shows color change from red to yellow upon addition of Hg^{2+} due to this conformation change of CP 8. This assay was conducted in a label-free detection style, and achieved the lowest detection limit down to 42 nM for Hg^{2+} with high selectivity relative to other metal ions such as Ca^{2+}, Mg^{2+}, Pb^{2+}, Cu^{2+}, Zn^{2+}, Mn^{2+}, and Co^{2+} ions. Nevertheless, this method employs the format of homogeneous assay in solution, and environmental perturbation may affect its detection selectivity.

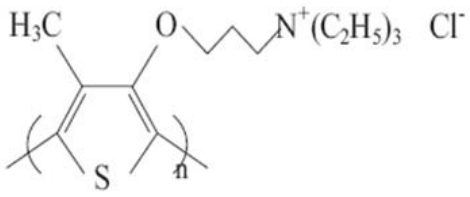

8

Figure 2.28 Molecular structure of CP 8 for Hg^{2+} detection [101].

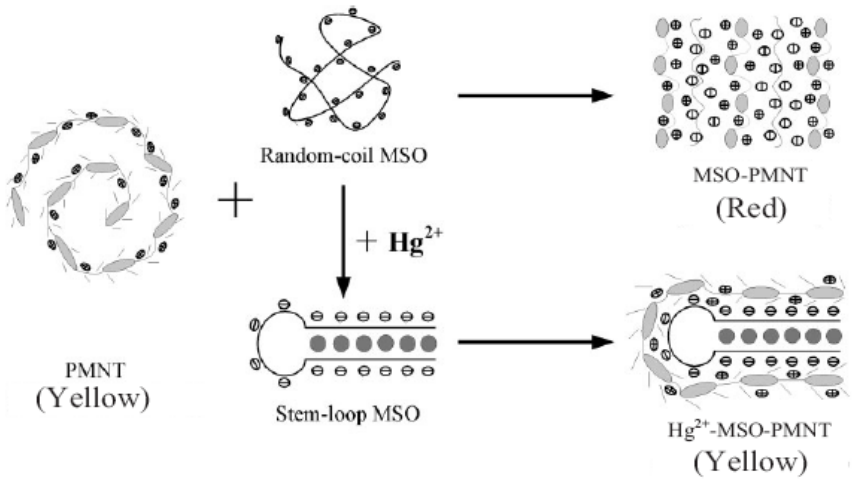

Figure 2.29 Schematic illustration of the optical mercury(II) sensing mechanism, based on a target induced conformational change of MSO oligonucleotide and a resultant optical change of CP 8 [101].

2.3.3.2 Detection of DNA

CP-based DNA detection has been studied extensively and intensively due to the vital application of DNA assays in biomedical research as well as the not-fully explored CP properties [26,75,81,82]. This section reviews some studies on DNA sensing using fluorescent conjugated polymers and oligomers, mainly focusing on the DNA detection based on superquenching mechanism, conformation change mechanism, and FRET mechanism.

DNA sensing based on superquenching mechanism

Superquenching-based sensing has been introduced in the previous section 'superqueching mechanism', using the avidin detection as an example. Nevertheless, this strategy could also be used for DNA detection. Whitten and coworkers developed a superquenching-based detection of DNA coding for the anthrax lethal factor [102]. To conduct the DNA sensing based on superquenching mechanism, the authors employed a

platform in which the biotinylated capture ssDNA and a biotinylated-PPE derivative are co-located on streptavidin-derivatized polystyrene microspheres. Later, the authors further improved the DNA assay by replacing the biotinylated capture DNA with a biotinylated peptide nucleic acid as capture probe, and investigated the assay temperature and resolution of single base-pair mismatches using this detection platform [103].

DNA sensing based on conformation change mechanism

DNA sensing based on conformation change is another important approach, which detection mechanism has been described in the previous section 'conformation change mechanism'. Some improvements of conformation change based DNA assay using PT derivatives have been done after the original discovery in 2002 [89]. To improve the assay operation temperature, Leclerc and coworkers found that the addition of 20% formamide as a denaturant allowed for DNA detection at ambient temperature, which is not possible in the original study [104]. To enhance detection sensitivity, they developed a tailored detection platform incorporating a light-emitting diode (LED) source with a narrow bandwidth for polymer excitation and a photomultiplier tube detector [105]. Meanwhile, the use of 0.3 mM of Triton X-100 was useful to improve the detection limit. Based on these improvements, the author achieved the detection of DNA at zeptomole levlel while retaining single-base mismatch differentiation [105].

DNA sensing based on FRET mechanism

DNA sensing based on FRET is an important approach, which mechanism has been described in the previous section 'Fluorescence resonance energy transfer mechanism' on the pioneering work done by Bazan and coworkers in 2002 [83]. The following section

mainly introduces two major efforts to improve FRET-based DNA assay using PF derivatives: 1) optimization of FRET efficiency for higher detection sensitivity, 2) improvement of assay operation for selectivity enhancement.

1) Optimization of FRET efficiency for higher detection sensitivity

The first major efforts are placed on optimization of FRET efficiency to generate higher signal output for detection sensitivity improvement. The efficiency of CP FRET depends on the distance between the CP and acceptor, orientation of the acceptor relative to the CP, as well as the spectral overlap between the emission of the CP and the absorption of the acceptor according to Förster theory [79]. Therefore, various parameters shown in Förster equation have been modulated by different experimental conditions to generate higher signal amplification.

For example, improved spectral overlap ($J(\lambda)$) between the absorption of a fluorescent dye and the emission band of a cationic conjugated polymer (CCP) has been reported to show improved signal amplification [29]. The distance (r_{DA}) effect has been used to explain more efficient FRET for complementary single-stranded DNA (ssDNA) rather than the noncomplementary when using CCP and the labelled ssDNA probe, where noncomplementary ssDNA partially screens the labelled ssDNA probe from the CP and increases the distance between the donor and acceptor resulting in the reduced FRET efficiency [106]. Thirdly, the effect of orientation (κ) on FRET efficiency was also reported by Bazan and coworkers. The authors found that poor FRET efficiencies between a linear CCP and dsDNA-intercalated ethidium bromide (EB) [107], and fluorescein as a FRET resonance gate from the CCP to the intercalated EB can improve DNA assay

performance. Further studies confirmed that the low FRET efficiency is due to a nonoptimal (orthogonal) orientation between the transition moment of the optically active polymer backbone and that of EB within the dsDNA structure [108]. Meanwhile, the authors also made synthetic entry into CCPs with increased conformational freedom, and they found that shape-adaptable polymers were able to improve FRET efficiency [109]. More recently, Bazan and Liu reported the design and synthesis of a water-soluble cationic conjugated oligomer, i.e. tetrahedralfluorene (9, structure shown in Figure 2.30) [110]. Compared with a cationic CP with similar repeat units, the 9 shows improved FRET efficiencies to dsDNA-Fl as well as improved selectivity between dsDNA and ssDNA. This improvement is ascribed to non-linear shape and spatial registry of 9, which is able to provide multiple-transition dipole moment orientations relative to that of rigid one-dimensional polymer backbone, and makes 9 very efficient energy donors for intercalated EB.

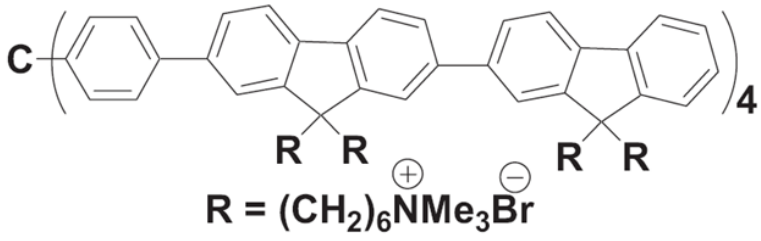

9

Figure 2.30 Molecular structure of the cationic tetrahedralfluorene in DNA sensing based on FRET mechanism[110].

Besides the modulation efforts based on Förster equation to improve FRET efficiency, photoinduced charge transfer (PCT), a detrimental process for FRET assays with a reduced intensity of reporter signal, is also received considerable attention [91]. The competition between FRET and PCT processes is determined by the molecular orbital

energy level alignment between CP (i.e. donor) and chromophore (i.e. acceptor/quencher), as shown in Figure 2.16 [80].

The first report addressing the molecular orbital energy level to improve CCP FRET-based DNA sensing is from Bazan and Liu in 2006 [80]. In this study, the authors designed and synthesized a series of cationic PF derivatives (CP 10, 11, and 12 with their structures shown in Figure 2.31) to probe the effect of the donor/acceptor orbital energy levels on FRET efficiency. Fluorescein-(Fl) or Texas Red-(TR) labelled ssDNA were chosen as the energy acceptor in this study. The molecular orbital energy levels of CP 10-12 were estimated by cyclic voltammetry coupled with optical measurements. The calculated highest occupied molecular orbital (HOMO) and lowest unoccupied molecular orbital (LUMO) levels are (−5.6 and −2.8 eV) for 10, (−5.4 and 2.6 eV) for 11, (−5.8 and −2.7 eV) for 12, respectively. The LUMO energy of Fl (−3.6 eV) is within the band gap of polymers 10–12. However, the HOMO energy of Fl (−5.9 eV) is lower than that of 10 (−5.6 eV), 11 (−5.4 eV). As a result, PCT process could occur between CP (10 or 11) and Fl, and to a less extent between 12 and Fl. The HOMO energy of TR (−5.4 eV) is higher than that of 10 and 12, but is close to that of 11. The FRET experimental results indicate the effect of donor/acceptor orbital energy levels on FRET efficiency. The most intense Fl emission was obtained for 12/ssDNA-Fl, which is approximately two-fold higher than that for 10/ssDNA-Fl and is over an order of magnitude higher than that for 11/ssDNA-Fl. This high FRET sensitized signal is due to the matched donor/acceptor orbital energy levels, which favors FRET between 12 and Fl. In addition, the authors found that the TR emission with 11/ssDNA-TR is more intense than the Fl emission with 11/ssDNA-Fl,

despite the less effective spectral overlap ($J(\lambda)$) between 11 and TR relative to that between 11 and Fl. This is due to a better-matched energy levels between 11 and TR than that between 11 and F1. This study demonstrated that the energy level alignment between the donor and acceptor plays a significant role in generating the CP FRET sensitized dye emission [80].

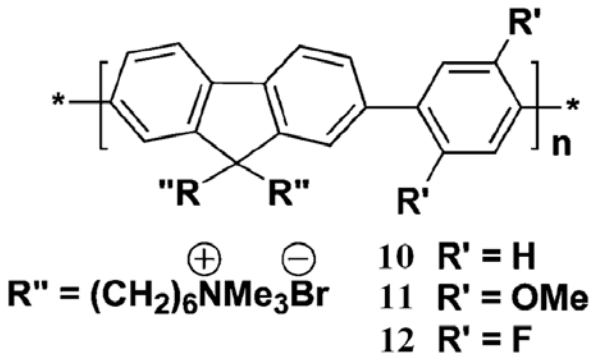

Figure 2.31 Molecular structures of the CPs (CP 10-12) used in DNA sensing based on FRET mechanism [80].

Apart from the concern on molecular orbital energy level alignment, Bazan and coworkers further revealed the importance of the CP molecular structure which can affect the contribution of FRET and PCT to the sensitized dye emission, and suitable molecular design that fine-tune distances at subnanoscale levels is worthy of consideration to favor FRET against quenching by PCT [111].

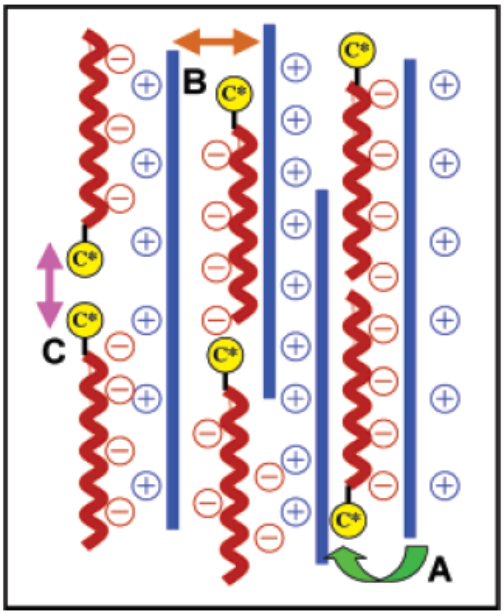

Figure 2.32 Major interactions within CCP/DNA-C* complexes that influence optical performance [80].

Meanwhile, attention should also be paid to the fluorescence quenching of the CP or the acceptor dye within the FRET pair complexes [80]. As shown in Figure 2.32, within CCP/DNA-chromophore (C*) complexes, there are cross interaction between CCP and C* and self-interaction among C* or CCPs. Close association between CCP and DNA-C* (A in Figure 2.32) favors FRET. However, self-interaction among CCPs (B in Figure 2.32) leads to polymer aggregation and reduces the polymer quantum yield in solution. Self-interaction among C* (C in Figure 2.32) causes dye fluorescence quenching and ultimately leading to reduced signal amplification. This viewpoint has been used to explain higher CCP-sensitized C^* emission from a variety of approaches [82], such as the reduction of CCP charge density which minimizes dye fluorescence quenching within the CCP/DNA-C^* complexes [112].

2) Improvement of assay operation for selectivity enhancement

The second major efforts are simultaneously placed on selectivity improvements by optimizing assay operation conditions. Compared with the use of ssDNA-C* probe in FRET-based assay to differentiate complementary ssDNA from noncomplementary ssDNA, various improved approaches have been developed such as the use of neutral ssPNA-C* probe [83], EB with Fl as FRET resonance gate [107], and EB with shape-adaptable polymers [109] or tetrahedralfluorene [110]. Nevertheless, few report on single-nucleotide polymorphisms (SNP)-level discrimination in FRET-based DNA sensing.

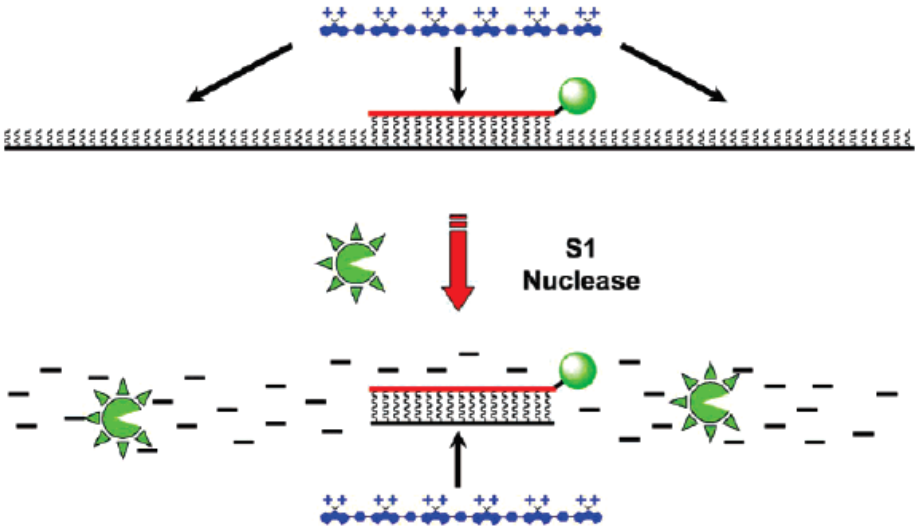

Figure 2.33 Long ssDNA target sequences are digested by S1 nuclease, leaving intact only those regions bound to the PNA-Fl probe. CP 10 (shown in the top of the figure) added directly to the resulting solutions can only associate with the remaining PNA-Fl/DNA duplex. Any PNA/DNA mismatches will result in complete DNA digestion; therefore, energy transfer from the CP 10 occurs only for the perfect PNA-Fl/DNA complement [113].

SNP-level DNA differentiation was first reported by Bazan and co-workers after the introduction of S1 nuclease enzyme into FRET-based DNA sensing in 2005 [113]. As shown in Figure 2.33, the assay starts with the recognition by sequence-specific

hybridization between the neutral PNA-Fl probe and the ssDNA sequence. Addition of S1 nuclease leads to digest all unbound ssDNA after PNA/ssDNA annealing, and therefore increases the detection selectivity. The combination of S1 nuclease enzyme and the CP 10/PNA design enable the assay capable of differentiating the normal, wild-type human DNA sequences from those sequences containing a single-base mutation. Using similar enzyme digestion strategy with CCP as signal amplifier and PNA as the probe, Liu and coworker further developed a label-free SNP DNA assay after introduction of an intercalation dye in homogeneous solution [114]. On the other hand, particle-supported format has been introduced into FRET-based DNA sensing to improve the detection selectivity [115]. In this study, Fan and coworkers adopted magnetic microsphere as a support to detect target DNA followed by CP signal amplification, and achieved SNP-level DNA detection [115].

Besides the above mentioned DNA sensing based on superquenching mechanism, conformation change mechanism, and FRET mechanism, other research efforts have also been made from different approaches. For example, Leclerc and co-workers developed a combined sensing strategy incorporating conformation change mechanism and FRET mechanism, and achieved a DNA detection as low as 3 zM target DNA with mismatched DNA discrimination [116]. In addition, to apply CP to DNA assays in real samples such as blood or serum, covalent bioconjugation of recognition element to PPE derivatives have been developed by Tan and coworkers [117], and Kim and coworkers [118].

2.3.3.3. Other application

Besides the above mercury(II) and DNA detection in our previous review sections, CP-based chemo/biosensing have been developed for other applications such as the detection of Pd[26 119], human a-thrombin [120], protease [121], kinase [122], phosphatase [122], Concanavalin A [123], and bacteria [124]. With further exploration and understanding of CP materials, CP-based chemo/biosensing will make a fast and great progress.

CHAPTER 3

SYNTHESIS AND CHARACTERIZATION OF SILICA AND SILVER NANOPARTICLES

3.1 Introduction

As discussed in the section of nanoparticle-based detection in Chapter 2, novel detection systems based on nanostructure features can be highly specific and extremely sensitive when combined with appropriate signal transduction and amplification mechanisms. In this thesis, silica NPs and silver NPs are chosen as the building blocks for the construction of CP-based nanoplatforms in chemo/biosensing. This is due to the unique properties of the selected nanomaterials for CP-based optical sensors.

Silica NPs (100 nm in diameter) are transparent in dilute solutions and their optical properties do not interfere with fluorescent conjugated polymers and oligomers. Silica materials have versatile bioconjugation methods [125], and their NP suspension provides a nearly homogeneous environment that facilitates DNA immobilization and hybridization. As a solid-state system, silica NP-supported assay enables the separation of specific binding from non-specific interactions to improve detection performance. As a result, the use of silica NPs as the solid support for CP-based DNA assay is first considered. Secondly, silver NPs have been known as their surface plasmonic effect for various

applications such surface enhanced Raman scattering (SERS) and metal-enhanced fluorescence (MEF) [24,53]. To investigate the MEF of a CP (PFBT) for DNA detection, a suitable choice is the use of silver NPs (~75 nm) since good plasmonic coupling between silver NPs and PFBT can occur, and this coupling has been regarded as a key contribution to MEF [24,53]. In this sense, silver NPs are preferred. Therefore, the synthesis of both silica and silver NPs are considered.

To prepare the NPs, simple and convenient synthesis methods are preferred for our purpose. Silica NP synthesis methods have been well documented in the literature such as Stöber method [126] and microemulsion method [127]. Due to the simplicity of synthesis, Stöber method in which silica NPs are formed in water-alcohol medium through a polymerization and condensation of tetraethoxysilane (TEOS) using ammonia as the catalyst, was chosen to prepare the NPs with slight modification. For the silver NP synthesis, a variety of methods are also available such as Lee–Meisel method [128], photo-reduction by laser irradiation [129], and laser ablation of bulk metal [130]. Considering the simplicity of synthesis, Lee–Meisel method [128] in which silver NPs are produced in aqueous medium through reduction of silver nitrate by sodium citrate, was used to synthesize the NPs with slight modification. In Chapter 3, the synthesis and characterization of both silica and silver NPs will be described in detail.

3.2 Materials and methods

3.2.1 Preparation and characterization of silica nanoparticle

Materials

Tetraethoxysilane (TEOS, 98%, Fluka), ethanol (99.9%, Merck), ammonia solution (30%Wt, SINO Chemical Company). MilliQ water (18.2 MΩ) was used to prepare all solutions.

Characterization

The synthesized silica NPs were imaged using a field-emission scanning electron microscope (FE-SEM JEOL JSM-6700 F) after coating a thin Pt layer (~5 nm in thickness) via a platinum coater (JEOL JFC-1300, Auto Fine Coater). A polished copper tape was used as the supporting substrate for the silica NP imaging.

Synthesis of silica NPs

Silica NPs were synthesized using a modified Stöber method [126]. An amount of 1.5 mL of TEOS dissolved in 15.24 mL of ethanol was added rapidly to a mixture of 6.37 mL of ethanol, 10.05 mL of Milli-Q water and 0.32 mL of 30% ammonia while vigorously stirring. The mixture was further stirred at room temperature for 8 h and the NPs in solution had an average size of ~55 nm by analyzing the samples under FE-SEM. An amount of 4.5 mL of the as-prepared NP suspension was diluted with 5.08 mL of ethanol and 0.27 mL of 30% ammonia. Another 1.84 mL of TEOS in 9.20 mL of ethanol was added dropwise into the diluted NP suspension. The mixture was stirred at room temperature for 6 h. The obtained NPs were centrifuged and washed with ethanol and

MilliQ water. In between the washing steps, the NPs were re-dispersed into the solutions by ultrasonication. The purified NPs were dispersed in MilliQ water and stored at 4°C for further use.

3.2.2 Preparation and characterization of silver nanoparticle

Materials

Silver nitrate (sigma-aldrich, reagent plus, >99.8%), sodium citrate tribasic dihydrate (sigma, ACS reagent, ⩾99.0%). MilliQ water (18.2 MΩ) was used to prepare all solutions.

Characterization and instrumentation

The extinction spectrum of silver NPs in MilliQ water was measured by Shimadzu UV-1700 spectrometer, and corrected after subtraction of the corresponding background. The prepared silver NPs were characterized by field-emission scanning electron microscopy (FE-SEM) on a JEOL JSM-6700F operating at 5 kV, and by transmission electron microscopy (TEM) on a JEOL JEM-2010F operating at 200 kV. The silver ion concentration was determined by inductively coupled plasma-mass spectroscopy (ICP-MS, Agilent 7500A).

Silver NP synthesis in aqueous solution

The silver NPs were synthesized by citrate reduction using a modified Lee–Meisel method [128]. All glassware and stir bars used in synthesis were thoroughly cleaned in aqua regia (HCl: HNO_3 = 3:1), rinsed with MilliQ water and oven-dried prior to use. The stock

solutions of silver nitrate (10.8 mg/mL) and sodium citrate tribasic dihydrate (22.8 mg/mL) were prepared in advance and stored in the dark. Other solutions were made freshly as needed. During preparation of the silver colloid, 1 mL of silver nitrate stock solution (10.8 mg/mL) was first diluted with 28.55 mL of MillQ water, and the resulting solution was brought to boil with vigorous stirring (700 rpm) in a 50 mL two-neck round-bottom flask with a condenser. 0.45 mL of sodium citrate solution (22.8 mg/mL) was added dropwise into the reaction solution (45 µL/12 seconds). Boiling was continued for ~40 mins before an icy bath was used to quench the whole reaction with vigorous stirring. The resulting colloidal solution had a maximum extinction peak at ~ 440 nm. The synthesized silver colloid was initially filtered with 0.22 µm filter. After centrifugation at 2000 g for 40 min, the supernatant was removed thoroughly from the silver NP precipitates, and the silver precipitates were redispersed in MilliQ water followed by the filtration with 0.22 µm filter. The obtained silver colloid was covered with Al-foil and stored in a 4 °C refrigerator. The silver ion concentration in the above silver colloid was estimated at ~193 ppm by ICP-MS after dissolving the silver NPs by aqua regia, while the silver NPs show an extinction maximum ~0.0552 @ 440 nm for 4 µL stock/800 µL water by UV/Vis measurement. Field-emission scanning electron microscopy (FE-SEM) showed that the obtained particles have an average size of ~75 nm.

3.3 Results and discussion

3.3.1 Synthesis and characterization of silica nanoparticles

Bare silica nanoparticles (NPs) were synthesized using a modified Stöber method via a seed-mediated growth process [126]. A two-step method was conducted during this process. A polymerization and condensation of TEOS using ammonia as a catalyst lead to silica NP seeds, which have a small size ~55 nm in diameter as shown in Figure 3.1. After further growth based on these NP seeds, the size of silica NPs increases to ~100 nm in average. These final NPs have a uniform and spherical shape, as well as a narrow size distribution (polydispersity (δ/D): ~5% based on calculating 150 NPs), as shown in Figure 3.2. The synthesized silica NPs have negative charged hydroxyl group on their surface arising from original synthesis stage. These negative charges enable silica NPs separate from each other by repulsive force, and keep them stable in aqueous solution (see the well-dispersed silica NPs in the Figure 3.3).

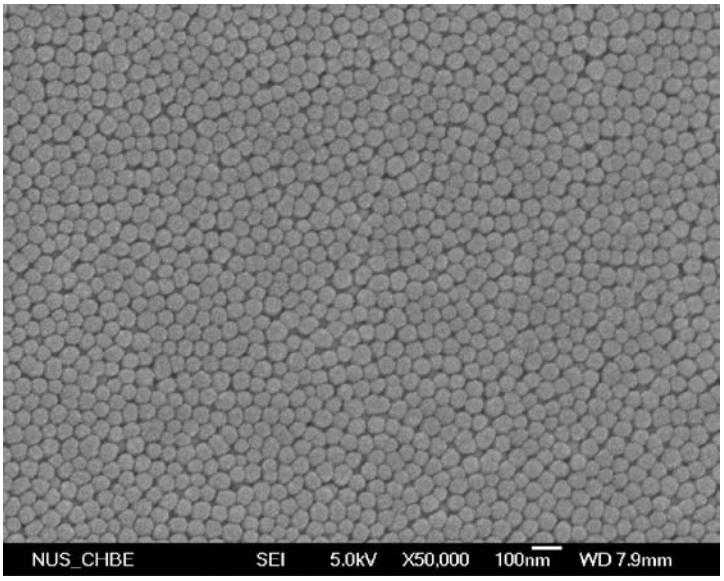

Figure 3.1 FE-SEM image of the synthesized silica nanoparticle (NP) seeds in the closely packed form after coating a thin conductive Pt layer (~5 nm in thickness) via a platinum coater. The average diameter of the seed silica NPs is ~55 nm.

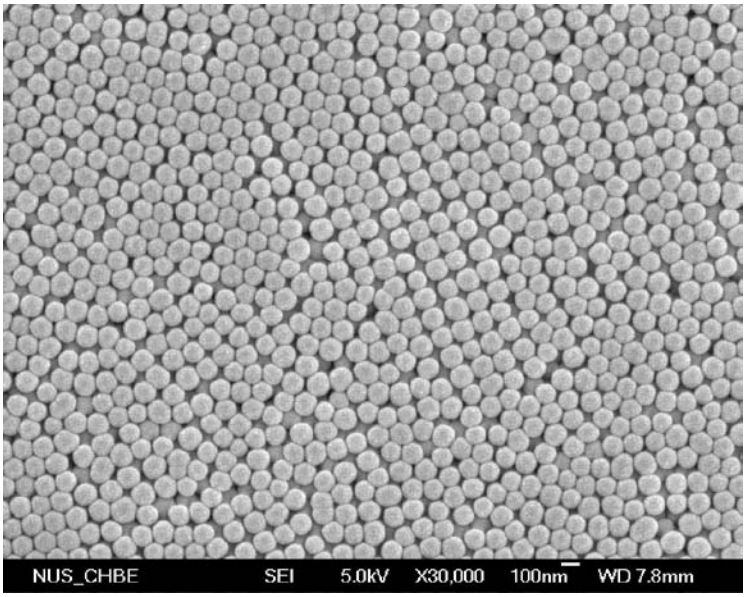

Figure 3.2 FE-SEM image of the synthesized final silica NPs in the closely packed form after coating a thin conductive Pt layer (~5 nm in thickness) via a platinum coater. The average diameter of the final silica NPs is ~100 nm.

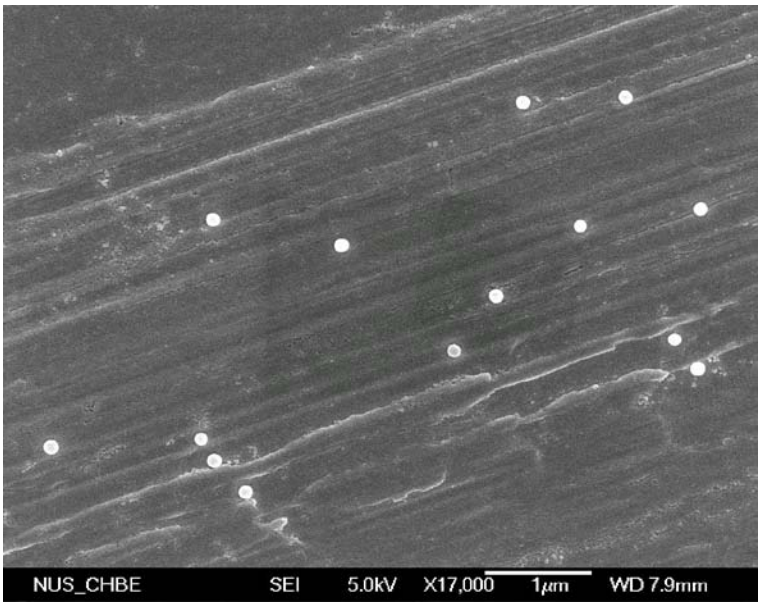

Figure 3.3 FE-SEM image of well-dispersed final silica NPs after coating a thin conductive Pt layer (~5 nm in thickness) via a platinum coater. The average diameter of the final silica NPs is ~100 nm.

3.3.2 Synthesis and characterization of silver nanoparticles

The silver NPs were synthesized by citrate reduction using a modified Lee–Meisel method [128]. After purification by centrifugation and filtration, the collected silver NPs have a size of ~75 nm in average, as shown in Figure 3.4 and Figure 3.5. FE-SEM images from Figure 3.4 show that the synthesized silver NPs have irregular shapes, and the TEM images in Figure 3.5 confirm that the silver NPs are composed of irregular polycrystalline structures. UV/Vis spectrum shows that the silver NPs have an extinction maximum wavelength at ~440 nm (see Figure 3.6). These synthesized silver NPs bear negative charges on their surface due to the absorbed citrate molecules during the NP synthesis stage. These negative charges enable repulsive force between silver NPs and make them quite stable in aqueous medium (see the well-dispersed silver NPs in the inset of Figure 3.4).

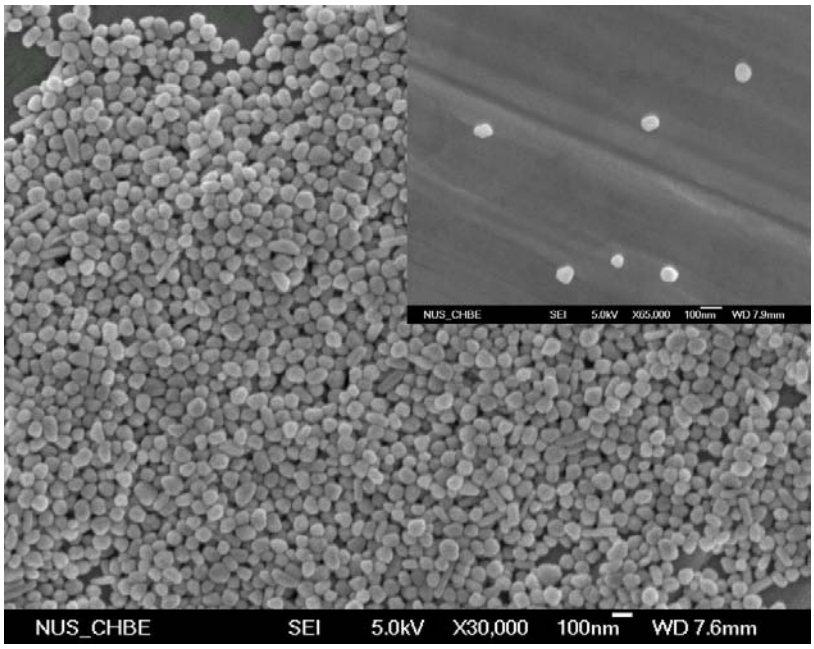

Figure 3.4 FE-SEM images of the synthesized silver NPs. The inset shows the well-dispersed silver NPs.

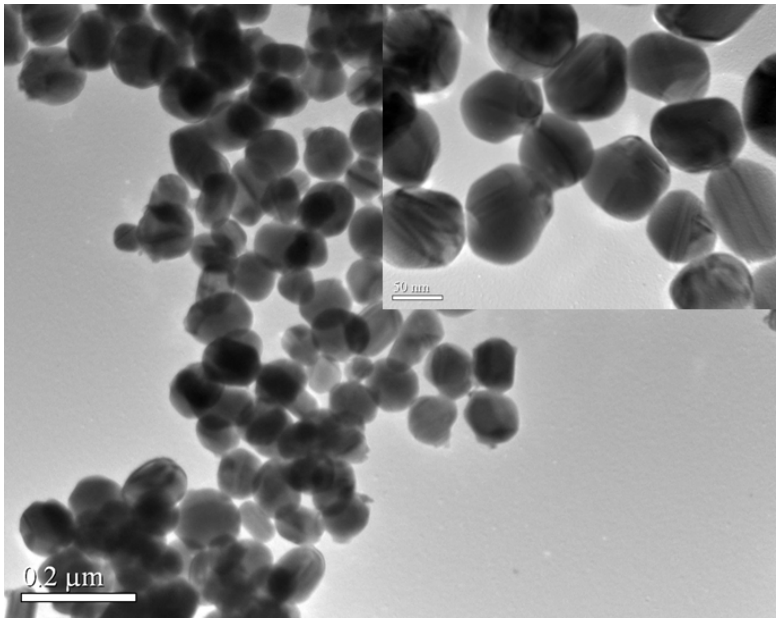

Figure 3.5 TEM images of the synthesized silver NPs. The inset shows the silver NPs in high magnification.

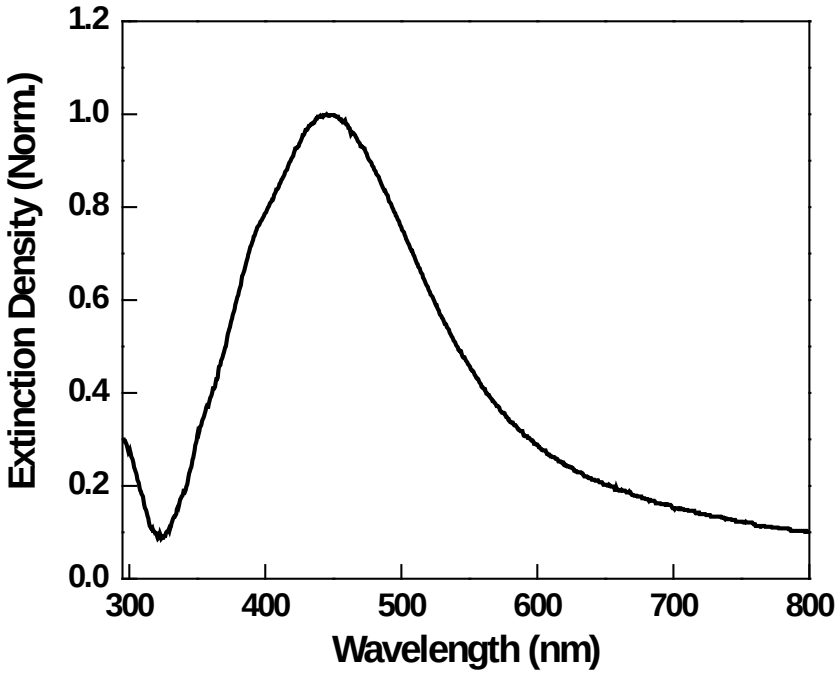

Figure 3.6 The extinction spectrum of the synthesized silver NPs in MilliQ water.

3.4 Conclusions

In Chapter 3, we describe the synthesis and characterization of two types of nanoparticles, namely silica NPs and silver NPs. Silica NPs with a diameter of ~100 nm in average were synthesized via a seed-mediated growth process by polymerization and condensation of TEOS catalyzed by ammonia. FE-SEM confirms that these prepared silica NPs have uniform spherical shape with a narrow size distribution. Meanwhile, silver NPs were synthesized by citrate reduction in aqueous medium. FE-SEM and TEM confirm the formation of silver NPs with a size of ~75 nm in average, and UV/Vis spectrometer shows that the silver NPs have an extinction maximum wavelength at ~440 nm. These prepared nanomaterials will constitute the elements of nanoplatform for the applications of CP/oligomer based chemo/biosensing.

CHAPTER 4

SILICA NANOPARTICLE-SUPPORTED DNA ASSAYS FOR OPTICAL SIGNAL AMPLIFICATION OF CONJUGATED POLYMER BASED FLUORESCENT SENSORS

4.1 Introduction

Methods for real-time, highly selective and sensitive polynucleotide detection are of vast scientific and economic importance because of their wide applications in identification of numerous biological pathogens and environmental contaminants [131,132]. Many DNA detection assays have been developed using different principles [133], such as fluorescence [10,11,134], electrochemical [135,136], microgravimetric [137,138], enzymatic [139], electroluminescence [140], and recently nanostructure based methods [41,141]. In general, the detection is constrained or limited by the levels of targets available in a particular sample. One has to rely on enzymatic sample replication (polymerase chain reaction) to increase the concentration of specific nucleic sequences to detectable levels or turn to complex labelling steps (dye multiplicity) or enhanced optical (or instrumentation) systems [142,143]. Such remedies are often reagent and instrumentation intensive, inciting higher levels of complexity and cost.

The unique optoelectronic properties of conjugated polymers (CPs) make them useful light-harvesting antennae for signal amplification in DNA sensor applications [89,144,145]. Their delocalized structure allows for electronic coupling between optoelectronic segments and efficient intra- and interchain energy transfer [25,29]. One specific approach that improves the sensitivity of homogeneous fluorescent DNA assays involves using a cationic conjugated polymer (CCP) and a chromophore (C*) labelled probe (*e.g.* DNA-C* or PNA-C*), which are selected to favor fluorescence resonance energy transfer (FRET) from the CCP to C* [28,83,106]. In addition to the factors such as spectral overlap, orientation and distance, recent studies reveal that the C* self-quenching upon CCP–DNA-C* complex formation and the mismatched energy levels between CCP and C* also affect the signal amplification [80]. Although this strategy has been proved successful for strand specific detection of DNA and RNA in aqueous media [28,83,106], high selectivity is only observed with PNA-C* as the probe [83]. Replacement of PNA-C* with DNA-C* leads to reduced selectivity as a result of the strong Coulomb attraction between the CCP and the negatively charged DNA probe [28,106].

Nanoparticle(NP)-based assays possess the advantage of solid-state sensors, allow the separation of specific binding from nonspecific interactions to improve assay selectivity [115], and have been applied to a wide variety of biological applications [96,115,146]. Among various nanomaterials, silica NPs (100 nm in diameter) are transparent in dilute solutions and their optical properties do not interfere with fluorescent conjugated polymers and oligomers. Silica materials also have versatile bioconjugation methods, and their NP suspension provides a nearly homogeneous environment that facilitates DNA

immobilization and hybridization. In this context, incorporation of the CP FRET assay into a silica NP-supported format would provide a favorable condition to improve the detection selectivity of CP-based homogeneous DNA assay while maintaining the advantages of CP signal amplification. In Chapter 4, we report a new strategy of using probe-immobilized silica NPs in conjunction with a CCP (PFP-2F, structure shown in Scheme 4.1) to simultaneously achieve high sensitive and selective DNA detection. Importantly, instead of fluorescence quenching of CPs on the particle surface [96], CP fluorescence signal amplification on NP-supported format was first investigated for sensitive DNA assay.

4.2 Materials and methods

General

The UV-Vis absorption spectra were recorded on a Shimadzu UV-1700 spectrometer. Fluorescence was measured using a Perkin Elmer LS-55 equipped with a xenon lamp excitation source and a Hamamatsu (Japan) 928 PMT, using 90 degree angle detection for solution samples. The NPs are imaged using a field-emission scanning electron microscope (FE-SEM JEOL JSM-6700 F) after coating a thin conductive Pt layer (~5 nm in thickness).

Materials

DNA oligonucleotides are ordered from Research Biolabs, Singapore. Tetraethoxysilane (98%, Fluka), ethanol (99.9%, Merck), ammonia solution (30%Wt, SINO Chemical Company), 3-aminopropyl triethoxysilane (99%, Aldrich), Sodium Chloride (99.5%,

Merck), Tween 20 (Aldrich), acetonitrile (anhydrous 99.8+%, Alfa Aesar), 2,4,6-trichloro-1,3,5-triazine (98%, Alfa Aesar), boric acid (99+%， Alfa Aesar), sodium tetraborate decahydrate (99+%，Alfa Aesar), and 10× phosphate buffer saline (ultrapure grade, 1st BASE) are commercial products and are used as received without further purification. MilliQ Water (18.2 Ω) was used to prepare all the buffers. The conjugated polymer, poly[9,9'-bis(6''-*N,N,N*-trimethylammonium)-hexyl)fluorene-*co*-*alt*-2,5-difluoro-1,4-phenylene) dibromide] (PFP-2F), was synthesized according to the procedures reported previously [80].

Synthesis and surface functionalization of silica NPs

The bare silica NPs were synthesized according to the procedure described in Chapter 3. After that, 3-amino-propyl-trimethoxysilane (140 μL) was added to the bare silica NPs (6.4 mg) in ethanol (1 mL). The mixture was stirred at room temperature for 2 h. It was followed by heating at 50 Celsius degree (˚C) for additional 1 h. After centrifugation and washing with ethanol (8×) and acetonitrile (5×), the NPs were further reacted with 2,4,6-trichloro-1,3,5-triazine (38.4 mg) in acetonitrile (1 mL) at room temperature for 2 h [147]. The surface activated NPs were centrifuged and washed with acetonitrile (3×), ethanol (1×), MilliQ water (4×), and borate buffer (3×).

5'-amine modified oligonucleotide (5'-NH_2-AGCACCCACATAGTCAAGAT-3', 25 μL of 100 μM) was added to the activated NPs (3.2 mg) in borate buffer (85μL, pH = 8.5), and the mixture was slightly votexed at room temperature for 16 h. The obtained NPs

were centrifuged and washed with MilliQ water (3×) to remove the free DNA. The supernatant was collected for UV/Vis absorbance measurement.

Hybridization of DNA-immobilized NPs

The probe immobilized NPs were washed twice with PBST buffer (137 mM NaCl, 2.7 mM KCl, 10 mM phosphate and 0.1% Tween 20) before hybridization. Different amount of fluorescein (Fl) labelled target DNA (DNA_T: 5′-Fl-ATCTTGACTATGTGGGTGCT-3′) was mixed with NP (1.6 mg) in PBST buffer and the total volume was adjusted to 100 uL. The mixture was shaken at room temperature for 2 h. The solution was centrifuged and the residue was thoroughly washed with PBST buffer (5×). Finally the nanoparticles were dispersed in ~100 μL PBST buffer. The supernatant was kept for fluorescence analysis.

Base mismatch detection with salt washing

15 μL (100 μM) of a DNA_T, a two-base mismatched sequence (5′-Fl-ATCTTGACTTTCTGGGTGCT-3′) and a random sequence (5′-Fl-CGTACGTACGTACGTACGTA-3′) were added separately to three probe-immobilized NP (0.2 mg) solutions in PBST buffer (85 μL), and shaken at room temperature for 2 h. After that, the resulting mixture was centrifuged and the residue was thoroughly washed with PBST buffer (4×). The collected NPs were further washed with a diluted PBST buffer (10 mM NaCl in 10 mM phosphate buffer, 0.1% Tween 20) for additional four times before FRET test.

FRET experiments and analysis

To study the effect of DNA strands/NP on FRET, the hybridized NPs (0.2 mg) were dispersed in PBST buffer (2 mL) in a quartz cuvette. Before CCP addition, the solution fluorescence was measured upon excitation at 490 nm. Different volumes of CCP at a [CCP] = 100 μM (CCP concentrations were based on CCP repeat unit) were then added to each NP solution, where 38 μL for $7DNA_T$/NP, 40 μL for $24DNA_T$/NP and 42 μL for $56DNA_T$/NP were used to maintain a charge ratio of +/- close to 3. The emission spectra were collected upon excitation of the CCP at 370 nm. Fl emission was also monitored upon excitation at 490 nm in the presence of CCP. For all the Fl emission spectra, the background emission and the polymer emission tail were subtracted.

4.3 Results and discussion

4.3.1 Strategy for the CP-assisted NP-supported DNA assay

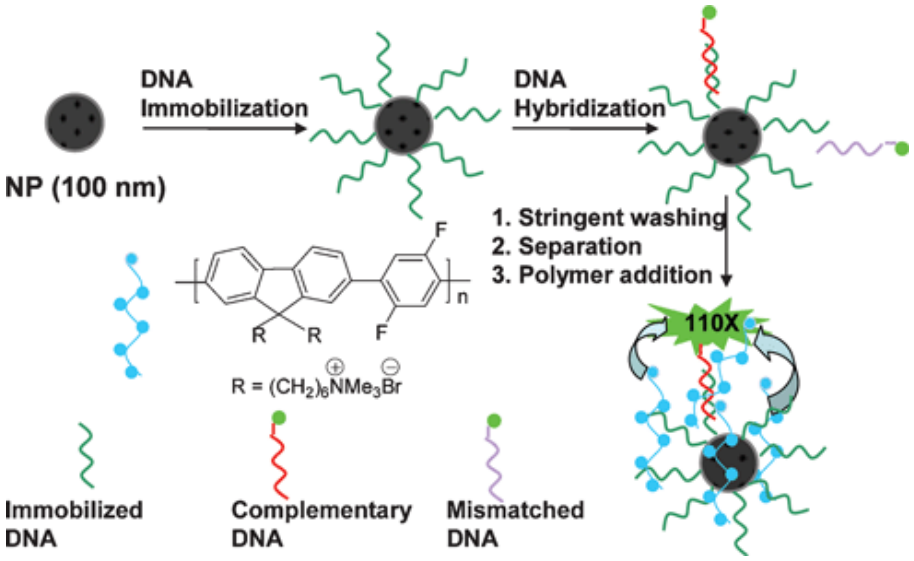

Scheme 4.1 Schematic illustration of NP-supported DNA assay using CCPs as signal amplifiers.

Scheme 4.1 was designed to take advantage of the optical amplification of CCPs and easy separation of NPs for sensitive and selective DNA detection. The approach begins with probe-immobilized NPs in solution. If the added DNA-C* is complementary to the probe, the probe-immobilized NPs can capture the target and bring C* close to the NP surface. In the absence of the complementary sequence, no C* will be attracted to the NPs after salt washing and separation steps. Only when the complementary sequence is present in the initial solution will CCP (donor) and C* (acceptor) be present in the final mixture, allowing intense acceptor emission upon CCP excitation.

The CCP, poly[9,9'-bis(6''-*N*,*N*,*N*-trimethylammonium)-hexyl)fluorene-*co*-*alt*-2,5-difluoro-1,4-phenylene) dibromide] (PFP-2F, structure shown in Scheme 4.1), and C* (Fluorescein: Fl) used in this study were selected to have matched molecular orbital energy level. According to recent reports [80,91], mismatched molecular orbital energy levels can lead to photoinduced electron transfer (PCT), which competes with the FRET process resulting in a reduced intensity of reporter signal. To get better FRET efficiency, matched orbital energy levels is important to against PCT for higher detection sensitivity. The use of PFP-2F and Fl as FRET pair has been found to satisfy this condition [80]. In other words, to get highest FRET signal output, the FRET pair (PFP-2F as the energy donor and Fl as the energy acceptor) is better than other FRET pairs. Therefore, we choose the FRET pair (PFP-2F and Fl) in this study. On the other hand, silica NPs in the 100 nm size range were selected since they are transparent in dilute solutions and their optical properties do not interfere with conjugated polymers. Moreover, particle-supported FRET assay allows the separation of specific binding from non-specific

interactions to improve detection selectivity [115]. In this context, incorporation of the PFP-2F/Fl FRET pair into a NP-supported assay should provide a favorable condition for sensitive and selective DNA detection. This consideration constitutes the guideline for our DNA assay strategy development.

4.3.2 Synthesis and surface functionalization of silica nanoparticles

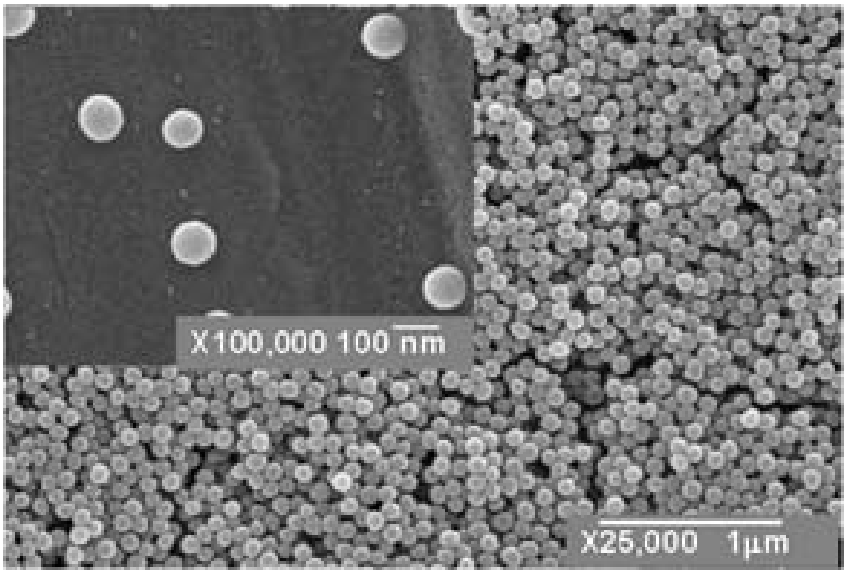

Figure 4.1 FE-SEM images of the synthesized silica nanoparticles. Inset: probe-immobilized silica nanoparticles.

The bare silica NPs were synthesized according to the procedure described in Chapter 3. After surface modification with (3-aminopropyl)trimethoxysilane, followed by activation with 2,4,6-trichloro-1,3,5-triazine, the modified NPs were reacted with amino labelled synthetic oligonucleotide (5′-NH_2-AGCACCCACATAGTCAAGAT-3′). After purification, the average number of DNA probes on each NP was calculated to be ~400 based on the UV absorbance measurement. Field-emission scanning electron microscope

(FE-SEM) images showed that the NPs before and after DNA immobilization are spherical in shape with an average size of ~100 nm (Figure 4.1).

4.3.3 Signal amplification dependent on number of Fl-DNA per NP

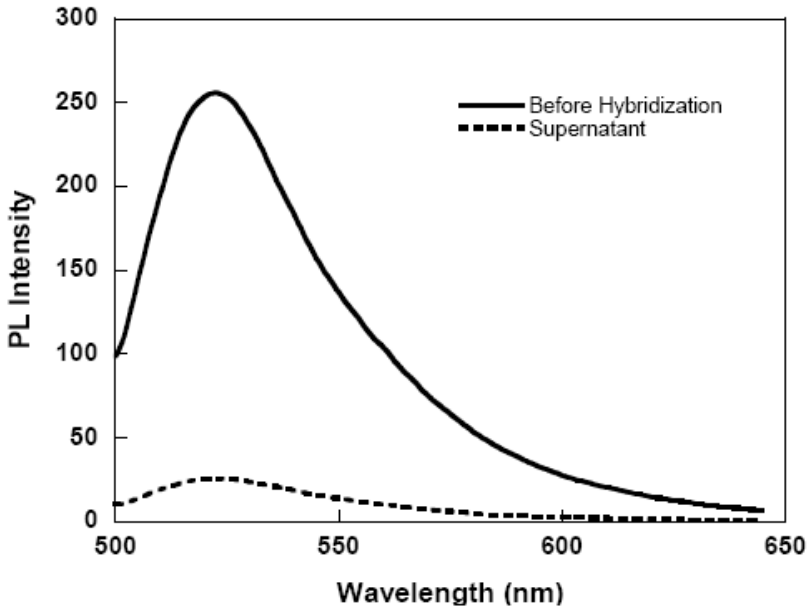

Figure 4.2 The emission spectra of DNA_T solution (0.18 μM) before hybridization and the supernatant (after hybridization and NP removal) with NPs (0.1 mg/mL).

Hybridization of probe-immobilized NPs (1.6 mg per 100 μL) with Fl labelled target DNA (DNA_T: 5′-Fl-ATCTTGACTATGTGGGTGCT-3′) of varying concentrations has been studied in PBST buffer (137 mM NaCl, 2.7 mM KCl, 10 mM phosphate buffer and 0.1% Tween 20, pH = 7.0). There was a linear increase in the total number of DNA_T molecules captured by each NP when [DNA_T] was in a range of 0 to 3 μM, which was followed by saturation at higher [DNA_T]. From the fluorescence change in DNA_T solutions before and after hybridization and removal of NPs, the number of DNA_T strands captured by each NP was calculated to be on average ~7 ± 1 for 0.18 μM, ~24 ±

2 for 0.75 μM, ~56 ± 5 for 2.0 μM, and ~83 ± 5 for 3.0 μM, respectively. The representative fluorescence emission spectra change for DNA_T solutions before and after hybridization with NP removal for $7DNA_T$–NP is shown as Figure 4.2.

Upon excitation at 490 nm, the solution ([NP] = 0.1 mg/mL) fluorescence increases almost linearly from 7 to $56DNA_T$–NP (Figure 4.3 inset), indicating that there is almost no Fl self-quenching on the NP surface. We now examine how the number of DNA_T strands on each silica NP influences FRET. Measurements were carried out in PBST buffer upon CCP addition ([NP] = 0.1 mg/mL). Figure 4.3 compares the Fl emission from NP solutions containing 7, 24 and $56DNA_T$–NP at a charge ratio (CCP/DNA probe and DNA_T, +/–) of 3.2, upon excitation at 370 nm. The most intense Fl emission was observed for CCP–$56DNA_T$–NP, which is approximately 40% more intense as compared to that for CCP–$24DNA_T$–NP and is about 4-fold greater than that for CCP–$7DNA_T$–NP. For $56DNA_T$–NP, the integrated Fl emission is approximately 40-fold greater than that obtained by excitation of Fl at 490 nm in the absence of the CCP, while over 75- and 110-fold enhancement is observed for 24- and $7DNA_T$–NP, respectively. The integrated fluorescence signals used for the calculation of signal amplification is shown in the Table 4.1.

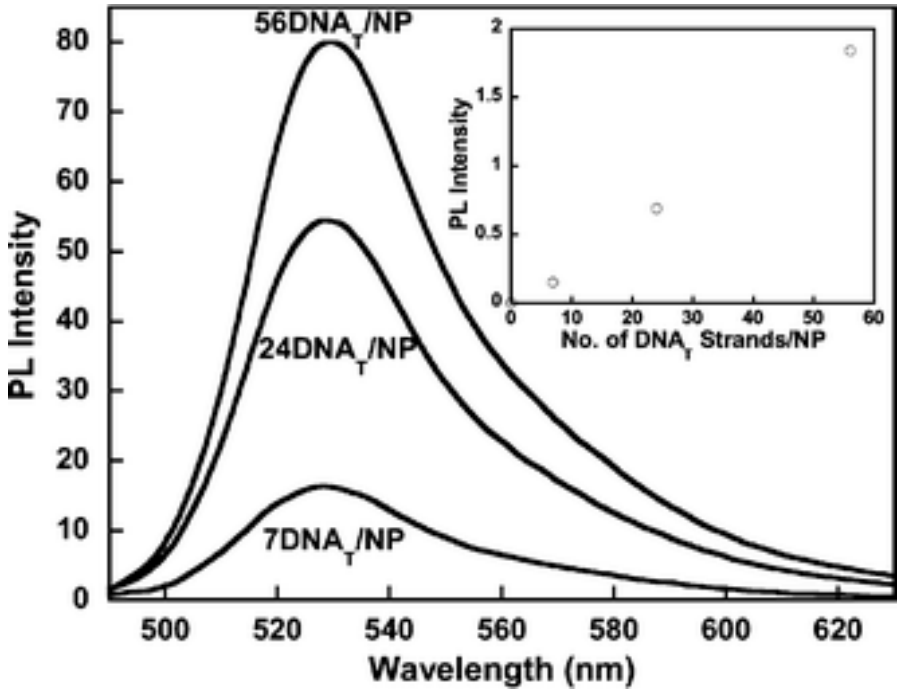

Figure 4.3 Fl emission spectra of DNA_T–NP solutions in the presence of CCP upon excitation at 370 nm. Inset: Fl intensity of DNA_T–NP solutions upon excitation at 490 nm in the absence of CCP. [NP] = 0.1 mg/mL and the charge ratio (+/–) is 3.2.

Table 4.1 The integrated fluorescence intensity of the hybridized NP in the absence and presence of CCP[a] and corresponding signal amplification

Integrated fluorescence intensity[b]	7 DNA_T/NP	24 DNA_T/NP	56 DNA_T/NP
Hybridized NP (under 490 nm excitation)	7.15	36.43	106.59
Hybridized NP with CCP (under 370 nm excitation)	827.64	2823.13	4135.20
Signal amplification fold	116	78	39

[a] All tests were done in the PBST buffer. [b] The integrated fluorescence intensity spanning the wavelength from 490 nm to 630 nm (area under the curve).

4.3.4 Signal amplification comparison of hybridized Fl-DNA in the free state and NP-bound state

Under similar experimental conditions, a solution of free $dsDNA_T$ with [Fl] the same as that of $7DNA_T$–NP generated only a 14-fold signal amplification (Figure 4.4). Specifically, to study the FRET for free $dsDNA_T$ in solution, the hybridized DNA_T (1×10^{-9} M, which corresponds to the same [Fl] of a $7DNA_T$/NP solution (0.1 mg/mL)) in 2 mL of PBST buffer was added in a quartz cuvette. The Fl emission was measured upon excitation at 490 nm in the absence of the CCP. After addition 3.5 μL of CCP ([CCP] = 20 μM, an amount corresponds to a charge ratio +/- of 3), the solution fluorescence were measured by excitation at 370 nm and 490 nm, respectively. The corresponding Fl emission spectra of the solutions are shown in Figure 4.4.

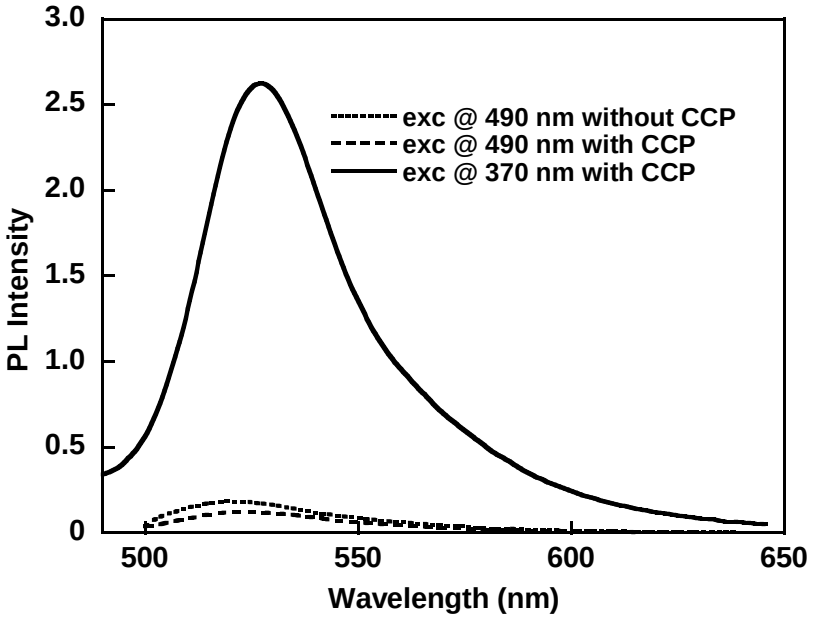

Figure 4.4 Fl emission spectra of free $dsDNA_T$ in the presence (exc @ 370 nm) and absence (exc @ 490nm) of CCP. Note: [$dsDNA_T$] = 1×10^{-9} M, and [CCP] = 0.035 μM based on CCP repeat unit.

Monitoring Fl emission upon direct excitation in the absence and presence of CCP showed a 25% decrease in fluorescence intensity for the free dsDNA_T solution while there was no obvious intensity change observed for DNA_T–NP solutions. This indicates that Fl quenching upon DNA_T–CCP complex formation is minimized with NP based sensor design, which is due to the limited movement and the large distance of Fl molecules on the NP surface (for 7DNA_T–NP, on average, there is one Fl molecule every 4500 nm^2 on the surface).

From the above results and the observed signal amplification dependent on number of Fl-DNA per NP (Figure 4.3 and Table 4.1), it is possible that the higher signal amplification in the presence of NPs could be attributed to the increased local concentration of donor units. When DNA_T-CCP complex is formed on NP surface, compared with that without NP support, CCP has the increased local concentration which is due to the complexation between the CCP and unhybridized ssDNA strands on the NP. Since CCP has the delocalized electronic backbone, exciton migration can happen along inter-polymer chains and intra-polymer chains on NP surface. Therefore, the increased local [CCP] can enable CCP donor to absorb more photon and deliver more exciton for a single acceptor (Fl) on NP surface, which favors FRET process and results in higher acceptor signal amplification relative to that without NP support. This agrees well with the observation that with an increased number of DNA_T strands on each NP there is a decrease in signal amplification, as shown in Table 4.1.

4.3.5 Specific and sensitive DNA detection

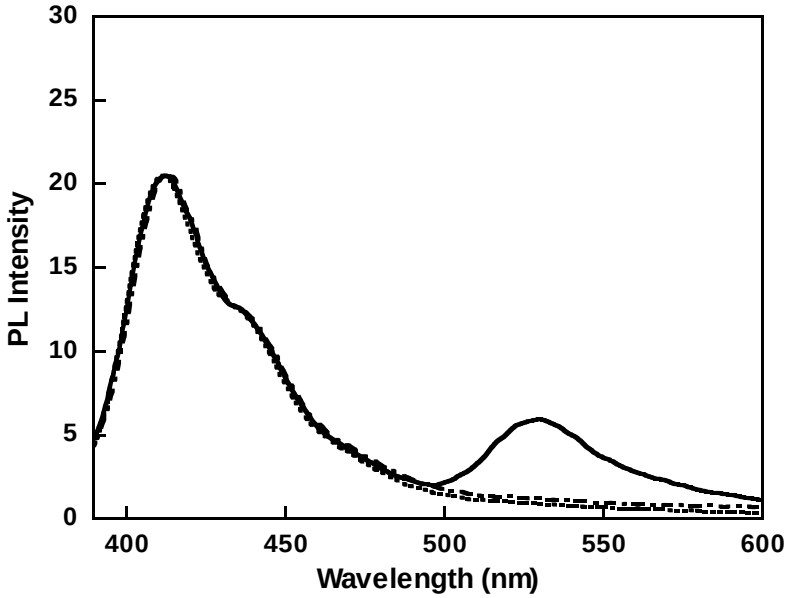

Figure 4.5 Normalized emission spectra for NP hybridization with DNA_T (solid line), a random sequence (dotted line) and a two-base mismatched sequence (dash-dotted line) upon excitation at 370 nm. Note: [NP] = 0.1 mg/mL and [CCP] = 0.15 μM.

To evaluate probe-immobilized NPs in DNA hybridization detection, 1.5 nmol of a DNA_T, a two-base mismatched sequence (5′-Fl-ATCTTGACTTTCTGGGTGCT-3′) and a random sequence (5′-Fl-CGTACGTACGTACGTACGTA-3′) were added separately to three probe-immobilized NP solutions in PBST buffer ([NP] = 1.6 mg per 2 mL), followed by hybridization and salt washing steps [45]. Figure 4.5 shows the normalized fluorescence spectra for NP hybridization with the three sequences. Strong Fl emission is observed when in the presence of the complementary sequence, while there is almost no Fl signal from solutions containing random or two-base mismatched sequences. This result demonstrated excellent specificity of the CCP-assisted NP-supported DNA assay. In addition, to determine the low detection limit of the developed assay, different [DNA_T] was tested with a standard fluorometer. With the signal amplification provided by the

CCP, this NP-supported assay allows detection of Fl emission for [DNA_T] = 10 pM, as shown in Figure 4.6.

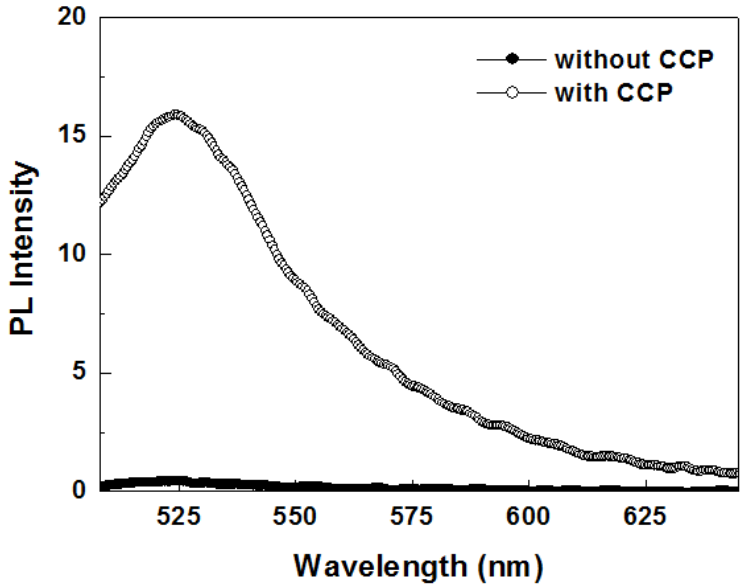

Figure 4.6 Fl emission spectra of DNA_T-NP at [DNA_T] = 10 pM in the presence and absence of CCP ([CCP] = 0.027 μM). Note: Fl emission spectrum in the presence of CCP was collected upon excitation at 370 nm, and that in the absence of CCP was collected upon excitation at 490 nm.

4.4 Conclusions

In summary, we have developed a silica NP based assay for highly sensitive and selective DNA hybridization detection. The NP based sensor strategy minimizes C* self-quenching within DNA_T–CCP complexes, and excess DNA probes on the NP surface could complex with CCP to increase the local concentration of donor units and deliver excitations to C*. In addition, the homogeneous suspension of silica NPs facilitates DNA hybridization and meanwhile provides the advantage of solid state sensors that allow separation and base mismatch detection. The optimized detection system amplified a

fluorescence signal up to over 110-fold in real time, and allowed the detection of 10 pM target DNA as well as two-base mismatch discrimination. This strategy of using silica NP-DNA probe and fluorescent CP could be used to detect other biomolecules in bio-analytical areas. More general, the successfully demonstrated assay indicates that homogeneous CP-based FRET assay could be potentially transferred to NP-supported format while maintaining some advantages of both homogenous solution assay and heterogeneous assay.

Nevertheless, the high signal amplification in the developed assay is obtained with well-controlled conditions such as matched donor/acceptor molecular orbital energy level, and confined fluorescence behaviors of CCP and Fl on the NP surface [82]. Other attempts deviated these special conditions may not get ideal signal amplification of FRET from CCP to C* [148]. Further optimization of CCP/diagnostic C* optical properties in silica NP-supported format to favor FRET signal amplification will likely yield practical platforms for real time detection [82].

CHAPTER 5

LABEL-FREE SINGLE-NUCLEOTIDE POLYMORPHISM (SNP) DETECTION USING A CATIONIC TETRAHEDRALFLUORENE AND SILICA NANOPARTICLES

5.1 Introduction

Sequence-specific detection of nucleic acids has become the subject of intense research in molecular diagnostics for both genetic and pathogenic diseases [149-151]. The detection and analysis of a single-nucleotide polymorphism (SNP), occurring as often as every few hundred to few thousand base pairs in genomic DNA, is of high importance to identify the disease-causing genes, and for early disease diagnosis and treatment [152,153] [154]. Fluorescently labelled SNP-specific hybridization probes, such as TaqMan probes and the stem-loop molecular beacons have been developed to satisfy the needs for rapid and reliable detection of DNA mutations [155-157]. The effectiveness of these probes is often limited by the sensitivity of the fluorescent reporters. Although multiple labels could provide improved detection sensitivity, the sophisticated probe design introduces complexity and cost [38,158,159]. Extensive efforts have been directed toward the design of label free sequence-specific detection systems, which include electrochemical [160-163],

colorimetric [164], surface plasmon resonance [165,166], and magnetically assisted biobarcode detection [41].

Fluorescent intercalator based detection is one of the classical methods that has been widely used to monitor DNA hybridization [167-169]. Intercalation dyes, such as ethidium bromide (EB) and SYBR Green, can intercalate within the internally stacked bases of double-stranded DNA (dsDNA) which result in an increase of their fluorescence quantum yields [167,170,171]. This type of detection is simple and effective, but it lacks specificity since the intercalation dye can interact with any dsDNA molecule in the solution to generate signals. In addition, intercalation dyes sometimes give false signals in the presence of single-stranded DNA (ssDNA) due to non-specific interactions [115,172,173].

One strategy to improve the selectivity of the intercalator based assay is to take advantage of the energy transfer process, so that fluorescence resonance energy transfer (FRET) occurs from the donor molecule to the intercalation dye [174,175]. Light harvesting cationic conjugated polymers (CCPs), in conjunction with reporter dyes on specific probes, have proven useful for strand-specific DNA detection with high detection sensitivity [28,80,83,84,86,106,116]. The signal amplification is a result of the large absorption cross section and the delocalized electronic structure of the polymers, which allow efficient intra- and interchain FRET [25,26,29]. However, FRET study between a linear CCP and EB intercalated into dsDNA showed poor energy transfer efficiencies [107]. Time dependent anisotropy measurements revealed that the low FRET efficiency was due to a non-optimal (orthogonal) orientation between the transition dipole moment of the optically active

polymer backbone and that of EB within the dsDNA structure [108]. Improved signal amplification has been demonstrated with shape-adaptable polymers, which have shown more conformational freedom and improved registry with the analyte shape [109].

Very recently, we found that cationic tetrahedral conjugated oligomers are better energy donors relative to CCPs [110]. The spatial registry of tetrahedral molecules is able to provide multiple transition dipole moment orientations relative to that of rigid one-dimensional polymer backbone, which makes them very efficient energy donors for intercalated EB. In homogeneous assays in solution, the tetrahedralfluorene sensitized EB emission could only be used to differentiate single-stranded sequences from double-stranded sequences. This is due to the limitation that EB could interact with any double-stranded sequences to generate enhanced signals, and this nonselective interaction prevents the sequence specific and base mutation detection. Although great progress has been made toward improving the sensitivity of the homogeneous intercalator based detection, the sequence specific detection remains an issue.

Meanwhile, nanoparticle (NP)-based assays have been extensively used for nucleic acid detection with sequence specific selectivity [18-20,176]. NP-based DNA assays possess the advantage of solid-state sensors, which allow the separation of specific binding from non-specific interactions to achieve sequence specific detection [45,115,177]. Among various nanomaterials, silica NPs (100 nm in diameter) are transparent in dilute solutions and their optical properties do not interfere with fluorescent conjugated oligomers. In addition, silica materials also have versatile bioconjugation methods, and their NPs have

large surface-to-volume ratio facilitating the DNA probe immobilization with a high density. The silica NP suspension also provides a nearly homogeneous environment that facilitates DNA immobilization and hybridization. In this context, incorporation of the FRET assay into a silica NP-supported format would provide a favorable condition to improve the detection selectivity of homogeneous FRET DNA assay while maintaining the advantages of conjugated oligomer signal amplification. In Chapter 5, we report a simple detection scheme that takes advantage of the DNA immobilized silica NP-supported format and a cationic tetrahedralfluorene sensitized EB emission so as to achieve label-free sequence specific DNA SNP detection with large signal amplification (Scheme 5.1). The overall detection does not require usage of complex instruments and could be achieved within several minutes.

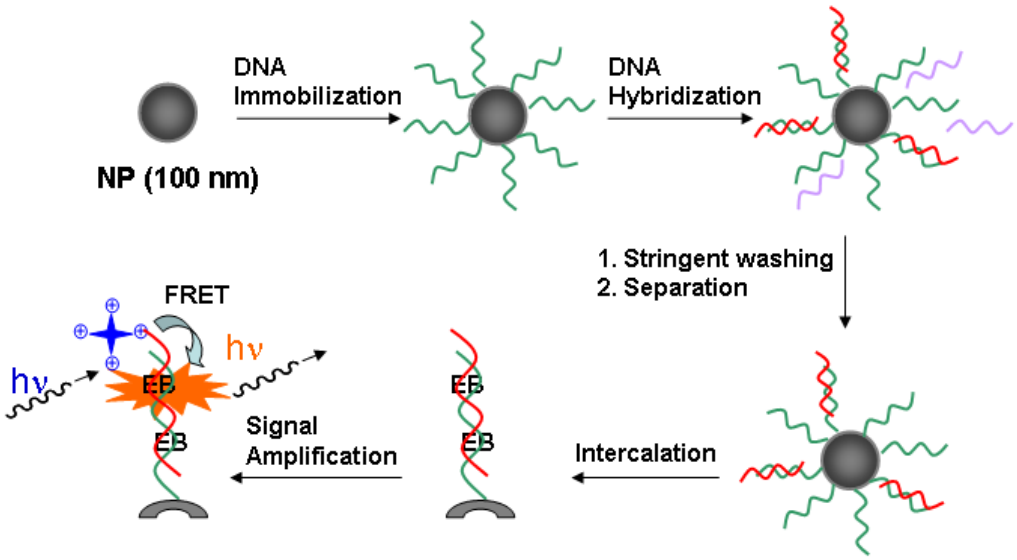

Scheme 5.1 Schematic illustration of the label-free SNP DNA detection strategy.

5.2 Materials and methods

Materials

DNA oligonucleotides, which include 5'-amine labelled DNA (DNA_p), 5'-Amine-AGCACCCACATAGTCAAGAT-3'; the target DNA with a complementary sequence (DNA_c), 5'-ATCTTGACTATGTGGGTGCT-3'; the target DNA with single-base mutation (DNA_1), 5'-ATCTTGACTAT*C*TGGGTGCT-3'; the target DNA with two-base mutation (DNA_2), 5'-ATCTTGACT*T*T*C*TGGGTGCT-3', were purchased from Research Biolabs, Singapore. Tetraethoxysilane (98%, Fluka), ethanol (99.9%, Merck), ammonia solution (30%Wt, SINO Chemical Company), 3-aminopropyl triethoxysilane (99%, Aldrich), sodium chloride (99.5%, Merck), Tween-20 (Aldrich), acetonitrile (anhydrous 99.8+%, Alfa Aesar), 2,4,6-trichloro-1,3,5-triazine (98%, Alfa Aesar), ethidium bromide (Aldrich), boric acid (99+%，Alfa Aesar), sodium tetraborate decahydrate (99+%，Alfa Aesar), sodium hydroxide (99+%, Merck), formamide (99.5+%, Alfa Aesar), and 10× phosphate buffer saline (PBS buffer, ultrapure grade, 1st BASE) are commercial products and were used as received without further purification. MilliQ water (18.2 MΩ) was used to prepare all the buffers. The buffer solutions in the assay include borate buffer (50 mM sodium borate, pH = 8.5), the hybridization buffer (1087 mM NaCl, 2.7 mM KCl, 10 mM phosphate buffer, 0.1% Tween-20, and 20% formamide, pH = 7.4), PBST buffer (75 mM PBS buffer with 0.1% Tween-20, pH = 7.4), and the washing buffer (10 mM phosphate buffer, 10 mM NaCl and 0.1% Tween-20, pH = 7.0). The cationic tetrahedralfluorene, tetrakis[4-(2-(9,9,9',9'-tetrakis(*N*,*N*,*N*-trimethylammoniumhexyl)-7,2'-bifluorenyl))-phenyl]methane hexadecanebromide, was synthesized according to the literature

procedure [110]. The molecular structures of the tetrahedralfluorene and ethidium bromide are shown in Scheme 5.2.

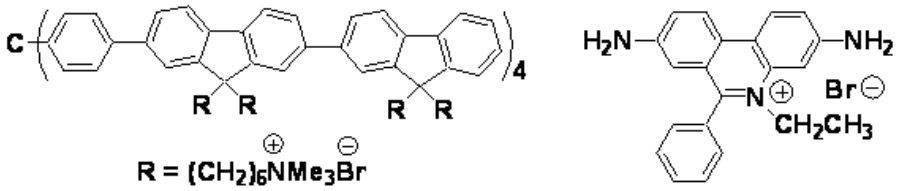

Tetrahedralfluorene Ethidium Bromide

DNA_p: 5'-NH_2-AGC ACC CAC ATA GTC AAG AT-3'
DNA_c: 5'-ATC TTG ACT ATG TGG GTG CT-3'
DNA_1: 5'-ATC TTG ACT AT*C* TGG GTG CT-3'
DNA_2: 5'-ATC TTG ACT *TTC* TGG GTG CT-3'

Scheme 5.2 Molecular structures of the tetrahedralfluorene, ethidium bromide, and the sequences of DNA molecules in this study.

Characterization

The UV/Vis absorption spectra were obtained from a Shimadzu UV-1700 spectrometer. Photoluminescence was measured using a Perkin Elmer LS-55 equipped with a xenon lamp excitation source and a Hamamatsu (Japan) 928 PMT, using 90 degree angle detection for solution samples. The synthesized NPs were imaged using a field-emission scanning electron microscope (FE-SEM JEOL JSM-6700 F) after coating a thin Pt layer via a platinum coater.

Synthesis and surface functionalization of silica NPs

The bare silica NPs were synthesized according to the procedure described in Chapter 3. After that, the surface functionalization of NPs was conducted according to the reference

with slight modification [147]. Briefly, 3-amino-propyltrimethoxysilane (~140 µL) was added to 1 mL of ethanol solution containing 6.4 mg of bare silica NPs. The mixture was reacted at room temperature for 2 h, which was followed by heating at 50°C for another 1 h. After cooling to room temperature, the NPs were centrifuged and washed with ethanol and acetonitrile. The obtained NPs were further reacted with 38.4 mg of 2,4,6-trichloro-1,3,5-triazine in 1 mL of acetonitrile at room temperature for 2 h. The obtained NPs were centrifuged and washed successively with acetonitrile, ethanol, MilliQ water and finally dispersed in 170 µL of borate buffer for DNA_p immobilization.

Immobilization of DNA probes onto silica NPs

DNA_p (50 µL, 100 µM) was added to the as-functionalized silica NP solution (6.4 mg in 170 µL borate buffer), which was followed by the addition of NaCl (180 µL, 2 M). The resulting mixture was incubated and shaken for ~16 h at room temperature. The NP suspension was centrifuged, and the supernatant was collected for UV/Vis absorption measurement. The DNA_p immobilized NPs were washed with MilliQ water and then dispersed in MilliQ water for further use. The number of DNA_p molecules immobilized on the silica NPs can be quantitatively calculated from the absorbance difference at 260 nm between the DNA_p solution before immobilization and the supernatant after immobilization and NP removal. The number of immobilized DNA_p on each NP was calculated based on the ratio of the total number of immobilized DNA_p to the total number of NPs in solution.

Hybridization of DNA_p immobilized NPs

The as prepared DNA_p-immobilized NPs (1.0 mg) in MilliQ water were centrifuged and re-dispersed in 70 μL of the hybridization buffer. The target DNAs (30 μL of [DNA_c or DNA_1 or DNA_2] = 10 μM) was added to each NP solution, and the mixture was incubated and shaken at room temperature for 12 h. After thorough washing to remove free target DNA molecules by three rounds of centrifugation with the hybridization buffer, the collected NPs were redispersed in 400 μL of the hybridization buffer. The supernatants were collected for UV/Vis analysis. The number of target DNAs captured by NPs can be calculated from the absorbance difference at 260 nm between the target DNA solutions before hybridization and the supernatants after hybridization and NP removal. The number of hybridized DNA molecules on each NP was calculated based on the ratio of the total number of captured DNA to the total number of NPs in solution.

EB intercalation

The hybridized NPs (0.4 mg) in the hybridization buffer was centrifuged and washed three times with a low ionic strength washing buffer. The NPs were centrifuged and then redispersed in 4 mL of the PBST buffer, among which 2 mL of the solution was transferred to a quartz cuvette. Aliquots of EB solution ([EB] = 2.54×10^{-4} M) were added dropwise at 4 μL each. Upon each addition, the mixture was gently shaken at room temperature before the fluorescence measurement. The excitation wavelength was 500 nm and the fluorescence was collected in the range of 510-750 nm. The unbound EB fluorescence from the hybridized NP/EB mixtures was also monitored by measuring the supernatant fluorescence for each mixture after centrifugation and NP removal. The

bound EB fluorescence upon each EB addition is thus the difference between the overall mixture fluorescence and the supernatant emission. The amount of EB required for maximized intercalation was studied based on the bound EB fluorescence intensity changes at EB emission maximum (~615 nm).

FRET experiments with tetrahedralfluorene

On the basis of the optimized amount of EB required for intercalation of the hybridized NPs (NP-DNA_p/DNA_c) in PBST buffer, aliquots of tetrahedralfluorene (concentration based on fluorene unit, [fluorene unit] = 8×10^{-5} M) were added dropwise into the solution. The mixture was gently shaken at room temperature before measurement. The fluorescence was monitored upon excitation at 352 nm and the emission was collected in the range of 360-700 nm. The amount of tetrahedralfluorene added was optimized to achieve the maximal sensitized EB emission intensity at ~605 nm.

SNP detection

The hybridized NPs (0.2 mg of NP-DNA_p/DNA_c, or NP-DNA_p/DNA_1, or NP-DNA_p/DNA_2) after washing with the low ionic strength washing buffer were dispersed in 2 mL of PBST buffer. An amount of 24 μL of EB ([EB] = 2.54×10^{-4} M) was added to the NP solutions in one shot, and the solution was gently shaken at room temperature. The EB emission from the solutions was monitored upon excitation at 500 nm. An amount of 36 μL of tetrahedralfluorene ([fluorene unit] = 8×10^{-5} M) was then added to the solution at one shot, and the emission was monitored upon excitation at 352 nm.

Tetrahedralfluorene sensitized EB emission was obtained from the solution fluorescence after subtracting any residual tetrahedralfluorene emission tail in the EB emission region.

5.3 Results and discussion

5.3.1 Strategy for the label-free SNP DNA detection using a cationic tetrahedralfluorene and silica NPs

As shown in Scheme 5.1, the overall detection could be separated into two consecutive stages: specific DNA recognition and signal amplification. Target hybridization to probes that have been pre-immobilized onto the NP surface was used to differentiate target DNA sequences from mismatches. Since various NP technology has been widely used for DNA and protein detection [141,176,178], standard DNA hybridization protocol and washing steps that have been well documented in the literature have been directly adopted to maximize the sequence recognition specificity. The signal amplification is also performed according to the protocols developed in our group [28,80,83,84,106].

The general detection scheme (Scheme 5.1) contains DNA_p (shown in green) immobilized NPs, an intercalating dye (EB), and a cationic tetrahedralfluorene molecule (shown in blue). The DNA_p-NP is first prepared by immobilization of amine-terminated DNA_p onto silica NPs. The recognition is accomplished by sequence-specific hybridization between the DNA_p on the silica NPs and the targets of interest (the complementary sequence DNA_c, shown in red, one-base or two-base mismatched sequences DNA_1 or DNA_2, shown in purple), which is followed by salt washing steps to retain the complementary sequence. After subsequent treatment of intercalation dyes

(EB), the cationic tetrahedralfluorene is added, which could be electrostatically associated with the DNA molecules on the NP surface. In the case of complementary DNA, addition of DNA_c results in the formation of a double helix (NP-DNA_p/DNA_c) and the intercalation of EB within the duplex structure. Excitation of the tetrahedralfluorene leads to energy transfer from tetrahedralfluorene to EB, resulting in the sensitized EB emission. In the case of non-complementary sequences, the hybridization products can not sustain the salt washing step. Little or no EB intercalation is possible. The distance between the tetrahedralfluorene and EB remains too large for efficient energy transfer.

5.3.2 Preparation of DNA immobilized silica nanoparticles

Silica NPs were first synthesized using a modified Stöber method via a seeded growth process [126]. The seeded method provides the uniform silica NPs (~100 nm in diameter) with a narrow size distribution (FE-SEM images shown in Figure 3.2 and Figure 3.3). We are particularly interested in silica NPs in the 100 nm size range since they are transparent in dilute solutions and their optical properties do not interfere with those of fluorescent molecules. Based on the size and the density of silica (1.96 g/cm^3), we estimate that 1.0 mg of the synthesized NPs contain ~ 1×10^{12} number of NPs [179].

The prepared NP surface was functionalized by silane followed by triazine activation, and ready for immobilization of amine-modified DNA_p. The successful immobilization of DNA_p on the NP surface was observed from the absorbance difference between the DNA_p solution before immobilization and the supernatant after immobilization. A surface coverage density was determined to be ~320 DNA_p/NP, which is comparable to the

surface coverage of the oligonucleotide immobilized on the carboxylic acid functionalized silica NPs reported by Mirkin et al [180].

5.3.3 Salt-wash assisted DNA detection using NP-DNA bioconjugate

After the surface immobilization, incubation of the DNA_p immobilized NPs (NP-DNA_p) with the target DNA sequences (DNA_c, DNA_1, or DNA_2) in the hybridization buffer led to the formation of DNA duplexes on the NP surface. The degree of hybridization varied, dependent on the sequence of the target DNA molecules. The extent of hybridization between NP-DNA_p and the complementary DNA_c was measured from the absorbance difference between the DNA_c solution before hybridization and the supernatant after hybridization and NP removal, which corresponds to ~140 ± 15 DNA_c/NP-DNA_p based on three batches of hybridization. Therefore, ~43 ± 4% of the surface immobilized DNA_p molecules participated in the hybridization with DNA_c. This number is comparable to the previous report, where a hybridization of ~40% was reported for oligonucleotide immobilized on the surface of silicon wafers [181]. Under similar hybridization condition, about 30% of the surface immobilized DNA_p could hybridize with DNA_1.

The SNP detection is conventionally achieved through thermal-stringent washing steps, which is based on the fact that the melting point of mismatched DNA is lower than that of the perfectly matched DNA [182]. The thermal assisted SNP detection method is generally time-consuming and is not suitable for NP based assay since the particles may not be stable at a high temperature. However, the duplex stability is known to be sensitive to the ionic strength of the solutions. Since DNA strands are negatively charged, cations

are required to screen the Coulomb repulsion that could prevent the dsDNA duplex formation. Recently, Mirkin and coworkers demonstrated that mismatched DNA is much more susceptible to solutions of low ionic strength than perfectly matched DNA [45]. Although this strategy was first demonstrated for gold NP based assays, recently, the same strategy has also been applied for a magnetically assisted assay for SNP detection [115]. Here, we performed the salt washing steps in order to selectively destabilize the imperfect duplexes containing single nucleotide mismatches. A low ionic strength washing buffer was used to wash all the hybridized particles. We assume that the DNA sequences containing a SNP could be largely removed during the salt washing steps, while majority of the complementary sequence remains bound on the NP surface. The selectivity will be evaluated from the EB fluorescence in solution.

5.3.4 Optimization of ethidium bromide (EB) intercalation

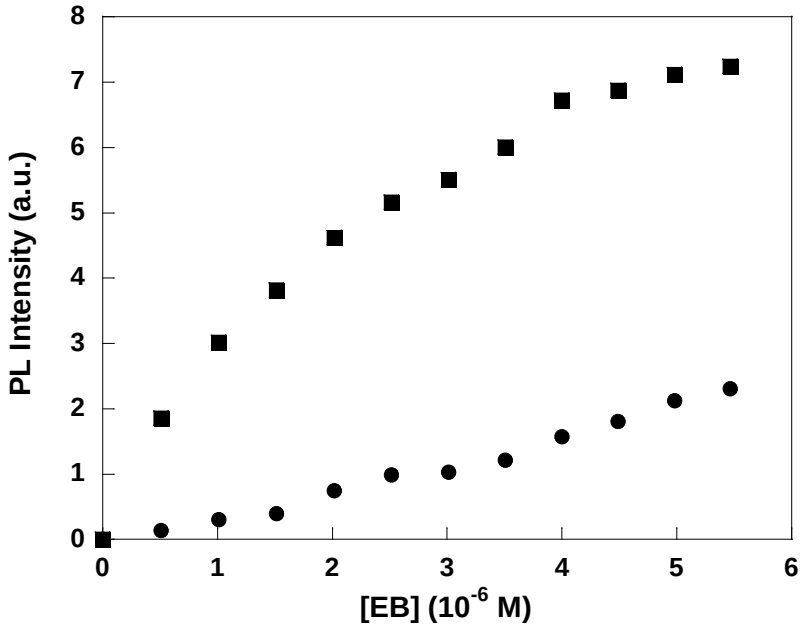

Figure 5.1 The bound EB emission intensities for NP-DNA_p (shown in circles) and NP-DNA_p/DNA_c (shown in squares) in PBST buffer as a function of [EB] upon 500 nm excitation. [NP] = 0.1 mg/mL.

The intercalation of EB into NPs (after salt washing) was studied by varying the concentration of EB in the NP-DNA_p/DNA_c solution. The EB emission from the solution containing DNA_p-NP with increased amount of EB was also studied. Figure 5.1 shows how the EB emission intensity for the NP-DNA_p/DNA_c and DNA_p-NP solutions changes with the addition of EB. For both solutions, there is an increase in EB emission with the increased amount of EB added. At the low concentration range of EB ([EB] = 0-3 μM), the increase of EB emission for NP-DNA_p/DNA_c solution is faster than that for the DNA_p-NP solution. The higher intensity for NP-DNA_p/DNA_c solution indicates the intercalation of EB with the dsDNA duplex, which in turn results in fluorescence enhancement [167]. The maximum difference in EB emission is observed at [EB] ~3 μM, after which the difference is nearly constant. This observation indicates that the saturation of the EB intercalation for NP-DNA_p/DNA_c occurs at [EB] ~3 μM, after which the increase in EB intensity is due to the non-specific interaction between EB and the DNA_p immobilized NP. During EB intercalation, a relatively high ionic strength buffer (75 mM) was used to avoid the secondary binding of EB on the outside of the DNA helix, which was reported to occur when the ionic strength of the solution is less than 0.01 M [183].

5.3.5 Spectrum overlap between the emission of the tetrahedralfluorene and the absorbance of EB

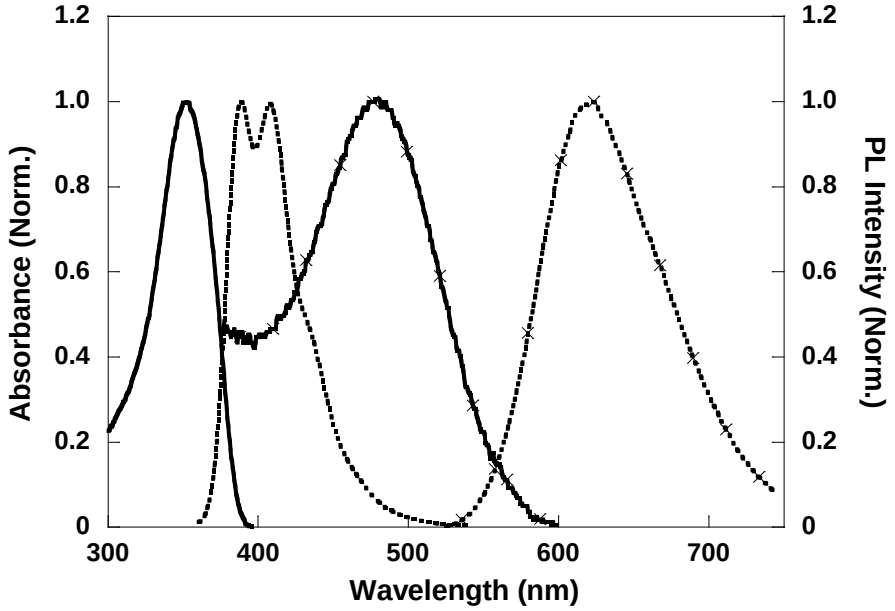

Figure 5.2 The absorption (solid line) and photoluminescence spectra (dashed line) of the cationic tetrahedralfluorene and EB (line with crosses) in PBST buffer. The excitation wavelength is 352 nm for the tetrahedralfluorene and 500 nm for EB.

As shown by Förster, dipole-dipole interactions lead to long-range energy transfer from a donor chromophore to an acceptor chromophore [79]. The energy transfer rate is dependent on the donor-acceptor distance, the orientation between the dipole moment of the donor and the acceptor, and the spectral overlap [79]. The spectral overlap describes how the donor emission overlaps with the absorption of the acceptor. The absorption and photoluminescence spectra of the cationic tetrahedralfluorene and EB in PBST buffer are shown in Figure 5.2. There is a good spectral overlap between the emission of the tetrahedralfluorene and the absorption of EB, which should favor FRET.

5.3.6 FRET sensitized EB emission with different tetrahedralfluorene concentration

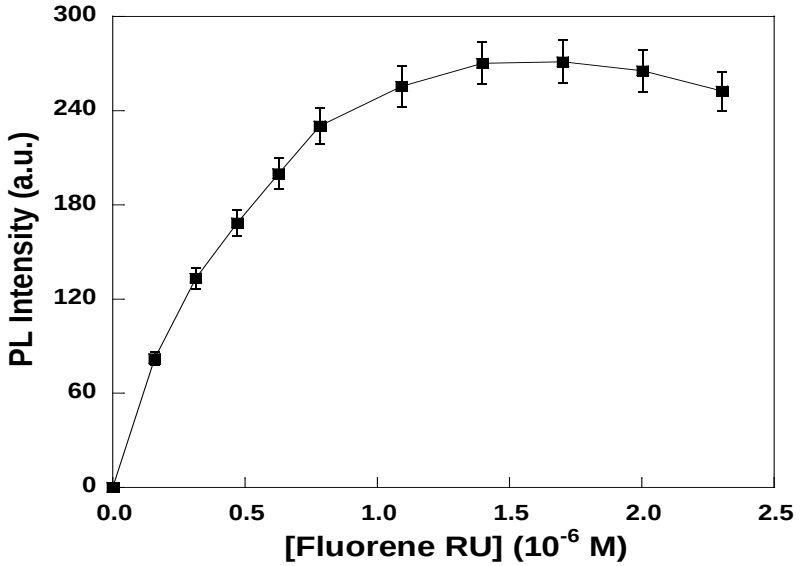

Figure 5.3 The intensity of EB emission at 605 nm for NP-DNA_p/DNA_c/EB/tetrahedralfluorene as a function of [fluorene unit]. Measurement was done in PBST buffer upon 352 nm excitation. [NP] = 0.1 mg/mL, and [EB] = 3.0 μM.

With optimized amount of EB (3 μM) in NP-DNA_p/DNA_c solution ([NP] = 0.2 mg in 2 mL of PBST buffer), the cationic tetrahedralfluorene was added to serve as the energy donor for sensitized EB emission. As shown in Figure 5.3, initial addition of the tetrahedralfluorene causes an immediate rise of EB intensity. The most intense FRET signal was observed at a concentration of [fluorene unit] = 1.4 μM, which corresponds to the charge ratio (+/-) close to 2. Here "+" refers to all the positive charges from tetrahedralfluorene, and "-" refers to all the negative charges from the NP-DNA_p/DNA_c, assuming the salt washing does not affect the number of DNA_c on the NP surface. Upon further addition of the tetrahedralfluorene, the FRET signal shows a tendency to decrease. As reported earlier [107,184], the co-existence of intercalated EB and cationic molecules

might lead to EB displaced from dsDNA due to the electrostatic repulsion between tetrahedralfluorene and EB since EB has a low binding affinity (~10^5 M^{-1}) upon intercalation with dsDNA [185]. In addition, under charge neutralization, the DNA molecules could also collapse into packed forms and prevent EB intercalation [186]. As a consequence, the condition of [fluorene unit] = 1.4 μM, which corresponds to the maximized EB emission, has been selected for SNP detection experiments.

5.3.7 Label-free SNP DNA assay with high signal amplification

The NP based SNP detection in the presence and in the absence of the cationic tetrahedralfluorene was studied and the results are shown in Figure 5.4. In the absence of the tetrahedralfluorene, although EB emission from NP-DNA_p/DNA_c/EB is the highest, the intensity is about 2.5-fold higher than that from the NP-DNA_p/DNA_1/EB, and about 4-fold higher than that from the NP-DNA_p/DNA_2/EB. As shown in the inset of Figure 5.4, the absolute intensity from NP-DNA_p/DNA_c/EB is rather low and the difference between complementary and non-complementary strands is small which can easily bring false-positive information. Similar results have been observed before when a dT_{20} sequence was immobilized on an optical fiber [187]. Upon hybridization with dA_{20} and intercalation with EB, the signal from dsDNA is 40-60% higher than that from the dT_{20}/EB. Such a poor sensitivity is due to the high background signal and the partial association of the positively charged EB with negatively charged ssDNA. Although the overall detection performance is not very satisfactory, the difference in signal between NP-DNA_p/DNA_c/EB and NP-DNA_p/DNA_1/EB indicates the effectiveness of the salt washing steps.

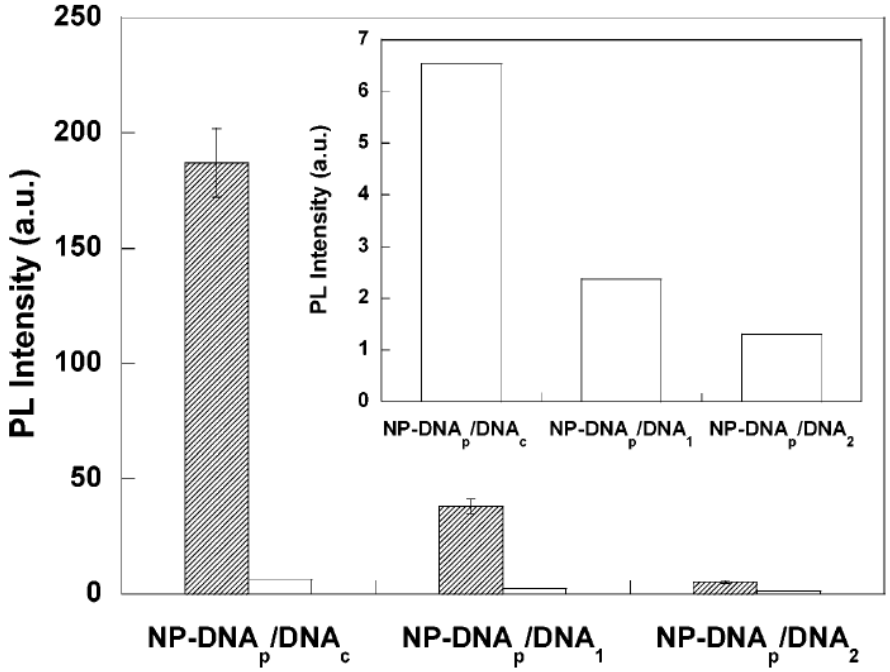

Figure 5.4 The maximum EB emission intensity from solutions containing NP-DNA_p/DNA_c/EB, NP-DNA_p/DNA_1/EB, and NP-DNA_p/DNA_2/EB in the presence (bar with shadow) of the tetrahedralfluorene. The bound EB emission intensity from the same solutions in the absence of tetrahedralfluorene is shown with the empty bar and is enlarged in the inset. Measurement was done in PBST buffer, with [NP] = 0.1 mg/mL, [EB] = 3.0 μM and [fluorene unit] = 1.4 μM. Excitation was at 352 nm for tetrahedralfluorene and 500 nm for EB.

Upon addition of the cationic tetrahedralfluorene, the difference in EB emission could be easily used to identify the target DNA molecules with different sequences. As shown in Figure 5.4, as compared to the solutions containing nonperfectly matched DNA targets, EB emission predominates when in the presence of NP-DNA_p/DNA_c/EB complexes. Under excitation at 352 nm, the tetrahedralfluorene sensitized emission is approximately 35-fold greater than that upon direct excitation of EB at 500 nm in the absence of the tetrahedralfluorene, indicative of FRET signal amplification provided by the tetrahedral molecule. In contrast, NP suspension containing SNP (NP-DNA_p/DNA_1/EB) has shown an intensity which is about 20% as that for the NP-DNA_p/DNA_c/EB. There is only very

weak fluorescence observed from the NP-DNA_p/DNA_2/EB. When one compares the detection in the presence and in the absence of the tetrahedralfluorene, it is obvious that there is an improvement for both detection sensitivity and selectivity when tetrahedralfluorene is used as the energy donor. Since the tetrahedralfluorene can only provide signal amplification to EB that has been intercalated within the dsDNA duplexes, the improved selectivity simply indicates the reduced background signal contribution to the overall intensity. These data demonstrate that the developed label-free DNA detection strategy is effective in differentiation of target DNA with different sequences.

5.4 Conclusions

In summary, we present a simple and efficient silica NP based platform with optically enhanced signals that allows label-free sequence-specific DNA detection with SNP selectivity. The signal transduction is achieved by a combination of two recognition events, i.e. the specific base pair recognition between the probes immobilized on the NP surface and the targets, and the electrostatic interaction between the tetrahedralfluorene and the DNA duplex that allows EB intercalation. Salt washing has proved to be effective in improving NP based SNP detection selectivity. The introduction of tetrahedralfluorene molecule as an energy donor significantly enhances the fluorescence signal of the intercalated EB, and the demonstrated signal amplification could be used in more circumstances to solve the background and sensitivity limits of the traditional NP based assay. As compared to the solution based homogeneous assay, which cannot offer sequence specific detection, this method provides a fast detection of oligonucleotides

with high signal amplification and SNP selectivity and opens up the possibilities for future development of integrated and portable devices for diagnostics or forensic investigations.

Nevertheless, during salt washing step in order to selectively destabilize the duplexes containing mismatched bases, the ionic strength of the washing buffer is not optimized. We directly use a low ionic strength washing buffer (10 mM phosphate buffer, 10 mM NaCl and 0.1% Tween-20, pH = 7.0) to wash all the hybridized particles, which may not be the best condition. Variation of washing buffer ionic concentration is needed to learn more about the effect of ionic strength on DNA duplex stability on silica NP surface. By doing so, we may further improve the detection signal/noise ratio and obtain higher selective DNA assay.

CHAPTER 6

AMPLIFIED FLUORESCENCE TURN-ON ASSAY FOR MERCURY(II) DETECTION AND QUANTIFICATION BASED ON CONJUGATED POLYMER AND SILICA NANOPARTICLES

6.1 Introduction

Recognition and detection of mercury ions (Hg^{2+}) and its derivatives is of vital importance because of their high toxicity and adverse effects on the environment and human health [188,189]. Different strategies for the analysis of Hg^{2+} have been developed, and the majority are based on fluorescence and colorimetric methods. Fluorescent Hg^{2+} sensors offer simple and rapid detection of mercury ions in environmental and biological samples. Most fluorescence based Hg^{2+} detection utilizes small organic molecules either in organic solution [190-193], or in aqueous solution [194-197]. Other detection strategies are also reported on the basis of nanoparticles [198,199], conjugated polymers (CP) [99,100], DNAzymes [200,201], foldamers [202,203], proteins [204,205], and oligonucleotides [206-209].

The complexation of metal ions with nucleotide purine and pyrimidine bases has attracted research interest recently [206-212]. The specific interaction between thymine-mercury(II)-thymine (T-Hg^{2+}-T) has been widely used for Hg^{2+} detection [101,206-209,213-216]. A doubly

labelled Hg^{2+} specific probe was firstly reported to detect Hg^{2+} based on Hg^{2+} induced probe folding which brought the dye (fluorescein) and the quencher (dabcyl) into close proximity to favor intramolecular energy/electron transfer[206]. A colorimetric assay based on the absorption change of a cationic polythiophene responding to Hg^{2+} induced oligonucleotide folding was subsequently reported [101]. Recently, an oligonucleotide-gold nanoparticle (Au NP) based assay was developed [213], which took advantage of the higher melting temperature for duplexes containing T-Hg^{2+}-T complexes as compared to that for duplexes with T-T mismatches. By introducing an appropriate complementary linker and more T-T mismatches to the DNA probes immobilized on the Au NPs, a room temperature colorimetric method was subsequently reported [214]. Very recently, two strategies for amplified detection of Hg^{2+} have also been reported. One was operated on the allosteric T-Hg^{2+}-T formation induced activation of a UO_2^{2+}-dependent DNAzyme [215], and the other was relied on T-Hg^{2+}-T formation induced activation of a DNA machine [216].

Fluorescent conjugated polymers (CPs) as optically sensitive materials have been widely used in chemical and biological sensors [26-28,86,217]. Their large absorption cross section and delocalized electronic backbone structure allow efficient light-harvesting and rapid intrachain and interchain energy transfer [25,26,28,29,218]. This results in huge signal amplification upon molecular-recognition events, and imparts the CP-based sensor high sensitivity, which offers a key advantage over small molecule counterparts. More often, CP-based Hg^{2+} detection were conducted in organic solution. For example, Fan et al. reported a PPETE conjugated polymer functionalized with N,N,N'-trimethylethylenediamino groups and used it for a turn-on Hg^{2+} detection in organic

solution [98]. Tang et al. also gave a report on a polythiophene containing thymine moieties for Hg^{2+} detection [99]. Although good performance with high sensitivity and selectivity was achieved in the above studies, this type of detection used neutral CP and its operation was conducted only in organic medium. In response to the restriction of detection in organic medium, water-soluble CP-based assays have been developed for heavy metal ion detection [26]. For instance, Bunz and coworker developed a Hg^{2+} assay in aqueous solution using a carboxylate-substituted poly(para-phenyleneethynylene) and a papain protein which contained Hg^{2+}-responsive sulfhydryl groups [100]. However, the above sensor worked only in the turn-off mode, and small environmental perturbation might affect the detection specificity. Instead of the turn-off detection, a turn-on assay in aqueous solution was recently reported by Liu et al [101]. The authors made use of a cationic conjugated polymer and a mercury-specific oligonuleotide (sequence: 5'-CATTTCTTTCTTCCCCTTGTTTGTTTCA -3') to detect Hg^{2+} in aqueous solution. This assay was conducted in a label-free detection style, and achieved the lowest detection limit down to 42 nM for Hg^{2+} with high selectivity relative to other metal ions such as Ca^{2+}, Mg^{2+}, Pb^{2+}, Cu^{2+}, Zn^{2+}, Mn^{2+}, and Co^{2+} ions. Nevertheless, the developed assay was conducted in homogeneous solution, and environmental perturbation may affect its detection selectivity.

In a meanwhile, nanoparticle(NP)-based assays have been applied to a wide variety of applications [96,115,146]. As the solid-state support, probe-immobilized NPs allow the separation of specific binding from nonspecific interactions to improve assay selectivity. Among various nanomaterials, silica NPs (100 nm in diameter) are transparent in dilute

solutions and their optical properties do not interfere with fluorescent conjugated polymers. Silica materials also have versatile bioconjugation methods, and their NP suspension provides a nearly homogeneous environment that facilitates probe immobilization and recognition. In this sense, incorporation of the CP FRET assay into a silica NP-supported format would provide a favorable condition to improve the detection selectivity of CP-based homogeneous assay while maintaining the advantages of CP signal amplification. In Chapter 6, by taking advantage of the signal amplification of cationic conjugated polymers (CCPs) and the specific T-Hg^{2+}-T interaction on the NP surface, we report an amplified fluorescence turn-on assay for mercury(II) detection and quantification in aqueous medium.

6.2 Materials and methods

Materials

The cationic conjugated polymer was synthesized according to a previous report [80]. DNA oligonucleotides were purchased from Research Biolabs (Singapore) with the sequences of 5'-NH_2-GTGACCATTTTGCAGTG-3' and 5'-fluorescein (Fl)-CACTGCATTTTGGTCAC-3'. Tween-20, sodium nitrate, silver nitrate was purchased from (Sigma Aldrich). Other metal salts used in this work are: Na(OAc), $Hg(OAc)_2$, $MgSO_4$, $Co(NO3)_2$, $Ni(OAc)_2$, $Ba(OAc)_2$, K(OAC), $Pb(NO_3)_2$, and $Cd(SO_4)$. Phosphate buffered saline (10× PBS buffer, ultrapure grade, 1st BASE) is a commercial product. The hybridization buffer is home-prepared 150 mM PBST buffer which contains 137 mM NaCl, 2.7 mM KCl, 10 mM phosphate and 0.1% Tween 20 (pH = 7.4). The acetate buffer

contains 140 mM sodium nitrate and 10 mM sodium acetate (pH = 7.1). The 25 mM PBST buffer is 25 mM PBS with 0.1% Tween-20 (pH = 7.2). MilliQ water (18.2 MΩ) was used to prepare all buffer solutions. The stock solution of Hg^{2+} (2 mM) was prepared by dissolving 6.78 mg of $Hg(OAc)_2$ in 10.64 mL acetate buffer with few droplets of concentrated HNO_3. Other metal ion stock solutions (2 mM) were prepared by dissolving metal salts in the acetate buffer.

Characterization

The concentration of DNA was determined by measuring the absorbance at 260nm using a Shimadzu UV-1700 spectrometer. Photoluminescence (PL) or fluorescence was measured using a Perkin Elmer LS-55 equipped with a xenon lamp excitation source and a Hamamatsu (Japan) 928 PMT, using 90 degree angle detection for solution samples. All spectra were measured in 25 mM PBST buffer. The as-prepared NPs were imaged using a field-emission scanning electron microscope (FE-SEM JEOL JSM-6700 F) after coating a Pt layer (~5 nm in thickness) via a platinum coater (JEOL JFC-1300, Auto Fine Coater).

Hybridization of DNA-immobilized NPs

Bare silica NPs and DNA immobilized NPs were prepared according to our previous report [219]. The ssDNA-NPs were washed twice with the hybridization buffer before hybridization. Fl-labelled oligonucleotide was then added to the ssDNA-NP solution in hybridization buffer ([Fl-DNA] = 1 μM, [NP] = 0.8 mg/100 μL). The mixture was shaken at room temperature for 2 h. After incubation, the suspension was centrifuged, and the

precipitate was washed with hybridization buffer while the supernatant was kept for fluorescence analysis. Finally, the hybridized dsDNA-NPs were dispersed in the hybridization buffer.

Ion incubation

The as prepared dsDNA-NP was transferred from the hybridization buffer to the acetate buffer, and packed into different tubes. Different amount of Hg^{2+} or the nonspecific ion mixture (including eight different ions, each has the same concentration as that of Hg^{2+}) in acetate buffer was added into the dsDNA-NP solutions, which were followed by shaking at room temperature for 45 minutes. After ion incubation, the above solutions were centrifuged and the residues were dispersed in acetate buffer.

Thermal wash

The Hg^{2+} or nonspecific ion treated dsDNA-NP was dispersed into the acetate buffer to yield a NP concentration of 0.1 mg/500 μL. The samples were then loaded into an incubator (45 °C, 1200 rpm) for 15 minutes. The treated DNA-NPs were centrifuged immediately. The residue was washed with hybridization buffer once, and then dispersed into 25 mM PBST buffer for PL measurement.

Fluorescence measurement and analysis

To study the selectivity of NP based sensor for Hg^{2+} detection, 0.1 mg of the hybridized NPs (after ion incubation and thermal wash) was dispersed in 1 mL of 25 mM PBST buffer in a 1.5 mL PMMA cuvette. The solution fluorescence was measured upon

excitation of Fl at 490 nm. CCP was then added dropwise to the metal ion treated NP solution. The emission spectra were collected again upon excitation of the CCP at 370 nm. Similar procedures have been used for assay sensitivity study.

6.3 Results and discussion

6.3.1 Strategy for the fluorescence turn-on mercury(II) assay based on conjugated polymers and silica NPs

The Hg^{2+} detection method is shown in Scheme 6.1. The assay begins with probe (NH_2-DNA, 5'-NH_2-GTGACCATTTTGCAGTG-3') immobilized silica nanoparticles (NPs) in solution. After hybridization with fluorescein (Fl) labelled DNA (Fl-DNA, 5'-Fl-CACTGCATTTTGGTCAC-3'), double-stranded DNA (dsDNA) containing three pairs of T-T mismatches is formed on the NP surface. The recognition is accomplished by Hg^{2+}-specific coordination between the T-T mismatches on the silica NPs (Hg^{2+}, shown in oval; non-specific ions, shown in triangle). In the presence of Hg^{2+}, T-Hg^{2+}-T complexation increases the melting temperature (T_m) of the resulting duplex, and Fl-DNA remains on the NP surface during thermal wash. In contrast, the non-specific ions can not form stable metal-DNA complex, and the duplex will denature during thermal wash, leaving weak or no fluorescent signals on the NP surface. In the final step, addition of CCP leads to amplified fluorescence signal of the Fl-DNA remained on the NP surface.

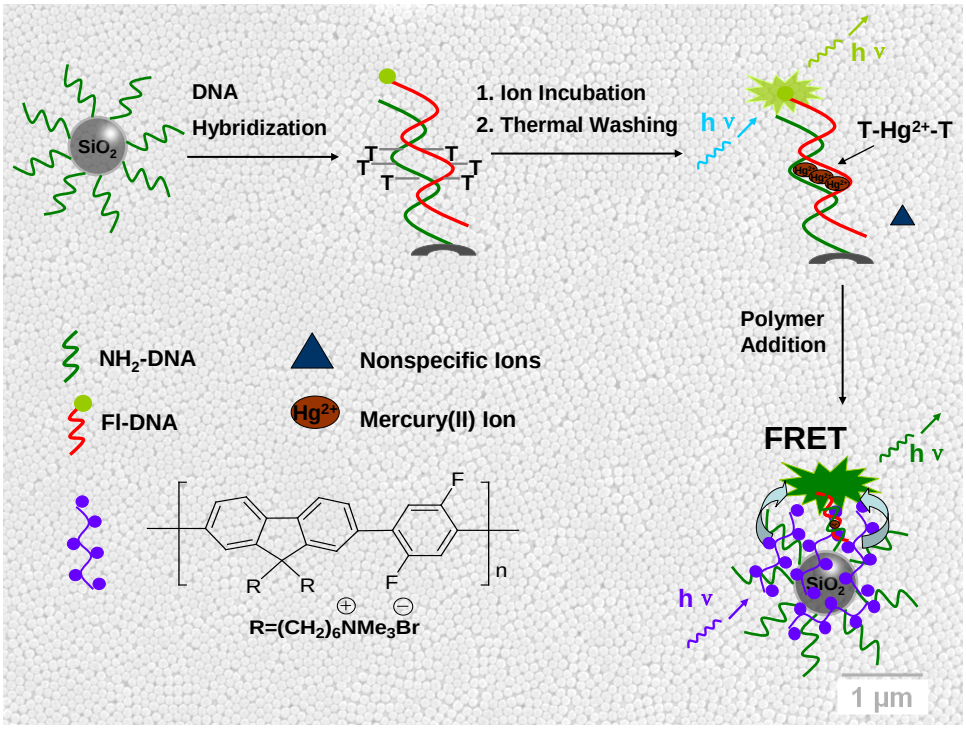

Scheme 6.1 Schematic illustration of a CCP-amplified fluorescence turn-on sensor for mercury(II) detection.

The CCP (structure shown in Scheme 6.1) and Fl used in this study were selected to have matched molecular orbital energy levels and good spectral overlap so that efficient FRET could occur [80]. Monodispersed silica NPs (~100 nm in diameter, FE-SEM images shown in Figure 3.2 and Figure 3.3) were chosen to allow separation and washing steps. The synthesis and modification of NPs are according to the previous report [219]. The probe pair of 5'-Fl-CACTGCATTTTGGTCAC-3' and 5'-NH_2-GTGACCATTTTGCAGTG-3' is specially chosen to allow efficient hybridization and meanwhile a large difference in T_m for the duplex before and after Hg^{2+} treatment. According to the previous report [210], the duplex with three pairs of T-T mismatch has a melting temperature of 43 ^oC, which increases to 61 ^oC upon treatment with excess Hg^{2+}. At 45 ^oC, there is no denaturation observed for the duplex containing three pairs of T-Hg^{2+}-T, while the duplex with three

T-T mismatches is almost completely denatured [210]. This result allows us to conduct thermal wash at 45 ^{o}C to selectively remove the hybridized Fl-DNA molecules from the NP surface in the presence of non-specific ions.

6.3.2 Preparation of hybridized DNA-NP bioconjugate

The oligonucleotide modified NPs have ~110 NH_2-DNA molecules on each NP. The number of DNA is calculated from the absorbance difference at 260 nm for the DNA solution before immobilization and the supernatant after immobilization, considering that 1.0 mg of 100 nm NPs contain ~1×10^{12} number of NPs [219]. After hybridization and centrifugation, the extent of hybridization is measured from the fluorescence difference between the Fl-DNA solution before hybridization and the supernatant after hybridization. On the average, there are ~64 Fl-DNA molecules captured by a single ssDNA-NP, which corresponds to a hybridization efficiency of ~60%. For 0.1 mg dsDNA-NP in 100 µL solution, the Fl-DNA has a concentration of ~0.103 µM, hence the perfect formation of three pairs of T- Hg^{2+}-T within each duplex requires at least ~0.31 µM [Hg^{2+}]. The hybridized NPs (dsDNA-NP) are further used for metal ion detection.

6.3.3 Fluorescence mercury(II) assay using the hybridized DNA-NPs

We first investigated the Fl emission of metal ion treated NP solution after thermal wash at 45 °C. Upon excitation at 490 nm, the Fl showed an emission maximum at 522 nm in 25 mM PBST buffer (Figure 6.1). Figure 6.2 shows the Fl emission intensity at 522 nm for dsDNA-NP suspensions (0.1 mg/mL) after the NPs were treated with different metal

ions at different concentrations, which was followed by thermal wash at 45 °C. The metal ions include Hg^{2+} and the nonspecific ion mixture, which contains Ag^{+}, Mg^{2+}, Co^{2+}, Ni^{2+}, Ba^{2+}, K^{+}, Pb^{2+}, and Cd^{2+} with each ion of the same concentration as that of Hg^{2+}. As shown in Figure 6.2, a sigmoidal working curve for Hg^{2+} in the concentration range of 0.1 μM to 3 μM is observed. The maximum transition in Fl emission intensity is observed at [Hg^{2+}] ~0.31 μM, where the [Hg^{2+}] is nearly three-fold as that for the concentration of DNA duplex (each probe contains three Hg^{2+} binding cites) bound to NPs, indicating nearly perfect formation of three pairs of T-Hg^{2+}-T within each duplex. Further decrease of the [Hg^{2+}] to lower than 0.1 μM resulted in large variations in Fl fluorescence intensity, which was not shown in the curve. When the same experiment was done for the nonspecific ion mixture, the solution fluorescence intensity was about one third as compared to that in the presence of Hg^{2+}. In addition, the solution fluorescence intensity did not change obviously with ion mixture concentrations. Direct excitation of the NH_2-DNA immobilized NPs with the same concentration as that of the dsDNA-NP (0.1 mg/mL) reveals that the solution fluorescence in the absence of Hg^{2+} is mainly from the silica NPs. We also compared the dsDNA-NP treated by Hg^{2+} (Hg^{2+}: 0.3 μM) and the one treated by mixed ions including Hg^{2+} (Hg^{2+}: 0.3 μM; non-specific mixture of Ag^{+}, Mg^{2+}, Co^{2+}, Ni^{2+}, Ba^{2+}, K^{+}, Pb^{2+} and Cd^{2+}: 3 μM for each ion). The results of the two treatments are similar to each other (see Figure 6.1), suggesting the selectivity of the assay for Hg^{2+}. Although comparison of the NP solution fluorescence intensity in the presence and absence of Hg^{2+} (shown in Figure 6.2) indicates the selectivity of the assay for Hg^{2+} detection, the absolute solution fluorescence intensity is rather low and the difference between Hg^{2+} and other metal ions is small.

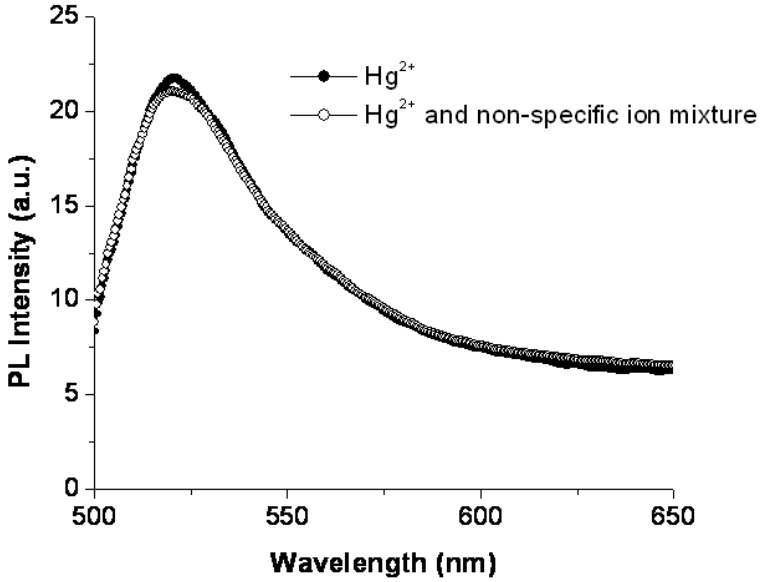

Figure 6.1 Fl emission spectra of metal ion treated dsDNA-NP in 25 mM PBST buffer upon excitation of FL at 490 nm, which showed a maximum emission peak at 522 nm. [Hg^{2+}] = 0.3 μM, non-specific ion mixture of Ag^{+}, Mg^{2+}, Co^{2+}, Ni^{2+}, Ba^{2+}, K^{+}, Pb^{2+} and Cd^{2+}: 3 μM for each ion. [NP] = 0.1 mg/mL. The result of treatment by Hg^{2+} is shown in dots, and the treatment by mixed ions including Hg^{2+} is shown in circles.

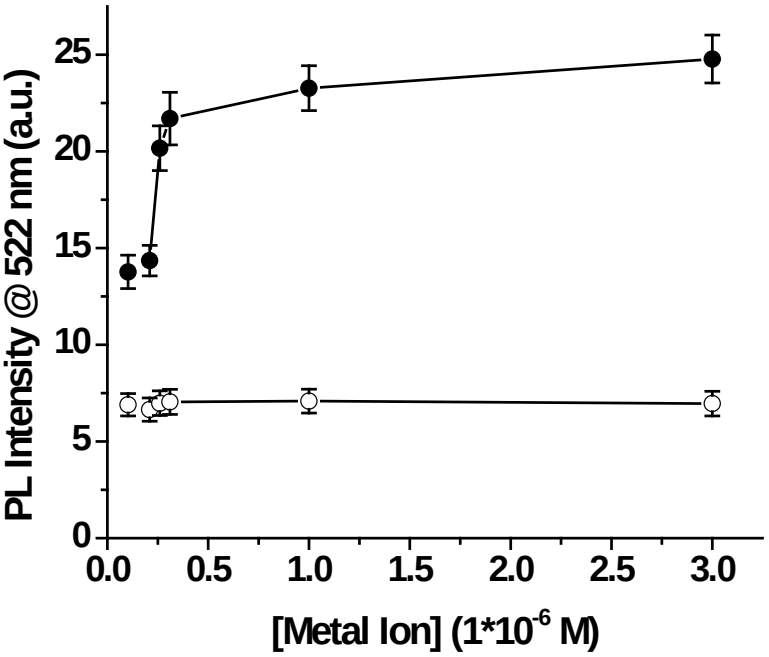

Figure 6.2 The maximum fluorescence intensity at 522 nm for dsDNA-NP suspensions as a function of metal ion concentration after thermal wash at 45 °C. Hg^{2+} is shown in solid circles and the mixture of Ag^{+}, Mg^{2+}, Co^{2+}, Ni^{2+}, Ba^{2+}, K^{+}, Pb^{2+} and Cd^{2+} is shown in hollow circles. Each metal ion has the same concentration as that of Hg^{2+}. Measurement was done in 25 mM PBST buffer upon excitation of Fl at 490 nm. [NP] = 0.1 mg/mL. The data are the average of three independent measurements with error bars indicated.

6.3.4 Conjugated polymer sensitized fluorescence mercury(II) detection

We then employed the CCP to amplify the Fl signal of metal ion treated NP solutions (0.1 mg/mL). For each solution, different amount of CCP was added until the Fl emission intensity reached the maximum through FRET. Upon excitation of the polymer at 370 nm, the maximum Fl emission wavelength was observed at 531 nm (see Figure 6.3), which was slightly red-shifted by 9 nm as compared to that upon direct excitation of Fl at 490 nm (see Figure 6.1). Figure 6.4 shows the polymer sensitized Fl emission intensities at 531 nm for NP solutions treated with metal ions (Hg^{2+} or the ion mixture) in the concentration range of 0.1 to 3 μM. In comparison with the Hg^{2+} detection under direct excitation of Fl at 490 nm (Figure 6.2), the polymer sensitized detection also shows a similar sigmoidal working curve with the maximum transition in Fl emission intensity occurred at [Hg^{2+}] of ~0.31 μM. However, for each solution, the polymer sensitized Fl emission intensity is ~20 fold higher than that upon direct excitation of Fl at 490 nm in the absence of the polymer, indicating signal amplification provided by the CCP. On the other hand, the polymer sensitized fluorescent signal from NP treated with nonspecific ion mixtures remains weak. The low signal for non-specific ions is due to the limited number of Fl-DNA remained on the NP surface after thermal wash. When one compares Figure 6.2 and Figure 6.4, the presence of CCP amplifies the detection signal, and the intensity ratio of non-specific ions relative to specific mercury(II) decreases from ~1/3 (without CCP) to ~1/6 (with CCP). Therefore, there is an obvious improvement in detection selectivity when the CCP is used as the energy donor (Figure 6.4).

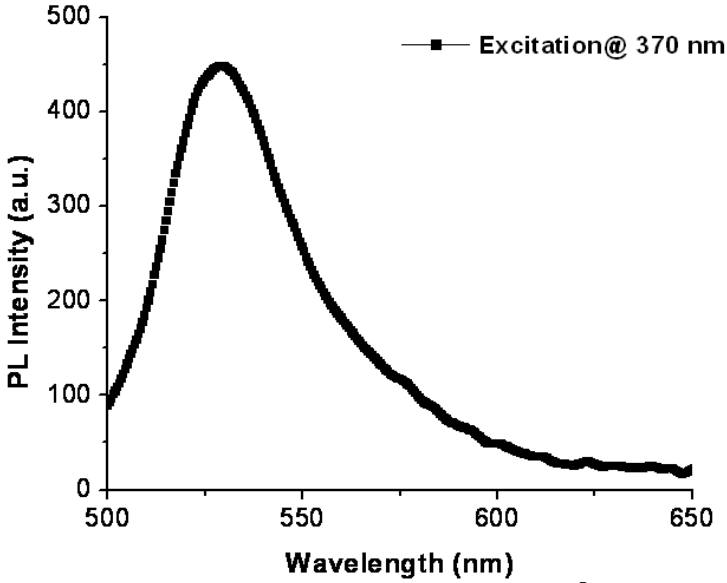

Figure 6.3 Polymer sensitized Fl emission spectrum for Hg^{2+} treated dsDNA-NP in 25 mM PBST buffer upon excitation of CCP at 370 nm, which shows an emission maximum at 531 nm. Measurement was done with [NP] = 0.1 mg/mL and [Hg^{2+}] = 0.31 µM.

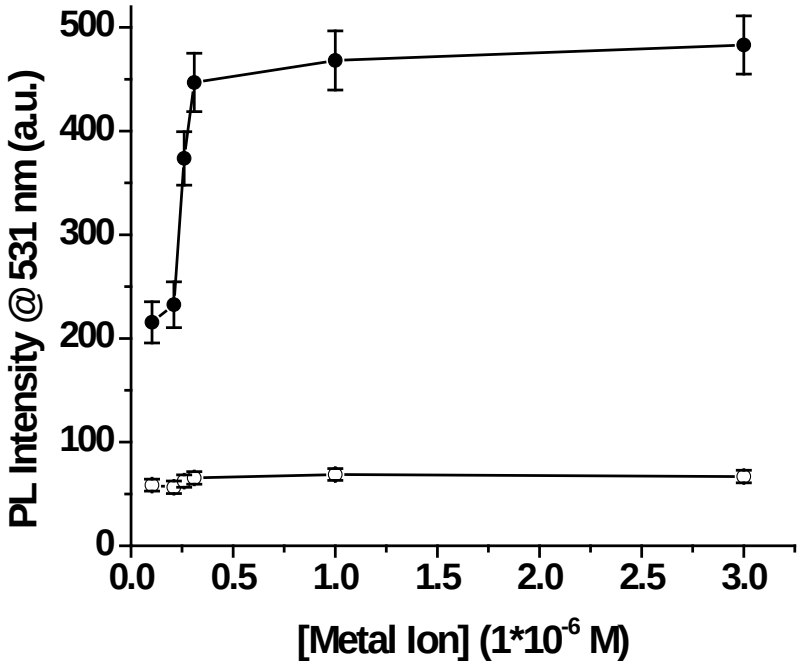

Figure 6.4 The CCP sensitized Fl emission intensity at 531 nm for dsDNA-NP suspensions as a function of metal ion concentration after thermal wash at 45 °C. Hg^{2+} is shown in solid circles and the mixture of Ag^{+}, Mg^{2+}, Co^{2+}, Ni^{2+}, Ba^{2+}, K^{+}, Pb^{2+} and Cd^{2+} is shown in hollow circles. Each metal ion has the same concentration as that of Hg^{2+}. Measurement was done in 25 mM PBST buffer upon excitation of CCP at 370 nm. [NP] = 0.1 mg/mL. The data are the average of three independent measurements with error bars indicated.

6.3.5 Fluorescence mercury(II) detection at [Hg^{2+}]/[DNA duplex] = 3/1

To understand the sigmodial working curve of the Hg^{2+} assay, Hg^{2+} detection experiments were conducted by simultaneously varying the concentration of Hg^{2+} and NP, while keeping [Hg^{2+}]:[DNA duplex] = 3:1. A linear curve for Fl emission intensity at 522 nm *vs.* [Hg^{2+}] is observed upon direct excitation of Fl at 490 nm in the absence of the polymer (Figure 6.5). On the other hand, upon addition of the CCP to solutions containing NPs treated with different concentrations of Hg^{2+} ([Hg^{2+}]:[DNA duplex] = 3:1), the polymer sensitized maximum Fl emission spectra are shown in Figure 6.6. The corresponding Fl emission intensity at 531 nm *vs.* [Hg^{2+}] is shown in Figure 6.7. A linear relationship between the solution fluorescence intensity and [Hg^{2+}] was observed in the concentration range of 0 to 465 nM. Based on the signal over noise ratio (S/N>3), we thus estimate that the detection limit could reach as low as ~5 nM. However, this strategy requires the prerequisite of [Hg^{2+}]:[DNA duplex] $\geq$ 3:1, which is not practical for Hg^{2+} detection in unknown samples.

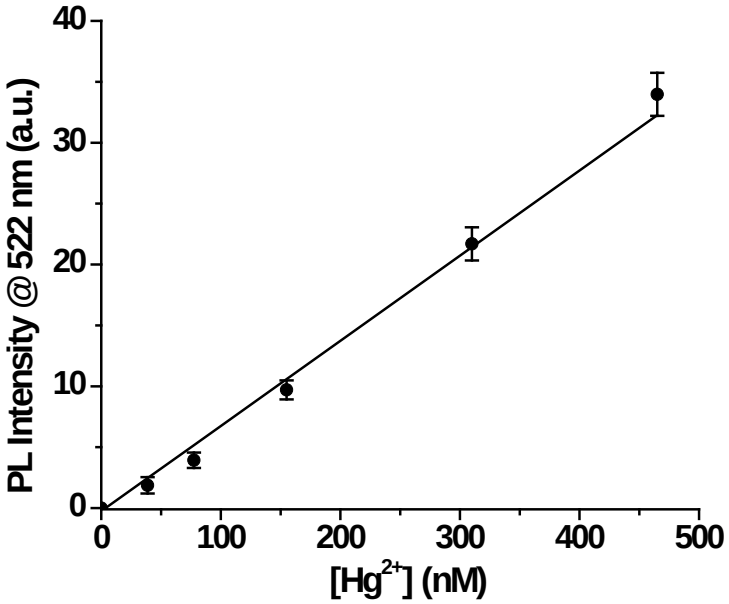

Figure 6.5 The Fl emission intensity at 522 nm for Hg^{2+} treated dsDNA-NP as a function of [Hg^{2+}]. The assay simultaneously varies [Hg^{2+}] and [NP] while keeping the [Hg^{2+}]:[DNA duplex] = 3:1. Measurement was done in the 25 mM PBST buffer upon excitation of Fl at 490 nm. The data are the average of three independent measurements with error bars indicated.

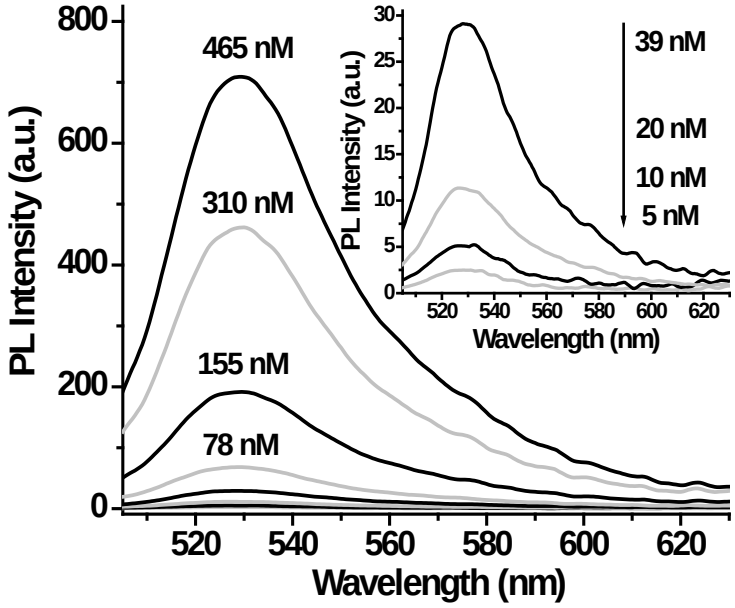

Figure 6.6 The CCP sensitized maximum Fl emission spectra for dsDNA-NP upon treatment with different [Hg^{2+}] after thermal wash at 45 °C. Inset: the enlarged spectra at low [Hg^{2+}]. The assay simultaneously varies [Hg^{2+}] and [NP], while keeping [Hg^{2+}]:[DNA duplex] = 3:1. Measurement was done in 25 mM PBST buffer upon excitation at 370 nm.

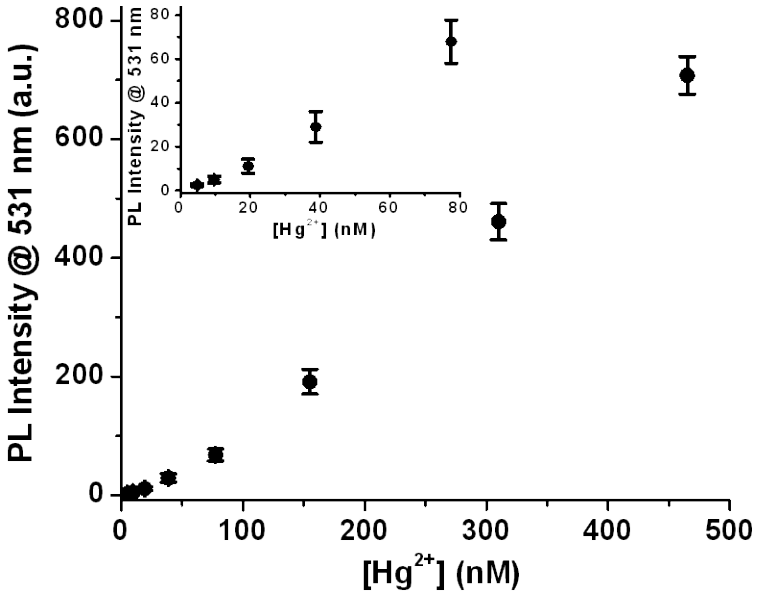

Figure 6.7 The maximum Fl emission intensity at 531 nm as a function of [Hg^{2+}]. Inset: the enlarged figure at low [Hg^{2+}] range. The assay simultaneously varies [Hg^{2+}] and [NP], while keeping [Hg^{2+}]:[DNA duplex] = 3:1. Measurement was done in 25 mM PBST buffer upon excitation at 370 nm. The data are the average of three independent measurements with error bars indicated.

The linear response between the Fl emission intensity *vs.* [Hg^{2+}] is thus dependent on whether all three Hg^{2+} binding cites in each probe are simultaneously involved in T-Hg^{2+}-T formation. While a sigmoidal working curve is obtained for random distribution of Hg^{2+} among the multiple binding sites in mercury-specific probes. A similar sigmoidal working curve was also reported for many other assays for Hg^{2+} detection. For doubly labelled mercury-specific probes [206], the response of the probe to Hg^{2+} was slow at the initial stage, which was ascribed to several Hg^{2+} ions binding to one probe molecule to induce the conformational change. For the DNAzyme-based assay [215], Hg^{2+} sensing was a cooperative process since Hg^{2+} is bound to multiple binding sites of DNAzyme, and the cleavage of the DNAzyme was estimated to occur when two out of five Hg^{2+} binding sites were bound to Hg^{2+}. For the room temperature Au NP based colorimetric assay

[214],[13] competition between the polyT probe hybridization and T-Hg^{2+}-T complexation easily led to random distribution of Hg^{2+} along the probe. On the other hand, Mirkin's group has developed an assay which uses an oligonucleotide probe containing only a single Hg^{2+} binding site for Hg^{2+} detection [213]. This assay allowed specific Hg^{2+} binding to form T-Hg^{2+}-T complex and resulted in a linear working curve for [Hg^{2+}] ranging from 0 to 2.0 μM. This result is similar to our data shown in Figure 6.5 and Figure 6.7. Suitable probe design will help us to circumvent the complicate interaction between Hg^{2+} and multiple binding sites to yield more accurate Hg^{2+} detection and quantification methods.

6.4 Conclusions

In summary, we have demonstrated a fluorescence turn-on assay for mercury(II) detection, which takes advantage of signal amplification of fluorescent conjugated polymers and silica NP based detection in addition to the specific thymine-Hg^{2+}-thymine interaction. By maintaining a constant NP concentration, while varying [Hg^{2+}], the working curve of mercury(II) shows a sigmoidal shape and gives a detection limit of 0.1 μM. However, by simultaneously reducing the NP and Hg^{2+} concentration, and keeping [Hg^{2+}]:[DNA duplex] = 3:1, a linear calibration curve for Hg^{2+} was observed with a detection limit of 5 nM in the presence of the CCP. The linear response between the Fl emission intensity *vs.* [Hg^{2+}] is dependent on whether all three Hg^{2+} binding sites in each probe are simultaneously involved in T-Hg^{2+}-T formation. While a sigmoidal working curve is obtained for random distribution of Hg^{2+} among the multiple binding sites in

mercury-specific probes. The use of CCP significantly enhances the detection selectivity and reduces false-positive signals.

Nevertheless, the developed mercury(II) sensing system needs 45 °C for thermal washing, which is not convenient compared with room-temperature operation. Recent advance on mercury(II) detection has shown the possibility of room-temperature assay through appropriate probe design [214]. Further improvement in the probe design in silica NP-supported format could yield efficient metal ion sensors operated at convenient temperature [212, 214].

CHAPTER 7

LAYER-BY-LAYER ASSEMBLY OF METAL-ENHANCED FLUORESCENCE (MEF) CONJUGATED POLYMER THIN FILMS FOR DNA DETECTION

7.1 Introduction

Highly sensitive and selective DNA detection is a continuous demand in quantitative studies for biomedical research [131,132]. Various detection systems have been developed in response to this demand, such as optical [10,11,134], electrochemical [135,136], microgravimetric [137,138]. Among different strategies, nanostructure based methods have been recently geared into the above systems to further harness detection performance [19,20,22-24,45,176].

Metal-enhanced fluorescence (MEF), constructed on metallic nanostructures, have recently received considerable attention as it can be used to increase the sensitivity of fluorescent sensors [22-24]. MEF reflects the interactions of the excited-state fluorophores with surface plasmon electrons in the metallic nanostructures such as silver [46,47], gold [48,49], and alumina [50], which in turn produce different effects on the fluorophores [22-24]. The overall fluorescence enhancement or quenching for a given system depends on the relative contributions among excitation rate enhancement (field enhancement), emission enhancement (radiative decay enhancement) and quenching (nonradiative decay enhancement) [22-24,51,52]. These contribution factors are sensitive to various parameters

such as the spectral properties of both fluorophores and metal nanoparticles (NPs) [53], the distance between fluorophores and metal NPs [54,55], and the orientation of fluorophores relative to metal NPs [55]. Understanding and controlling the fluorophore-metal interaction is critical to develop and improve various MEF-based applications such as biosensor, LEDs, and single-molecule studies [22-24,55,220,221]. Current reports about MEF in different systems include field enhancement [222-224], emission enhancement [225-227], or both [228,229]. However, few reports address the MEF for the system of large chromophores such as water-soluble conjugated polymers.

Water-soluble conjugated polymers (CPs) are macromolecules that contain π-delocalized backbones with pendant ionic groups, which have been widely used in chemical and biological sensors [26-28,30,218,230]. Their large absorption cross section and delocalized electronic structure allow efficient light-harvesting and rapid intra- and interchain fluorescence resonance energy transfer (FRET). This results in huge signal amplification upon molecular-recognition events, and imparts the CP-based sensor higher fluorescence intensity relative to small molecule counterparts [25-29,218]. This high response signal is essential to achieve high detection sensitivity for various fluorescence-based detection systems, and would enable probing samples with lower concentrations. To the aim of sensitive detection, great efforts have been made to develop the CP-based DNA detection, but few reports on MEF of CP [231] and, from our best knowledge, no report on MEF-CP based bioassay. This may be primarily because of 1) difficulty in fine-tuning of nanoscale distance between metal surface and CP chromophores, 2) poor understanding of MEF as a strategy for CP-based bioassays, and 3) lack of suitable experimental design and

protocol. Therefore, the development of MEF platform for CP and its application in DNA assays is highly desirable to further enhance biosensing capability.

In Chapter 7, we report a new strategy to prepare a CP-based MEF substrate, and successfully apply the MEF-CP substrate to sensitive and selective DNA detection. In our approach, layer-by-layer (LbL) process was used to fine control the nano-scale distance between silver NP surface and CP fluorophore using non fluorescent polymers (PDDA & PSS) as the spacer. Furthermore, a cationic, fluorescent, water-soluble polyfluorene derivative, poly[9,9-bis(9-*N*,*N*,*N*-trimethylammonium)ethoxy)ethoxy)ethyl)fluorene-*alt*-(4,7-(2,1,3-benzothiadiazole)dibromide)] (PFBT) [232], was selected for MEF study. Our previous studies demonstrated that biosensors using PFBT derivatives are effective in either solution [29,232,233] or solid state [90,234]. The extension of PFBT to MEF study is an effective strategy to further enhance DNA detection sensitivity and expand our established biosensing systems [29,90,232-234]. Moreover, the optical property of two PFBT absorption peaks (335 nm and 450 nm) provides an internal standard to better investigate MEF without considering the amount difference of PFBT on reference and sample slide. Finally, the first application of MEF-PFBT substrate in DNA detection was successfully demonstrated, which opens up new possibilities to improve the detection sensitivity of CP-based bioassays.

7.2 Materials and methods

Materials

The fluorescent cationic conjugated polymer (PFBT) was synthesized according to a previous report [232]. DNA oligonucleotides were purchased from IDT including Cy5-PNA: 5'-Cy5-OO-TCC ACG GCA TCT CA-Lys-Lys-3', complementary DNA (DNA_c): 5'-TGA GAT GCC GTG GA-3', and non-complementary DNA (DNA_{nc}): 5'-GGT CAT TAG CTT CT-3'. Poly(diallyldimethylammonium chloride) (PDDA) (medium molecular weight: 200,000-350,000; 20 wt% in water, Aldrich), Poly(styrene sulfonic acid) sodium salt (PSS) (M.W. 70,000; Alfa-aesar), 1-methyl-2-pyrrolidinone (NMP) (99.5+%, Biotech grade, Sigma-Aldrich), silver nitrate (sigma-aldrich, reagent plus, >99.8%), sodium citrate tribasic dihydrate (sigma, ACS reagent, ≥99.0%), sodium chloride (>=99.5%, Sigma), 3-aminopropyltriethoxysilane (APTES, 99%, Aldrich), sulphuric acid (98.0%, BDH), acetic acid (100%, Merck), methanol (99.8%, Merck), ethanol (99.9%, Merck), hydrogen peroxide (30%, Merck), ammonia solution (30%wt, SINO Chemical Company), phosphate buffered saline (PBS, 1500 mM), transparent waterproof tape (polar bear), glass microscope slide (VFM microscope slide, 26 × 76 mm, 1.0-1.2 mm; CellPath) and silicon wafer (dopant and one-side polished; Φ 100 ± 0.5 mm) were used as received. MilliQ water (18.2 MΩ) was used to prepare all solutions.

Characterization and instrumentation

The extinction spectra of silver colloid were measured by a Shimadzu UV-1700 spectrometer. The prepared silver colloid was characterized by field-emission scanning electron microscopy (FE-SEM) on a JEOL JSM-6700F operating at 5 kV, and by

transmission electron microscopy (TEM) on a JEOL JEM-2010F operating at 200 kV. The assembled Ag NP arrays on glass slides were imaged by FE-SEM after coating a Pt layer (~10 nm in thickness) via a platinum coater (JEOL JFC-1300, Auto Fine Coater), and by atomic force microscope (AFM) (Nanoscope III, Digital Instruments) operating in the tapping mode with a silicon tip. The thickness of the polymer films was measured on the surface of similarly prepared polished silicon wafer by using a spectroscopic ellipsometer (VB-250, VASE Ellipsometer, J. A. Woollam Co., Inc) after drying the samples. A wavelength ranging from 500 to 1000 nm and angles of incident light (65 and 75 °) were used for the spectroscopic ellipsometer, which was equipped with a 75 W light source and a high-speed monochromator (HS-190, J. A. Woollam Co., Inc). For each sample, three different locations were measured and the thickness was obtained by using the software provided by the manufacturer. The silver ion concentration was determined by ICP-MS (Agilent, 7500A ICPMS).

The absorbance change of PFBT solution before and after slide assembly was monitored by MicroplateReader (TECAN Infinite M200). Similar monitoring process was done for Cy5-PNA/DNA duplex solution before and after slide assembly. All sample slides were placed onto the bottom of 24-well mciroplates for the measurements of corresponding spectra using the MicroplateReader operated in the top reading mode. The fluorescence emission spectra of sample slides under different excitation wavelength were recorded. The excitation spectra for PFBT polymer on slide surface were obtained at a fixed emission wavelength of 550 nm. After the Cy5-PNA/DNA duplex assembly, fluorescence emission spectra of sample slides under the excitation of 335 and 440 nm were recorded over a range of 480 to 800 nm, and Cy5 emission spectra were collected

under the excitation of 645 nm for sample slides and 600 nm for Cy5 solution. All spectra of sample slides were measured in MilliQ water and corrected after subtraction of the corresponding background.

Experimental methods

Silver NP synthesis in aqueous solution

The silver NPs were synthesized according to the procedure described in Chapter 3.

Surface functionalization of glass slides

The microscope glass slides were cut into 7 mm × 12.5 mm dimension and pre-washed by detergent, water, ethanol upon sonication for 10 min in each step. The slides were then treated in piranha solution (H_2O_2 : concentrated H_2SO_4 = 1: 3) at 80 °C for 30 min, followed by RCA (H_2O: H_2O_2: NH_3 (v: v: v) = 5: 1: 1) treatment via 30 min sonication without temperature control. A rinse cycle of water-ethanol-water was done between different steps. After that, the pre-cleaned slides were dried and immersed in silane solution (2% APTES in methanol mixture (methanol, 95%; MilliQ water, 5%; acetic acid, 0.1%)) with gentle shaking for 30 mins to introduce NH_2-functinoal groups on slide surface. After that, the slides were rinsed with ethanol, sonicated for 2 min, and stored in ethanol for further process.

Silver nanoparticle (NP) self-assembly on NH_2-functionalized slide

Before silver NP assembly, the pretreated glass slides were dried with nitrogen gas and one side of slides was covered by a water-resistance & transparent adhesive tape. The

tape-patterned glass slides were rinsed thoroughly with deionised water and dried with nitrogen gas. Meanwhile, 60 µl of stock silver colloid is added into 540 µL MilliQ water in a plate well. The treated slides were then loaded into the silver colloid with the uncovered surface up while gently shaking overnight to form Ag NP arrays. The self-assembled Ag NP arrays were rinsed with water, and stored in 800 µL of citrate solution (0.342 mg/mL) in a 24-well microplate for UV/PL measurements by Tecan MicroplateReader. Typically, the prepared good Ag NP array has an extinction maximum of ~0.35 at 440 nm.

Layer-by-layer (LbL) self-assembly of charged polymers

LbL assembly of PSS/PDDA on NH_2-functionalized glass or Ag NP array slide was carried out manually. For Ag NP array slide, the substrates were immersed in 800 µL PDDA solution (PDDA concentration was based on polymer repeat unit (RU), [RU] = 1×10^{-2} M in 0.1 M NaCl aqueous solution) for 15 min, followed by a wash in water, and immersed again in the PSS solution (PSS concentration was based on polymer repeat unit (RU), [RU] = 1×10^{-2} M in 0.1 M NaCl aqueous solution) for 15 min, followed a wash in water. Multilayer assemblies consisting alternating charged layers of PDDA and PSS were prepared by consecutive adsorption of both polyelectrolytes. The final layer is always PSS layer to ensure negative charges on the top of multilayer assemblies based on NH_2-slide or Ag NP array slide. Finally, cationic PFBT deposition is conducted by incubating the above anionic slides in PFBT solution (PFBT concentration was based on polymer repeat unit (RU), [RU] = 2.5 µM, 800 µL) for 5 minute. After washing with

MilliQ water, the prepared slides were stored in 800 µL of water in a 24-well microplate for UV/PL measurements by Tecan MicroplateReader.

Adhesive layer deposition

After PFBT self-assembly, the obtained slides were assembled with one more layer of PDDA operated in the same condition as the previous step. After washing with water, these prepared slides were then immersed in incubation buffer (25mM PBS and 5% NMP) for DNA assay.

Annealing of Cy5-PNA and DNA

For DNA detection, Cy5-PNA (sequence: 5'-Cy5-OO-TCC ACG GCA TCT CA-Lys-Lys-3') and DNA_c (sequence: 5'-TGA GAT GCC GTG GA-3') were first mixed together in the incubation buffer to form duplex structure (12 µM for Cy5-PNA or DNA_c). Meanwhile, Cy5-PNA was mixed with DNA_{nc} (sequence: 5'-GGT CAT TAG CTT CT-3') in the incubation buffer (12 µM for Cy5-PNA or DNA_{nc}). These mixed solutions were then heated up to 80°C for 10 min, followed by naturally cooling to RT. The formed DNA_c duplex (Cy5-PNA hybridized with DNA_c) and DNA_{nc} mixture (Cy5-PNA mixed with DNA_{nc}) are stored in 4 °C refrigerator for further use.

DNA assay on PFBT film

For PFBT film-based DNA detection, the annealed Cy5-PNA/DNA mixture was diluted with incubation buffer to 300 µL to yield [DNA_c] or [DNA_{nc}] = 10^{-7} M. The assay slides were then incubated in the above mixture for 15 min. After washing with the incubation

buffer, the treated slides were placed into 800 µL of water in a 24-well microplate for UV/PL measurement by Tecan MicroplateReader.

7.3 Results and discussion

7.3.1 Strategy of layer-by-layer (LbL) preparation of MEF-PFBT substrate for DNA detection

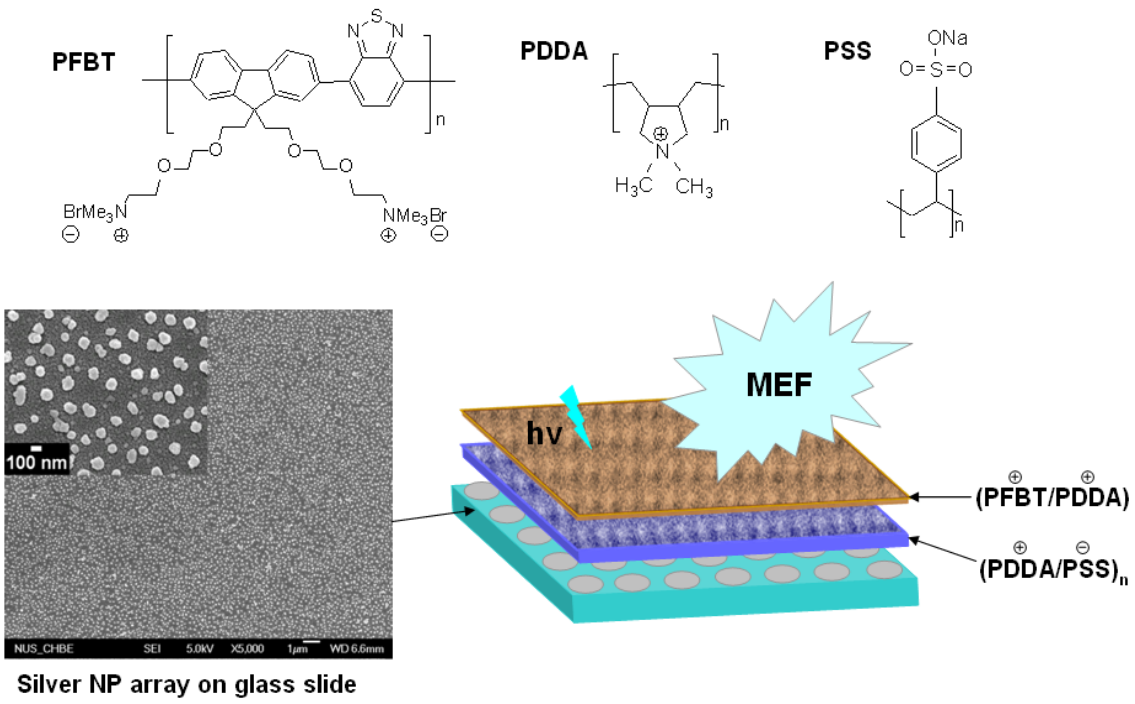

Scheme 7.1 Schematic illustration of layer-by-layer (LbL) preparation of MEF substrate for DNA detection, with the molecular structures of PFBT, PDDA and PSS, as well as the FE-SEM images of the silver NP array on the glass slide after coating a thin conductive Pt layer (~10 nm in thickness).

Scheme 7.1 shows the general strategy for MEF based DNA detection via layer-by-layer (LbL) self-assembly process driven by electrostatic interaction. The MEF substrate

preparation starts with immobilization of negative charged silver NP onto the surface of NH_2-functionalized glass slide. A polyelectrolyte layer-by-layer (LbL) process using poly(diallyldimethyl ammonium chloride) (PDDA) and poly(sodium 4-styrenesulfonate) (PSS) is then used to fine tune the nano-scale distance between the silver NPs and the PFBT layer. The prepared MEF-PFBT slide is further assembled with a thin layer of PDDA to increase the positive charge density on the top surface, and is ready for DNA bioassay.

7.3.2 MEF-PFBT platform components

The MEF-PFBT platform is composed of multiple key components, as shown in Scheme 7.1. Silver NPs were synthesized using a modified Lee–Meisel method [128]. After purification by centrifugation and filtration, the collected silver NPs showed a diameter of ~ 75 nm in average (see Figure 3.4 and Figure 3.5) with an extinction peak ~ 440 nm (see Figure 3.6). These silver NPs carry negative surface charges due to the adsorbed citrate molecules, which allow easy binding onto a NH_2-functionalized slide surface to form silver NP array. Typically, the prepared silver NP arrays supported by a transparent microscopy glass slide had an extinction maximum intensity of ~0.35 at ~440 nm in the wet state. After drying the silver NP array, the FE-SEM images (see Scheme 7.1) from the resulting surface show the interparticle distance of ~200 nm and no obvious aggregation. This indicates strong binding between NH_2-functionalized slide and citrate adsorbed silver NPs.

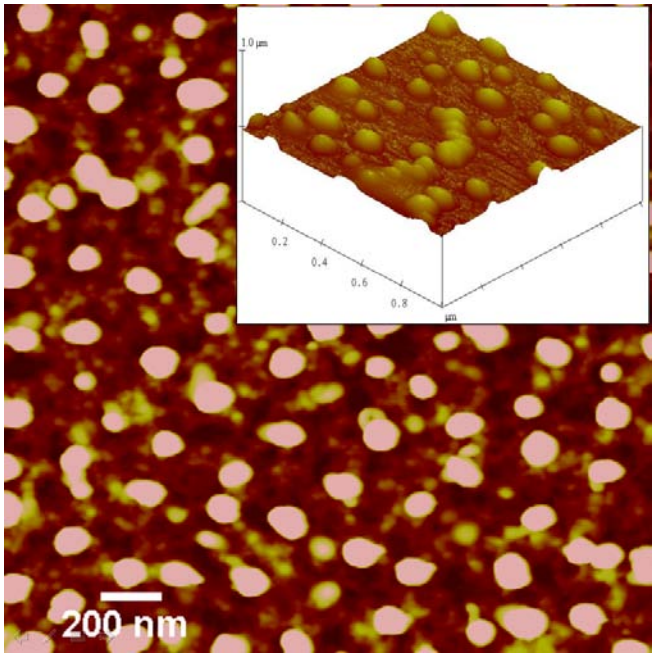

Figure 7.1 AFM images of the Ag NP array slide (PFBT/$(PDDA/PSS)_2$/Ag NP array). Inset: the three-dimensional image of the same slide.

Molecular structures of the PFBT, PDDA and PSS polymers are shown in Scheme 7.1. Due to the intrinsic charge from these polymers, electrostatically-driven LbL process could be used to construct the silver NP array-PFBT films using alternate charged polymers (PDDA & PSS) as the spacer. Figure 7.1 shows the AFM images of Ag NP array slide (PFBT/$(PDDA/PSS)_2$/Ag NP array) from the resulting surface in the dry state, indicating relatively ordered NP array structure with rough surface. Figure 7.2 shows the absorption and photoluminescence (PL) spectrum of the cationic PFBT film in water, as well as the extinction spectrum of Ag NP array in water. This BT-containing copolymer of PFBT bears two solid-state absorption peaks (335 nm and 450 nm). The Ag NP array plasmonic band at ~440 nm overlaps significantly with the low energy PFBT band at 450 nm and only weakly with the high energy PFBT band at 335 nm with the higher transition. Such selective overlap provides an excellent opportunity to dissect the MEF

contributions through monitoring PFBT fluorescence, in the presence and absence of the Ag NP array, as a function of excitation wavelength. This constitutes one of key reasons why PFBT conjugated polymer instead of others is selected for this study.

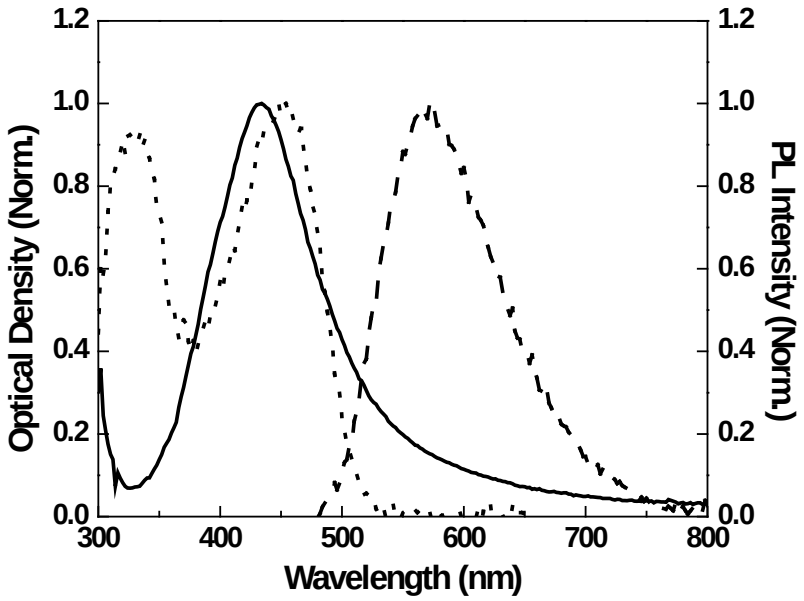

Figure 7.2 The absorption spectrum (dotted line) and photoluminescence (PL) spectrum (dashed line) of the cationic PFBT film in water, and the extinction spectrum (solid line) of silver NP array in water. The excitation wavelength is 335 or 440 nm for the PFBT.

7.3.3 Metal-enhanced fluorescence of PFBT with underlying Ag NP array

To study MEF of PFBT, we first prepared two types of slides bearing similar amount of PFBT with the polyelectrolyte spacer $(PDDA/PSS)_n$ (n=1-4): Ag NP array slide and the reference slide (without the Ag NP array). Conditions used for self-assembly were strictly same for each substrate. The size of each substrate was kept constant (~87.5 mm^2), and the net quantity of PFBT adsorbed on each substrate was controlled to be nearly the same by monitoring the absorbance change of a PFBT stock solution before and after assembly on slide surface (see the typical example in Figure 7.3).

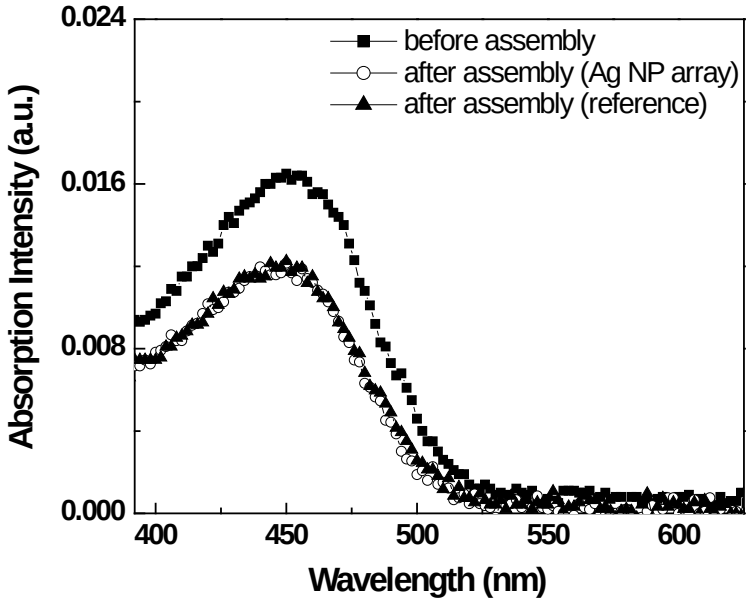

Figure 7.3 The absorption spectra of PFBT solution (2.5 μM in MilliQ water, 800 μL) before and after PFBT assembly onto the Ag NP array slide (PFBT/$(PDDA/PSS)_2$/Ag NP array) and the reference slide (PFBT/PSS/PDDA/PSS/NH_2-glass).

Based on the above, the photoluminescence (PL) spectra of the two types of PFBT slides were then collected and analyzed. Figure 7.4A shows the PL spectra of PFBT, when the wavelength of excitation is 440 nm, on the reference slide (PFBT/PSS/PDDA/PSS/NH_2-glass) and Ag NP array slides (PFBT/$(PDDA/PSS)_n$/Ag NP array) as the number of PDDA/PSS spacer bilayers (n) is varied from 1 to 4. As compared to the PL intensity from PFBT adsorbed on reference slides, the initial build-up of the spacer from one to two bilayers causes a 3-fold increase of the PFBT emission intensity. The PL intensity decreases when the spacer is further increased to three and four bilayers, however even for four bilayers, the PL intensity of PFBT on the Ag NP assay slide is higher than that observed from the reference slide. The average thickness of each bilayer was estimated to be ~3 nm by ellipsometry, which is similar to the literature report [235]. These

measurements indicate that the maximum MEF is observed at a distance of approximately 6-7 nm from the Ag NP surface. It is also important to note that there is no change in the PFBT emission intensity upon excitation at 335 nm, as shown in Figure 7.4B. This dramatic difference in PL spectra between Figure 7.4A and Figure 7.4B indicates the observed fluorescence enhancement is highly dependent on excitation wavelength and the spectral overlap between the plasmonic peak of Ag NP array and the absorption peak of the polymer.

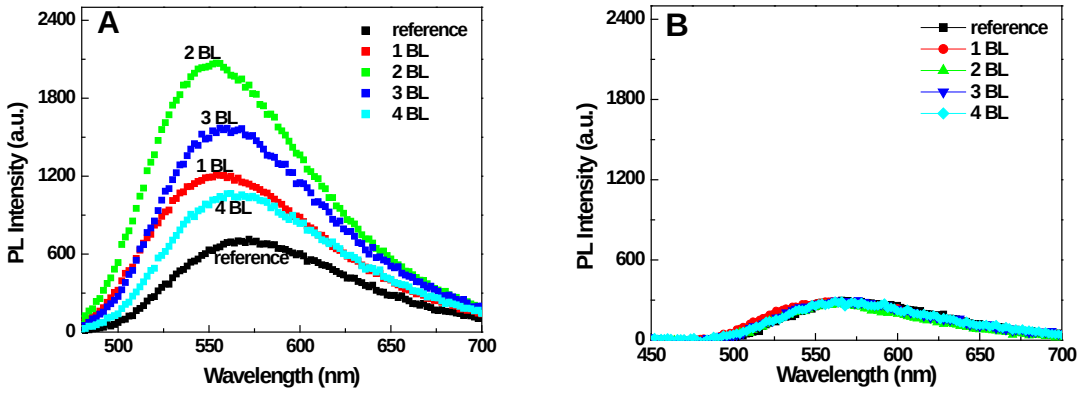

Figure 7.4 Distance-dependent fluorescence emission spectra of the PFBT on Ag NP array and reference slides under A) 440 nm excitation, and B) 335 nm excitation.

To systematically examine the variations in PL intensity as a function of excitation wavelength, the PFBT PL spectra were collected on the same spot of the Ag NP array slide with two bilayer spacers by varying excitation wavelength from 250 to 500 nm. In a meanwhile, the same experiments were conducted for PFBT on the reference slide. Figure 7.5 shows maximum PFBT fluorescence intensities of Ag NP array (squares) and reference slide (circles) from these spectra as a function of excitation wavelength. As typical examples of obtained spectra under each excitation wavelength, the PL spectra

under 440 nm excitation from Ag NP array slide and reference slide are shown in the inset of Figure 7.5.

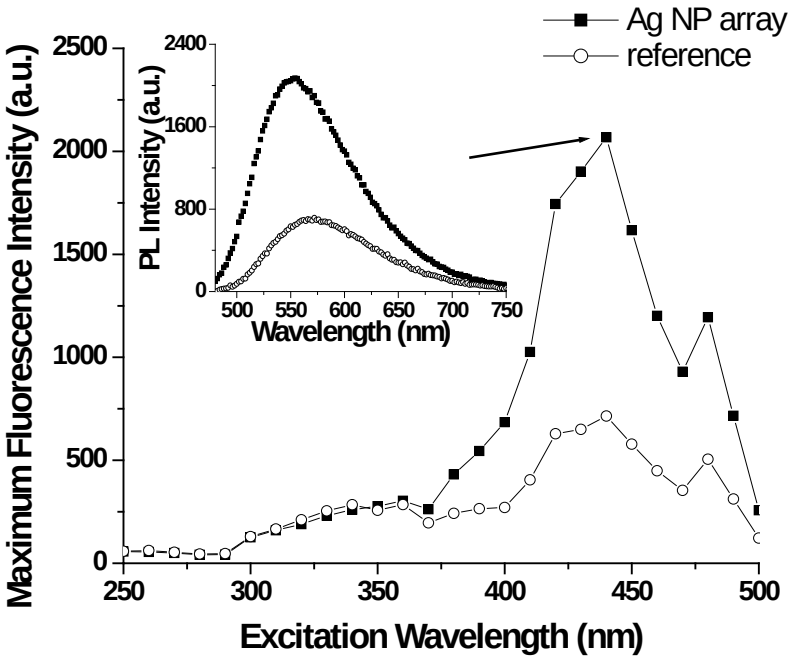

Figure 7.5 Maximum fluorescence intensity under different excitation wavelengths. Inset shows typical emission spectra under excitation of 440 nm for PFBT on Ag NP array slide (PFBT/$(PDDA/PSS)_2$/Ag NP array) and PFBT on the reference slide (PFBT/PSS/PDDA/PSS/NH_2-glass).

The PL intensity ratio of PFBT on the Ag NP array slide to that on the reference slide, was then calculated and is shown in Figure 7.6A as a function of excitation wavelength. The ratio at each wavelength follows the shape of the Ag NP array extinction spectrum. The maximum ratio is ~3 upon excitation of the PFBT film at 440 nm; there is virtually no enhancement at 335 nm and below. To better understand the MEF mechanism, the excitation spectra of the above two slides were also monitored at 550 nm, and the results are shown in Figure 7.6B. As compared to PFBT on the reference slide, the excitation spectrum of PFBT on the Ag NP array is significantly different in the 365 nm to 510 nm

region. However, the two spectra are nearly identical at wavelengths below 365 nm. Considering the selective spectral overlap of Ag NP array plasmonic band at ~440 nm with PFBT absorption band at 450 nm instead of that at 335 nm, these results from Figure 7.6A and Figure 7.6B indicate that plasmonic coupling strongly affects the local electric field around PFBT fluorophores, and the fluorescence enhancement of PFBT on Ag NP array slide relative to that on reference slide in Figure 7.4A is significantly contributed by field amplification. This is similar to the literature reports that MEF can be caused by absorption enhancement for several systems [222-224,231,236-238]. However, the MEF could also be affected by fluorophore's radiative decay rate [225-228]. To further elucidate the MEF mechanism, radiative decay studies of PFBT slides (reference slide and Ag NP array slide) are needed in the future. Nevertheless, our current exploration and finding provided valuable guidance for design of other metal-fluorophore systems using MEF, especially for conjugated fluorophore systems.

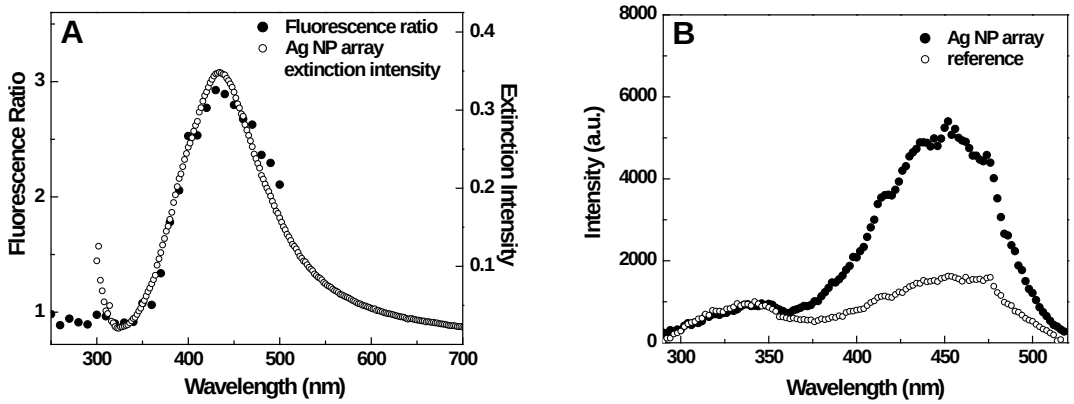

Figure 7.6 A) Fluorescence ratio *vs.* excitation wavelength (shown in dots) and the extinction spectrum of Ag NP array slide (shown in circles). B) Excitation spectra of PFBT on the same Ag NP array slide (shown in dots) and the reference slide (shown in circles) collected at the emission wavelength of 550 nm.

7.3.4 DNA detection based on MEF-PFBT platform

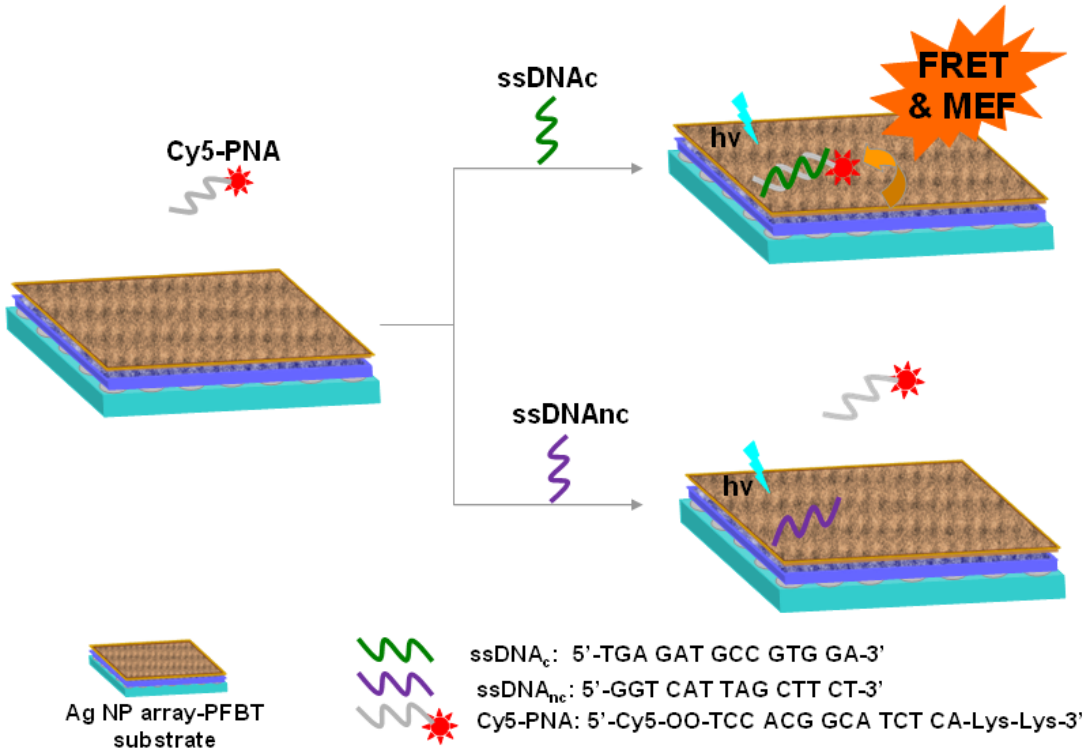

Scheme 7.2 Schematic illustration of DNA detection strategy using Ag NP array-PFBT substrate and Cy5-PNA probe.

Based on the above studies, MEF substrates with Ag NP array as support were prepared and their utility in ssDNA detection was then examined. The DNA assay starts with a Cy5-PNA (5'-Cy5-OO-TCC ACG GCA TCT CA-Lys-Lys-3') probe. Cy5 was selected as signal reporter in this assay because that there is good spectral overlap between the emission of PFBT and the absorbance of Cy5 (see Cy5 absorption spectrum in Figure 7.7), which should favor FRET from PFBT to Cy5, according to Förster theory [79]. As shown in Scheme 7.2, if the ssDNA is complementary (ssDNA$_c$: 5'-TGA GAT GCC GTG GA-3') to the Cy5-PNA, the formed negatively charged Cy5-PNA/DNA$_c$ duplex binds through electrostatic interactions to the positively charged PFBT/PDDA surface. These conditions allow for close proximity and FRET sensitization of Cy5 upon PFBT

excitation. However, if the ssDNA is non-complementary ($ssDNA_{nc}$: 5'-GGT CAT TAG CTT CT-3') to Cy5-PNA, no duplex will form and the neutral Cy5-PNA will remain in solution and be washed off from the slide. One can therefore determine whether the solution contains the target ssDNA sequence by monitoring Cy5 emission upon PFBT excitation.

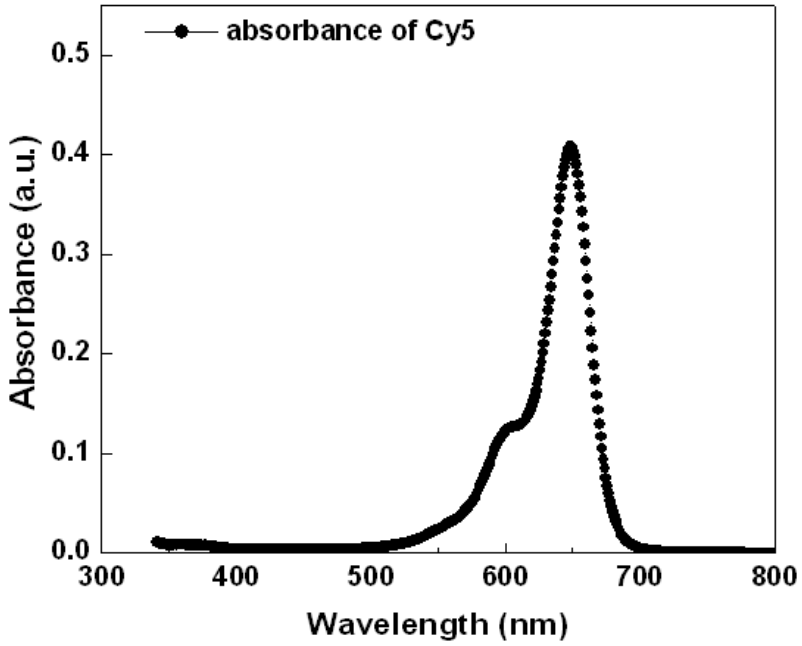

Figure 7.7 The absorption spectrum of Cy5 in 20 mM PBS buffer.

To test the selectivity of DNA assay protocol in Scheme 7.2, Cy5-PNA (10^{-7} M) and one equivalent of $ssDNA_c$ (or $ssDNA_{nc}$) were pre-hybridized before the control slide (PDDA-PFBT/PSS/PDDA/PSS/NH_2-glass) and Ag NP array slide (PDDA-PFBT/$(PDDA/PSS)_2$/Ag NP array) were dipped into the solution, which was followed by washing with 25 mM PBS buffer with 5% NMP. To make more straightforward comparisons between different slides, we note that the quantity of Cy5-PNA/DNA_c adsorbed on both slides was controlled to be the nearly the same by monitoring the Cy5 emission (600 nm excitation) in the depositing solution before and after the assay

procedure (Figure 7.8). As shown in Figure 7.9, upon excitation at λ_{exc} = 440 nm, the Cy5 emission in the range of 640-750 nm is only observed with $ssDNA_c$, demonstrating excellent selectivity for the assay. Considering that Cy5 does not have any absorbance at 440 nm (see Figure 7.7), the Cy5 emission signal upon excitation at 440 nm should be thus due to the formation of a FRET pair, which favors energy transfer from PFBT to Cy5 [90,234]. For the control slide, the Cy5 emission upon excitation at 440 nm (close to PFBT absorption maximum) is ~600 a.u., which is ~6.6-fold higher than that obtained upon direct excitation of Cy5 with λ_{exc} = 645 nm (Cy5 absorption maximum), indicative of signal amplification provided by PFBT. Comparison of the results in Figure 7.9 with λ_{exc} = 440 nm, shows that the Cy5 emission from the Ag NP array slide is approximately 2.6-fold higher (~1600 a.u.) than that from the control slide. Compared with Cy5 intrinsic emission (exc@645 nm) on surface, the developed detection system could provide ~17-fold signal amplification of the reporter dye (upon PFBT 440 nm excitation), indicating the strong influence from MEF and FRET process on Cy5 optical properties [239,240]. It is also interesting to note that upon excitation of PFBT at 335 nm, the Cy5 emission from both slides is similar (see Figure 7.9). The overall Cy5 emission intensity is much greater with λ_{exc} = 440 nm than that with λ_{exc} = 335 nm for the Ag NP array slide, indicates that the MEF effect previously observed with the PFBT substrates is translated to the assay platform.

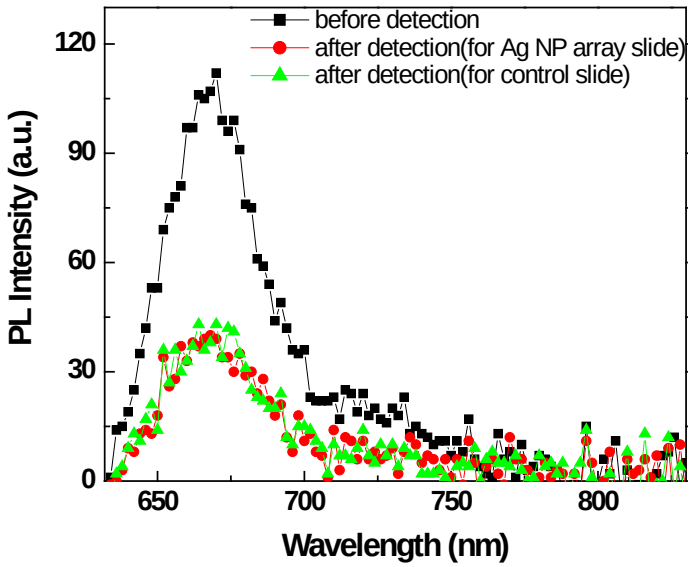

Figure 7.8 PL spectra of Cy5-duplex solution before and after self-assembly onto Ag NP array slide (PDDA-PFBT/$(PDDA/PSS)_2$/Ag NP array), and control slide (PDDA-PFBT/PSS/PDDA/PSS/NH_2-glass). Measurements were done in 300 µL incubation buffer held in 24-well microplate by Tecan MicroplateReader with the excitation at 600 nm.

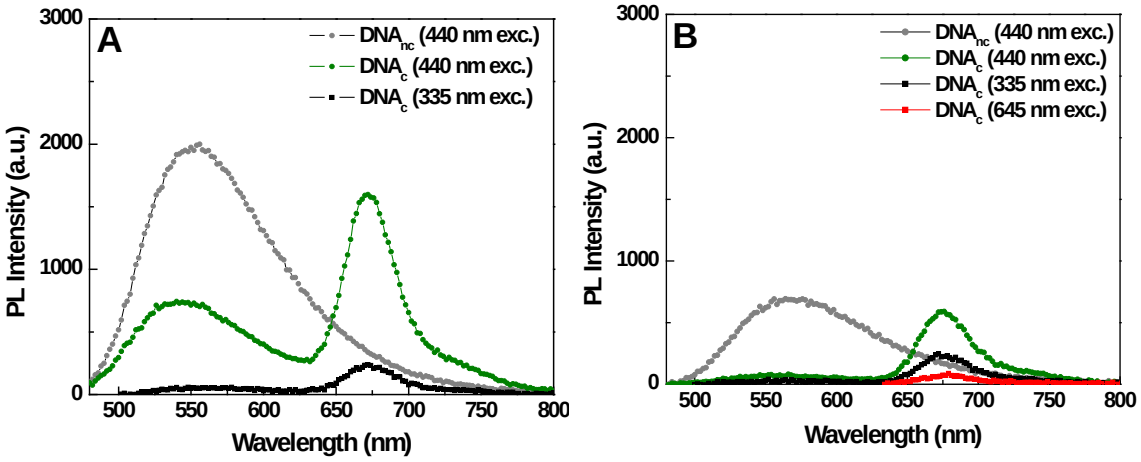

Figure 7.9 PL spectra after DNA assay ([DNA] = 10^{-7} M) under direct excitation (645 nm) and FRET excitation (335 nm and 440 nm) from: A) Ag NP array slide (PDDA-PFBT/$(PDDA/PSS)_2$/Ag NP array), and B) control slide (PDDA-PFBT/PSS/PDDA/PSS/NH_2-glass). Note that the same amount of Cy5-DNA_c was assembled onto each slide.

7.4 Conclusions

In summary, we have demonstrated MEF of the water-soluble PFBT by exploiting substrates with underlying Ag NP array. That PFBT has two nearly equally intense absorption bands make it possible to identify the significant contribution of field enhancement to the overall distance-dependent MEF by metallic nanostructures. In addition, the Ag NP array amplified PFBT emission is further utilized to develop a sensing surface that in the presence of PNA probes provides selective detection of ssDNA with signal intensities that are higher than those obtained by use of polymer alone. These findings open up new opportunities to improve the detection sensitivity of conjugated polymer based bioassays. In addition, the silver NP array enhanced excitation and fluorescence of conjugated polymers should find other applications in organic electronic devices.

Nevertheless, during our silver NP array fabrication, the inter-particle distance of our silver NP arrays is ~200 nm and may lack effective plasmonic coupling to generate higher MEF signal output [241]. Further work of the effect of silver NP surface density on CP optical response is necessary. In addition, the prepared silver NP has some size distribution, which would affect the fabrication of reproducible NP array. Lastly, current DNA assay based on MEF-CP substrate only demonstrate the differentiation between complementary and non-complementary DNA, and lack the capability to discriminate DNA with a few mutations. Further optimizing bioassay conditions (e.g. S1 nuclease digestion process for DNA SNP detection [113]) could lead to more efficient DNA detection with high selectivity.

CHAPTER 8

CONCLUSIONS AND RECOMMENDATIONS

8.1 Conclusions

In the Ph.D. study, conjugated polymer and oligomer based nanosensing systems have been developed and applied to the fluorescence detection of DNA and mercury(II) with high signal amplification and selectivity. This work started with the optimization of experimental conditions for silica NP-supported CP-assisted DNA detection, and demonstrated that conjugated polymers (PFP-2F) could provide over 110-fold signal amplification in real-time. The assay strategy was then developed for single-nucleotide polymorphism DNA detection using conjugated oligomers (tetrahedralfluorene). By modifying the DNA probe immobilized on the silica NP surface, the assay was further extended for mercury(II) study in solution. At last, by exploiting silver NP arrays as supporting substrates, metal-enhanced fluorescence of conjugated polymers (PFBT) was demonstrated and used for DNA detection, which opens up new possibilities to improve the detection sensitivity of conjugated polymer based bioassays. The major findings of this research include the following:

1. Silica NP assisted DNA assays with high signal amplification and selectivity were developed using fluorescent CP (PFP-2F) as an optical signal amplifier. ssDNA immobilized silica nanoparticles (~100 nm in diameter) were first synthesized after a

seed-mediated growth and triazine bioconjugation. The obtained NP bioconjugates were then used as probes to capture target DNA. The optimized detection system amplified a fluorescence signal up to over 110-fold in real time, and allowed detection of target DNA at 10 pM with a standard fluorometer. It also allowed the discrimination of base mutation down to two-base mismatch. The high performance was due to the rationally tailored sensing strategy. In this strategy, silica NP-DNA probes were designed to minimize dye self-quenching within target DNA-CP complexes. Moreover, excess DNA probes on the NP surface could form a complex with fluorescent CPs to increase the local concentration of donor units and deliver excitations to dye (fluorescein). These efforts result in high signal amplification for highly sensitive DNA detection. In addition, the monodispersed silica NPs took the advantage of solid-state sensors and allowed the separation of DNA-NP after centrifuge. This reduces non-specific interactions from the test medium, and improves DNA sequence-specific discrimination. The strategy of using silica NP-DNA probe and fluorescent conjugated polymers could be used to detect other biomolecules besides DNA in bio-analytical areas. More general, the successfully demonstrated assay indicates that homogeneous CP-based FRET assay could be potentially transferred to NP-supported format while maintaining some advantages of both homogenous solution assay and heterogeneous assay.

2. Label-free single-nucleotide polymorphism (SNP) detection using cationic conjugated oligomers (tetrahedralfluorene) and silica NPs was demonstrated. This label-free DNA assay was conducted by the combination of several recognition events: (1) the

specific base pair recognition between the probes immobilized on the NP surface and the DNA targets, and (2) the electrostatic interaction between the cationic tetrahedralfluorene and the DNA duplex containing pre-intercalated EB. The developed assay provided approximately 35-fold signal amplification and SNP selectivity. The high signal amplification was due to the flexible dipolar orientation of conjugated tetrahedralfluorene as an energy donor, which significantly enhanced the efficiency of FRET to the intercalated EB. SNP selectivity was achieved by salt washing on the silica NP-DNA platform. This signal amplification could be used in many circumstances to reduce the background signal and improve detection limit of the traditional NP-based assays. In addition, compared with the solution-based homogeneous assay, this method allows a quick detection of oligonucleotides with high signal amplification and SNP selectivity. Therefore, the developed method opens up possibilities for future development of integrated and portable devices for diagnostic or forensic application.

3. An amplified fluorescence turn-on assay was developed for mercury(II) detection and quantification using cationic CPs (PFP-2F) and silica NPs. This sensor system relied on specific thymine-Hg^{2+}-thymine coordination on NP surface and fluorescent conjugated polymers as signal amplifier. Through maintaining a constant [NP] with different [Hg^{2+}], the mercury(II) assay shows a sigmoidal working curve and gives a detection limit of 0.1 μM. In contrast, by simultaneously reducing the concentration of NP and Hg^{2+}, and keeping [Hg^{2+}]:[DNA duplex] = 3:1, a linear Hg^{2+} calibration curve was obtained. A detection limit of 5 nM was obtained in the presence of CP signal

amplification. This linear response between the Fl emission intensity *vs.* [Hg^{2+}] is dependent on whether all three Hg^{2+} binding sites in each probe are involved in thymine-Hg^{2+}-thymine coordination. In the case of random distribution of Hg^{2+} among the multiple binding sites in mercury-specific probes, a sigmoidal working curve is obtained. The introduction of CPs in the Hg^{2+} assay significantly enhances the detection selectivity and reduces false-positive signals. Further work on ion-specific probe design on NP surface could yield efficient metal ion sensor not limited to Hg^{2+}, and have convenient operation temperature.

4. Metal-enhanced fluorescence (MEF) of fluorescent conjugated polymers (PFBT) was investigated, and its application for selective DNA assay with high signal amplification was demonstrated. Silver NPs (~75 nm in average with extinction maximum at ~440 nm) were first synthesized and self-assembled onto glass slides to form Ag NP arrays. A distance-dependent fluorescence from PFBT assembled on the Ag NP array was observed, which shows initial increase of emission intensity followed with a decreasing tendency when further increasing the number of bilayer spacer (alternating PDDA/PSS). The maximum emission intensity occurred for PFBT-Ag NP array (with 2 bilayer spacer) showing ~3-fold higher intensity relative to that of reference slide. Our results show that the observed MEF is strongly contributed by the field enhancement as reflected in the resonance coupling between the plasmonic band of the Ag NP array and the PFBT absorption band at 450 nm. On top of that, MEF-PFBT substrate was further developed for highly sensitive and selective DNA detection using Cy5-labelled peptide nucleic acid as the probe. Upon

PFBT excitation at λ_{exc} = 440 nm, the Cy5 emission is only observed with complementary ssDNA, demonstrating excellent selectivity for the assay. Moreover, compared with Cy5 intrinsic emission on surface, the developed detection platform provides ~17-fold signal amplification of the reporter dye upon PFBT excitation. It is the first application of MEF-CP substrate in DNA detection, which opens up new possibilities to improve the detection sensitivity of conjugated polymer based bioassays. Further tuning MEF substrate preparation (e.g. inter-particle distance of metal NP array) and optimizing bioassay conditions (e.g. S1 nuclease digestion process for SNP assay) could lead to more efficient DNA detection with high sensitivity and selectivity. In addition, the silver NP array enhanced excitation and fluorescence of conjugated polymers should find other applications in organic electronic devices.

8.2 Suggestions for future work

The results obtained in this study showed the potential of conjugated polymer/oligomer based nanosensors. Nevertheless, specific limitations exist as stated at the end of each assay development Chapter. For instance, in Chapter 4, the large signal amplification in the developed assay is obtained with well-controlled conditions such as matched donor/acceptor molecular orbital energy level. Further work on optimization of CCP/diagnostic C* optical properties may be the next focus. In Chapter 5, ionic strength of the washing buffer is not optimized. Further investigation of the effect of buffer ionic strength on DNA duplex stability on silica NP surface may help us improve the detection

signal/noise ratio and obtain higher selective DNA assay. Overall, from assay design and development point of view, based on the developed systems in the PhD study, further work could be done as followed behind:

1. **Further biosensor development using new biocognition mechanisms based on silica NP-CP platform for protein detection**

   We have demonstrated that silica NP-CP assisted DNA assays could provide high signal amplification and selectivity in Chapter 4. This DNA detection strategy can be extended to the detection of other biomacromolecules. Instead of DNA base pairing for the target recognition in the Chapter 4, other biorecognition mechanisms could be used, e.g. the antibody–antigen binding, the protein-specific aptamer binding, and other receptor-ligand interaction [31,242]. For instance, protein-specific aptamer binding has been recently used for lysozyme detection in CP-based homogeneous assay in solution [87]. To transfer the homogeneous assay format into particle-supported format, lysozyme-specific aptamer with functional terminus can be conjugated with silica NP as lysozyme probe. After the recognition event following by a dye-labelled lysozyme-specific aptamer binding, fluorescent CP will be used as the signal amplifier. With further discovery and understanding of protein-involved receptor-ligand interaction, CP-assisted silica NP-supported assay could find new applications.

2. **Silica NP-CP system for the detection of metal ion**

   In Chapter 6, to detect mercury(II), 45 °C was used in our sensing system, which posed a problem for convenient operation. Recent advance on mercury(II) detection

based on NP-DNA conjugate has shown the possibility of room-temperature chemoassay [214]. Further improvement of the Hg^{2+}-specific duplex design (e.g. that with more T-Hg^{2+}-T binding sites, allowing full denature of mismatched duplex at room temperature but remain stable duplex structure after T-Hg^{2+}-T coordination) in our system could yield more efficient mercury(II) sensors operated at room temperature. Furthermore, using a strategy similar to that of mercury(II) sensing developed in Chapter 6, a variety of other metal ions could be detected. In this approach, suitable CCP as the signal amplifier of diagnostic dye, silica NP as the solid support, and functional nucleic acid (e.g. metal ion-specific nucleic acid duplex with either nature or artificial sequences [212], and metal ion-specific DNAzyme [31]) as metal ion probe will constitute key components of our sensing platform. Based on an appropriate design of the detection system, the high selective and sensitive chemoassays are practicable for the metal ion detection in the environment and for industry process control.

3. Further study on the MEF of PFBT and methods for SNP DNA detection with high sensitivity

In Chapter 7, during the MEF exploration, radiative decay of the prepared MEF substrate was not tested, which consists of another important MEF mechanism [22-24]. Therefore, to further elucidate the MEF mechanism, radiative decay studies of PFBT on Ag NP array are needed. In addition, the relatively large inter-particle distance of our silver NP arrays may lack effective plasmonic coupling for higher MEF [241]. Therefore, further improvement of NP density in our system may lead to higher signal

amplification, and future research in this direction is needed. As for the DNA assay based on MEF-PFBT substrate, further optimization of bioassay condition is desirable to achieve highly sensitive and selective detection. Specifically, for the detection selectivity, S1 nuclease can be used to digest duplex formed by Cy5-PNA and target DNA with complementary or single-base mutation sequence [113]. After that, following the developed methods in Chapter 7, the MEF-PFBT based DNA assay may be demonstrated with SNP level. In addition, for the detection sensitivity, different concentration of target DNA will be measured to determine the lowest detection limit following the same assay method in Chapter 7.

4. MEF-CP for detection of other biomacromolecules

Based on the developed MEF-PFBT strategy in Chapter 7, MEF-PFBT as the solid platform can be easily extended from DNA assay to the detection of enzyme protein such as protease and nuclease. The detection of enzymes and measurement of their activity is critical for the development of novel pharmaceuticals, and of vital importance for biological research [243-245]. For the proposed protease sensor for trypsin detection, anionic conjugated polymers such as sulphonated polyfluorene derivatives will be assemblied onto the MEF surface by electrostatic interaction via alternating LbL process. Meanwhile, the Fl-labelled positive charged peptides will be incorporated into the polymer layers to act as trypsin indicators and avoid the leakage. In the absence of trypsin, FRET will occur from the CP to the Fl, generating a green emission. In the presence of trypsin, the dye-labled peptide will be digested and released from the MEF-CP slide after washing, which prevents the occurrence of

FRET and leads to a blue emission. The key step in the above assay is the target-triggered digestion process which releases dye molecules away from the MEF-CP surface. This results in optical response change indicating the presence of target. Similar approach could be done for other enzyme proteins such as chymotrypsin [246] and S1 nuclease [114].

REFERENCES

(1) Cammann, G. G.; Guilbault, E. A.; Hal, H.; Kellner, R.; Wolfbeis, O. S. *The Cambridge Definition of Chemical Sensors, Cambridge Workshop on Chemical Sensors and Biosensors*; Cambridge University Press: New York, 1996.

(2) Kauffman, D. R.; Star, A. *Chem. Soc. Rev.* **2008**, *37*, 1197-1206.

(3) Wang, J. *Chem. Rev.* **2008**, *108*, 814-825.

(4) Caravan, P. *Chem. Soc. Rev.* **2006**, *35*, 512-523.

(5) Wolfbeis, O. S. *Anal. Chem.* **2006**, *78*, 3859-3873.

(6) Borisov, S. M.; Wolfbeis, O. S. *Chem. Rev.* **2008**, *108*, 423-461.

(7) Narayanaswamy, R.; Wolfbeis, O. S. *Optical Sensors: Industrial, Environmental and Diagnostic Applications*; Springer-Verlag: Berlin Heidelberg, 2004.

(8) McDonagh, C.; Burke, C. S.; MacCraith, B. D. *Chem. Rev.* **2008**, *108*, 400-422.

(9) Tyagi, S.; Kramer, F. R. *Nat. Biotechnol.* **1996**, *14*, 303-308.

(10) Bruchez Jr, M.; Moronne, M.; Gin, P.; Weiss, S.; Alivisatos, A. P. *Science* **1998**, *281*, 2013-2016.

(11) Chan, W. C. W.; Nie, S. *Science* **1998**, *281*, 2016-2018.

(12) Zeph, L. R.; Lin, X. Y.; Stotzky, G. *Curr. Microbiol.* **1991**, *22*, 79-84.

(13) Haugland, R. P. *The Handbook-A Guide to Fluorescent Probes and Labeling Technologies*; 10 th ed.; Molecular Probes: Eugene, OR, 2005.

(14) Nielsen, P. E.; Egholm, M. *Peptide Nucleic Acids: Protocols and Applications*; Horizon Scientific Press: Portland, 1999.

(15) Ellington, A. D.; Szostak, J. W. *Nature* **1990**, *346*, 818-822.

(16) Tuerk, C.; Gold, L. *Science* **1990**, *249*, 505-510.

(17) Zhang, J.; Campbell, R. E.; Ting, A. Y.; Tsien, R. Y. *Nature Reviews Molecular Cell Biology* **2002**, *3*, 906-918.

(18) Taton, T. A.; Mirkin, C. A.; Letsinger, R. L. *Science* **2000**, *289*, 1757-1760.

(19) Han, M.; Gao, X.; Su, J. Z.; Nie, S. *Nat. Biotechnol.* **2001**, *19*, 631-635.

(20) Cao, Y. C.; Jin, R.; Mirkin, C. A. *Science* **2002**, *297*, 1536-1540.

(21) Zhao, X. J.; Hilliard, L. R.; Mechery, S. J.; Wang, Y. P.; Bagwe, R. P.; Jin, S. G.; Tan, W. H. *Proc. Natl. Acad. Sci. U. S. A.* **2004**, *101*, 15027-15032.

(22) Aslan, K.; Gryczynski, I.; Malicka, J.; Matveeva, E.; Lakowicz, J. R.; Geddes, C. D. *Curr. Opin. Biotechnol.* **2005**, *16*, 55-62.

(23) Lakowicz, J. R. *Plasmonics* **2006**, *1*, 5-33.

(24) Stewart, M. E.; Anderton, C. R.; Thompson, L. B.; Maria, J.; Gray, S. K.; Rogers, J. A.; Nuzzo, R. G. *Chem. Rev.* **2008**, *108*, 494-521.

(25) Swager, T. M. *Acc. Chem. Res.* **1998**, *31*, 201-207.

(26) Thomas III, S. W.; Joly, G. D.; Swager, T. M. *Chem. Rev.* **2007**, *107*, 1339-1386.

(27) Ho, H. A.; Najari, A.; Leclerc, M. *Acc. Chem. Res.* **2008**, *41*, 168-178.

(28) Liu, B.; Bazan, G. C. *Chem. Mater.* **2004**, *16*, 4467-4476.

(29) Liu, B.; Bazan, G. C. *J. Am. Chem. Soc.* **2004**, *126*, 1942-1943.

(30) Feng, F.; He, F.; An, L.; Wang, S.; Li, Y.; Zhu, D. *Adv. Mater.* **2008**, *20*, 2959-2964.

(31) Liu, J.; Cao, Z.; Lu, Y. *Chem. Rev.* **2009**, *109*, 1948-1998.

(32) DNA. http://en.wikipedia.org/wiki/DNA

(33) Hermanson, G. T. *Bioconjugate Techniques*; Academic Press: San Diego,CA, 1996.

(34) Mirkin, C. A. *Inorg. Chem.* **2000**, *39*, 2258-2272.

(35) Bao, G.; Suresh, S. *Nature Materials* **2003**, *2*, 715-725.

(36) Peptide nucleic acid. http://en.wikipedia.org/wiki/Peptide_nucleic_acid

(37) Tan, W.; Wang, K.; Drake, T. J. *Curr. Opin. Chem. Biol.* **2004**, *8*, 547-553.

(38) Yang, C. J.; Lin, H.; Tan, W. *J. Am. Chem. Soc.* **2005**, *127*, 12772-12773.

(39) Yang, C. J.; Jockusch, S.; Vicens, M.; Turro, N. J.; Tan, W. *Proc. Natl. Acad. Sci. U. S. A.* **2005**, *102*, 17278-17283.

(40) Zhao, X.; Tapec-Dytioco, R.; Tan, W. *J. Am. Chem. Soc.* **2003**, *125*, 11474-11475.

(41) Nam, J. M.; Stoeva, S. I.; Mirkin, C. A. *J. Am. Chem. Soc.* **2004**, *126*, 5932-5933.

(42) Alivisatos, P. *Nat. Biotechnol.* **2004**, *22*, 47-52.

(43) Nie, S.; Xing, Y.; Kim, G. J.; Simons, J. W. *Annu. Rev. Biomed. Eng.* **2007**, *9*, 257-288.

(44) Xu, H.; Sha, M. Y.; Wong, E. Y.; Uphoff, J.; Xu, Y.; Treadway, J. A.; Truong, A.; O'Brien, E.; Asquith, S.; Stubbins, M.; Spurr, N. K.; Lai, E. H.; Mahoney, W. *Nucleic Acids Res.* **2003**, *31*, e43.

(45) Park, S. J.; Taton, T. A.; Mirkin, C. A. *Science* **2002**, *295*, 1503-1506.

(46) Guo, S. H.; Tsai, S. J.; Kan, H. C.; Tsai, D. H.; Zachariah, M. R.; Phaneuf, R. J. *Adv. Mater.* **2008**, *20*, 1424-1428.

(47) Sabanayagam, C. R.; Lakowicz, J. R. *Nucleic Acids Res.* **2007**, *35*, e13.

(48) Kulakovich, O.; Strekal, N.; Yaroshevich, A.; Maskevich, S.; Gaponenko, S.; Nabiev, I.; Woggon, U.; Artemyev, M. *Nano Lett.* **2002**, *2*, 1449-1452.

(49) Bardhan, R.; Grady, N. K.; Cole, J. R.; Joshi, A.; Halas, N. J. *ACS Nano* **2009**, *3*, 744-752.

(50) Ray, K.; Chowdhury, M. H.; Lakowicz, J. R. *Anal. Chem.* **2007**, *79*, 6480-6487.

(51) Chen, Y.; Munechika, K.; Ginger, D. S. *MRS Bull.* **2008**, *33*, 536-542.

(52) Aslan, K.; Wu, M.; Lakowicz, J. R.; Geddes, C. D. *J. Am. Chem. Soc.* **2007**, *129*, 1524-1525.

(53) Chen, Y.; Munechika, K.; Ginger, D. S. *Nano Lett.* **2007**, *7*, 690-696.

(54) Bek, A.; Jansen, R.; Ringler, M.; Mayilo, S.; Klar, T. A.; Feldmann, J. *Nano Lett.* **2008**, *8*, 485-490.

(55) Ray, K.; Szmacinski, H.; Enderlein, J.; Lakowicz, J. R. *Appl. Phys. Lett.* **2007**, *90*, 251116.

(56) Malicka, J.; Gryczynski, I.; Lakowicz, J. R. *Biochem. Biophys. Res. Commun.* **2003**, *306*, 213-218.

(57) Ferguson, J. A.; Steemers, F. J.; Walt, D. R. *Anal. Chem.* **2000**, *72*, 5618-5624.

(58) Giepmans, B. N. G.; Adams, S. R.; Ellisman, M. H.; Tsien, R. Y. *Science* **2006**, *312*, 217-224.

(59) Niemeyer, C. M.; Adler, M.; Wacker, R. *Trends Biotechnol.* **2005**, *23*, 208-216.

(60) McCrum, N. G.; Buckleym, C. P.; Bucknall, C. B. *Principles of Polymer Engineering*; Oxford Science Publications: Oxford, UK, 1997.

(61) Skotheim, T. A.; Reynolds, J. R. *Handbook of Conducting Polymers*; CRC: London, 2007.

(62) Shirakawa, H.; Louis, E. J.; MacDiarmid, A. G.; Chiang, C. K.; Heeger, A. J. *J. Chem. Soc., Chem. Commun.* **1977**, 578-580.

(63) The Nobel Prize in Chemistry 2000. http://nobelprize.org/nobel_prizes/chemistry/laureates/2000/index.html

(64) Kraft, A.; Grimsdale, A. C.; Holmes, A. B. *Angew. Chem. Int. Ed.* **1998**, *37*, 402-428.

(65) Burroughes, J. H.; Bradley, D. D. C.; Brown, A. R.; Marks, R. N.; Mackay, K.; Friend, R. H.; Burns, P. L.; Holmes, A. B. *Nature* **1990**, *347*, 539-541.

(66) Torsi, L.; Dodabalapur, A.; Rothberg, L. J.; Fung, A. W. P.; Katz, H. E. *Science* **1996**, *272*, 1462-1464.

(67) Sirringhaus, H. *Adv. Mater.* **2005**, *17*, 2411-2425.

(68) Pei, Q. B.; Yu, G.; Zhang, C.; Yang, Y.; Heeger, A. J. *Science* **1995**, *269*, 1086-1088.

(69) Heeger, A. J. *Solid State Commun.* **1998**, *107*, 673-679.

(70) Hide, F.; DiazGarcia, M. A.; Schwartz, B. J.; Heeger, A. J. *Acc. Chem. Res.* **1997**, *30*, 430-436.

(71) Gunes, S.; Neugebauer, H.; Sariciftci, N. S. *Chem. Rev.* **2007**, *107*, 1324-1338.

(72) Bunz, U. H. F. *Chem. Rev.* **2000**, *100*, 1605-1644.

(73) Perepichka, I. F.; Perepichka, D. F.; Meng, H.; Wudl, F. *Adv. Mater.* **2005**, *17*, 2281-2305.

(74) Scherf, U.; List, E. J. W. *Adv. Mater.* **2002**, *14*, 477-487.

(75) Peng, H.; Zhang, L. J.; Soeller, C.; Travas-Sejdic, J. *Biomaterials* **2009**, *30*, 2132-2148.

(76) Achyuthan, K. E.; Bergstedt, T. S.; Chen, L.; Jones, R. M.; Kumaraswamy, S.; Kushon, S. A.; Ley, K. D.; Lu, L.; McBranch, D.; Mukundan, H.; Rininsland, F.; Shi, X.; Xia, W.; Whitten, D. G. *J. Mater. Chem.* **2005**, *15*, 2648-2656.

(77) Chen, L.; McBranch, D. W.; Wang, H. L.; Helgeson, R.; Wudl, F.; Whitten, D. G. *Proc. Natl. Acad. Sci. U. S. A.* **1999**, *96*, 12287-12292.

(78) Dwight, S. J.; Gaylord, B. S.; Hong, J. W.; Bazan, G. C. *J. Am. Chem. Soc.* **2004**, *126*, 16850-16859.

(79) Förster, T. *Ann. Phys.* **1948**, *2*, 55-75.

(80) Liu, B.; Bazan, G. C. *J. Am. Chem. Soc.* **2006**, *128*, 1188-1196.

(81) Bazan, G. C. *J. Org. Chem.* **2007**, *72*, 8615-8635.

(82) Pu, K. Y.; Liu, B. *Biosens. Bioelectron.* **2009**, *24*, 1067-1073.

(83) Gaylord, B. S.; Heeger, A. J.; Bazan, G. C. *Proc. Natl. Acad. Sci. U. S. A.* **2002**, *99*, 10954-10957.

(84) Liu, B.; Baudrey, S.; Jaeger, L.; Bazan, G. C. *J. Am. Chem. Soc.* **2004**, *126*, 4076-4077.

(85) Wang, S.; Bazan, G. C. *Adv. Mater.* **2003**, *15*, 1425-1428.

(86) Béra Abérem, M.; Najari, A.; Ho, A. A.; Gravel, J. F.; Nobert, P.; Boudreau, D.; Leclerc, M. *Adv. Mater.* **2006**, *18*, 2703-2707.

(87) Wang, J.; Liu, B. *Chem. Commun.* **2009**, 2284-2286.

(88) He, F.; Tang, Y. L.; Wang, S.; Li, Y. L.; Zhu, D. B. *J. Am. Chem. Soc.* **2005**, *127*, 12343-12346.

(89) Ho, H. A.; Boissinot, M.; Bergeron, M. G.; Corbeil, G.; Doré, K.; Boudreau, D.; Leclerc, M. *Angew. Chem. Int. Ed.* **2002**, *41*, 1548-1551.

(90) Liu, B.; Bazan, G. C. *Proc. Natl. Acad. Sci. U. S. A.* **2005**, *102*, 589-593.

(91) Brédas, J. L.; Beljonne, D.; Coropceanu, V.; Cornil, J. *Chem. Rev.* **2004**, *104*, 4971-5003.

(92) Le Floch, F.; Ho, H. A.; Harding-Lepage, P.; Bedard, M.; Neagu-Plesu, R.; Leclerc, M. *Adv. Mater.* **2005**, *17*, 1251-1254.

(93) Le Floch, F.; Ho, H. A.; Leclerc, M. *Anal. Chem.* **2006**, *78*, 4727-4731.

(94) Lee, K.; Rouillard, J. M.; Pham, T.; Gulari, E.; Kim, J. *Angew. Chem. Int. Ed.* **2007**, *46*, 4667-4670.

(95) Jones, R. M.; Bergstedt, T. S.; McBranch, D. W.; Whitten, D. G. *J. Am. Chem. Soc.* **2001**, *123*, 6726-6727.

(96) Wosnick, J. H.; Liao, J. H.; Swager, T. M. *Macromolecules* **2005**, *38*, 9287-9290.

(97) Ogawa, K.; Chemburu, S.; Lopez, G. P.; Whitten, D. G.; Schanze, K. S. *Langmuir* **2007**, *23*, 4541-4548.

(98) Fan, L. J.; Zhang, Y.; Jones Jr, W. E. *Macromolecules* **2005**, *38*, 2844-2849.

(99) Tang, Y.; He, F.; Yu, M.; Feng, F.; An, L.; Sun, H.; Wang, S.; Li, Y.; Zhu, D. *Macromol. Rapid Commun.* **2006**, *27*, 389-392.

(100) Kim, I. B.; Bunz, U. H. F. *J. Am. Chem. Soc.* **2006**, *128*, 2818-2819.

(101) Liu, X.; Tang, Y.; Wang, L.; Zhang, J.; Song, S.; Fan, C.; Wang, S. *Adv. Mater.* **2007**, *19*, 1471-1474.

(102) Kushon, S. A.; Ley, K. D.; Bradford, K.; Jones, R. M.; McBranch, D.; Whitten, D. *Langmuir* **2002**, *18*, 7245-7249.

(103) Kushon, S. A.; Bradford, K.; Marin, V.; Suhrada, C.; Armitage, B. A.; McBranch, D.; Whitten, D. *Langmuir* **2003**, *19*, 6456-6464.

(104) Béra Abérem, M.; Ho, H. A.; Leclerc, M. *Tetrahedron* **2004**, *60*, 11169-11173.

(105) Dore, K.; Dubus, S.; Ho, H. A.; Levesque, I.; Brunette, M.; Corbeil, G.; Boissinot, M.; Boivin, G.; Bergeron, M. G.; Boudreau, D.; Leclerc, M. *J. Am. Chem. Soc.* **2004**, *126*, 4240-4244.

(106) Gaylord, B. S.; Heeger, A. J.; Bazan, G. C. *J. Am. Chem. Soc.* **2003**, *125*, 896-900.

(107) Wang, S.; Gaylord, B. S.; Bazan, G. C. *J. Am. Chem. Soc.* **2004**, *126*, 5446-5451.

(108) Xu, Q. H.; Wang, S.; Korystov, D.; Mikhailovsky, A.; Bazan, G. C.; Moses, D.; Heeger, A. J. *Proc. Natl. Acad. Sci. U. S. A.* **2005**, *102*, 530-535.

(109) Liu, B.; Wang, S.; Bazan, G. C.; Mikhailovsky, A. *J. Am. Chem. Soc.* **2003**, *125*, 13306-13307.

(110) Liu, B.; Dan, T. T. T.; Bazan, G. C. *Adv. Funct. Mater.* **2007**, *17*, 2432-2438.

(111) Woo, H. Y.; Vak, D.; Korystov, D.; Mikhailovsky, A.; Bazan, G. C.; Kim, D. Y. *Adv. Funct. Mater.* **2007**, *17*, 290-295.

(112) Pu, K. Y.; Fang, Z.; Liu, B. *Adv. Funct. Mater.* **2008**, *18*, 1321-1328.

(113) Gaylord, B. S.; Massie, M. R.; Feinstein, S. C.; Bazan, G. C. *Proc. Natl. Acad. Sci. U. S. A.* **2005**, *102*, 34-39.

(114) Li, K.; Liu, B. *Anal. Chem.* **2009**, *81*, 4099-4105.

(115) Xu, H.; Wu, H.; Huang, F.; Song, S.; Li, W.; Cao, Y.; Fan, C. *Nucleic Acids Res.* **2005**, *33*, e83.

(116) Ho, H. A.; Doré, K.; Boissinot, M.; Bergeron, M. G.; Tanguay, R. M.; Boudreau, D.; Leclerc, M. *J. Am. Chem. Soc.* **2005**, *127*, 12673-12676.

(117) Yang, C. Y. J.; Pinto, M.; Schanze, K.; Tan, W. H. *Angew. Chem. Int. Ed.* **2005**, *44*, 2572-2576.

(118) Lee, K.; Povlich, L. K.; Kim, J. *Adv. Funct. Mater.* **2007**, *17*, 2580-2587.

(119) Huang, H. M.; Wang, K.; Tan, W. H.; An, D.; Yang, X. H.; Huang, S. S.; Zhai, Q.; Zhou, L.; Jin, Y. *Angew. Chem. Int. Ed.* **2004**, *43*, 5635-5638.

(120) Ho, H. A.; Leclerc, M. *J. Am. Chem. Soc.* **2004**, *126*, 1384-1387.

(121) Kumaraswamy, S.; Bergstedt, T.; Shi, X. B.; Rininsland, F.; Kushon, S.; Xia, W. S.; Ley, K.; Achyuthan, K.; McBranch, D.; Whitten, D. *Proc. Natl. Acad. Sci. U. S. A.* **2004**, *101*, 7511-7515.

(122) Rininsland, F.; Xia, W. S.; Wittenburg, S.; Shi, X. B.; Stankewicz, C.; Achyuthan, K.; McBranch, D.; Whitten, D. *Proc. Natl. Acad. Sci. U. S. A.* **2004**, *101*, 15295-15300.

(123) Kim, I. B.; Wilson, J. N.; Bunz, U. H. F. *Chem. Commun.* **2005**, 1273-1275.

(124) Disney, M. D.; Zheng, J.; Swager, T. M.; Seeberger, P. H. *J. Am. Chem. Soc.* **2004**, *126*, 13343-13346.

(125) Iler, R. K. *The Chemistry of Silica: Solubility, Polymerization, Colloid and Surface Properties, and Biochemistry*; Wiley-Interscience: New York, 1979.

(126) Stöber, W.; Fink, A.; Bohn, E. *J. Colloid Interface Sci.* **1968**, *26*, 62-69.

(127) Zhao, X.; Bagwe, R. P.; Tan, W. *Adv. Mater.* **2004**, *16*, 173-176.

(128) Lee, P. C.; Meisel, D. *J. Phys. Chem.* **1982**, *86*, 3391-3395.

(129) Abid, J. P.; Wark, A. W.; Brevet, P. F.; Girault, H. H. *Chem. Commun.* **2002**, 792-793.

(130) Mafuné, F.; Kohno, J. Y.; Takeda, Y.; Kondow, T.; Sawabe, H. *J. Phys. Chem. B* **2000**, *104*, 9111-9117.

(131) Wang, J. *Nucleic Acids Res.* **2000**, *28*, 3011-3016.

(132) Schork, N. J.; Fallin, D.; Lanchbury, J. S. *Clin. Genet.* **2000**, *58*, 250-264.

(133) Sutherland, G.; Mulley, J. *Nucleic Acid Probes*; CRC Press: Florida, 1989.

(134) Niemeyer, C. M.; Blohm, D. *Angew. Chem. Int. Ed.* **1999**, *38*, 2865-2869.

(135) Boon, E. M.; Ceres, D. M.; Drummond, T. G.; Hill, M. G.; Barton, J. K. *Nat. Biotechnol.* **2000**, *18*, 1096-1100.

(136) Fan, C.; Plaxco, K. W.; Heeger, A. J. *Proc. Natl. Acad. Sci. U. S. A.* **2003**, *100*, 9134-9137.

(137) Su, X.; Robelek, R.; Wu, Y.; Wang, G.; Knoll, W. *Anal. Chem.* **2004**, *76*, 489-494.

(138) Mannelli, I.; Minunni, M.; Tombelli, S.; Mascini, M. *Biosens. Bioelectron.* **2003**, *18*, 129-140.

(139) Patolsky, F.; Lichtenstein, A.; Willner, I. *Nat. Biotechnol.* **2001**, *19*, 253-257.

(140) Avouris, P.; Chen, J. *Mater. Today* **2006**, *9*, 46-54.

(141) Nam, J. M.; Thaxton, C. S.; Mirkin, C. A. *Science* **2003**, *301*, 1884-1886.

(142) Nuovo, G. J. *Methods in molecular biology (Clifton, N.J.)* **2000**, *123*, 217-238.

(143) Saiki, R. K.; Scharf, S.; Faloona, F. *Science* **1985**, *230*, 1350-1354.

(144) Tyler McQuade, D.; Pullen, A. E.; Swager, T. M. *Chem. Rev.* **2000**, *100*, 2537-2574.

(145) Kim, I. B.; Erdogan, B.; Wilson, J. N.; Bunz, U. H. F. *Chemistry - A European Journal* **2004**, *10*, 6247-6254.

(146) Yao, G.; Wang, L.; Wu, Y.; Smith, J.; Xu, J.; Zhao, W.; Lee, E.; Tan, W. *Anal. Bioanal. Chem.* **2006**, *385*, 518-524.

(147) Steinberg, G.; Stromsborg, K.; Thomas, L.; Barker, D.; Zhao, C. *Biopolymers* **2004**, *73*, 597-605.

(148) Wang, Y.; Liu, B. *Biosens. Bioelectron.* **2009**, *24*, 3293-3298.

(149) Shuber, A. P.; Michalowsky, L. A.; Nass, G. S.; Skoletsky, J.; Hire, L. M.; Kotsopoulos, S. K.; Phipps, M. F.; Barberio, D. M.; Klinger, K. W. *Hum. Mol. Genet.* **1997**, *6*, 337-347.

(150) Weidenhammer, E. M.; Kahl, B. F.; Wang, L.; Duhon, M.; Jackson, J. A.; Slater, M.; Xu, X. *Clin. Chem.* **2002**, *48*, 1873-1882.

(151) Wilson, W. J.; Strout, C. L.; DeSantis, T. Z.; Stilwell, J. L.; Carrano, A. V.; Andersen, G. L. *Mol. Cell. Probes* **2002**, *16*, 119-127.

(152) Chakravarti, A. *Nature* **2001**, *409*, 822-823.

(153) Tsongalis, G. J.; Coleman, W. B. *Clin. Chim. Acta* **2006**, *363*, 127-137.

(154) National Cancer Institute, U. S. National Institutes of Health. Understanding Cancer Series: Genetic Variation (SNPs). http://nci.nih.gov/cancertopics/understandingcancer/geneticvariation

(155) Holland, P. M.; Abramson, R. D.; Watson, R.; Gelfand, D. H. *Proc. Natl. Acad. Sci. U. S. A.* **1991**, *88*, 7276-7280.

(156) Piatek, A. S.; Tyagi, S.; Pol, A. C.; Telenti, A.; Miller, L. P.; Kramer, F. R.; Alland, D. *Nat. Biotechnol.* **1998**, *16*, 359-363.

(157) Wang, H.; Li, J.; Liu, H.; Liu, Q.; Mei, Q.; Wang, Y.; Zhu, J.; He, N.; Lu, Z. *Nucleic Acids Res.* **2002**, *30*, e61.

(158) Iwahana, H.; Fujimura, M.; Takahashi, Y.; Iwabuchi, T.; Yoshimoto, K.; Itakura, M. *Biotechniques* **1996**, *21*, 510-519.

(159) May, J. P.; Brown, L. J.; Rudloff, I.; Brown, T. *Chem. Commun.* **2003**, 970-971.

(160) Hahm, J. I.; Lieber, C. M. *Nano Lett.* **2004**, *4*, 51-54.

(161) Star, A.; Tu, E.; Niemann, J.; Gabriel, J. C. P.; Joiner, C. S.; Valcke, C. *Proc. Natl. Acad. Sci. U. S. A.* **2006**, *103*, 921-926.

(162) Gao, Z.; Agarwal, A.; Trigg, A. D.; Singh, N.; Fang, C.; Tung, C. H.; Fan, Y.; Buddharaju, K. D.; Kong, J. *Anal. Chem.* **2007**, *79*, 3291-3297.

(163) Lubin, A. A.; Lai, R. Y.; Baker, B. R.; Heeger, A. J.; Plaxco, K. W. *Anal. Chem.* **2006**, *78*, 5671-5677.

(164) Li, H.; Rothberg, L. J. *J. Am. Chem. Soc.* **2004**, *126*, 10958-10961.

(165) Endo, T.; Kerman, K.; Nagatani, N.; Takamura, Y.; Tamiya, E. *Anal. Chem.* **2005**, *77*, 6976-6984.

(166) Kim, D. K.; Kerman, K.; Saito, M.; Sathuluri, R. R.; Endo, T.; Yamamura, S.; Kwon, Y. S.; Tamiya, E. *Anal. Chem.* **2007**, *79*, 1855-1864.

(167) Lepecq, J. B.; Paoletti, C. *J. Mol. Biol.* **1967**, *27*, 87-106.

(168) Yamamoto, N.; Okamoto, T. *Nucleic Acids Res.* **1995**, *23*, 1445-1446.

(169) Yguerabide, J.; Ceballos, A. *Anal. Biochem.* **1995**, *228*, 208-220.

(170) Yin, J. L.; Shackel, N. A.; Zekry, A.; McGuinness, P. H.; Richards, C.; Van Der Putten, K.; McCaughan, G. W.; Eris, J. M.; Bishop, G. A. *Immunol. Cell Biol.* **2001**, *79*, 213-221.

(171) Rajeevan, M. S.; Ranamukhaarachchi, D. G.; Vernon, S. D.; Unger, E. R. *Methods* **2001**, *25*, 443-451.

(172) Simon, L. D.; Abramo, K. H.; Sell, J. K.; McGown, L. B. *Biospectroscopy* **1998**, *4*, 17-25.

(173) Abramo, K. H.; Pitner, J. B.; McGown, L. B. *Biospectroscopy* **1998**, *4*, 27-35.

(174) Talavera, E. M.; Bermejo, R.; Crovetto, L.; Orte, A.; Alvarez-Pez, J. M. *Appl. Spectrosc.* **2003**, *57*, 208-215.

(175) Algar, W. R.; Massey, M.; Krull, U. J. *Journal of Fluorescence* **2006**, *16*, 555-567.

(176) Penn, S. G.; He, L.; Natan, M. J. *Curr. Opin. Chem. Biol.* **2003**, *7*, 609-615.

(177) Wang, J.; Kawde, A. N.; Erdem, A.; Salazar, M. *Analyst* **2001**, *126*, 2020-2024.

(178) Cognet, L.; Tardin, C.; Boyer, D.; Choquett, D.; Tamarat, P.; Lounis, B. *Proc. Natl. Acad. Sci. U. S. A.* **2003**, *100*, 11350-11355.

(179) Bangs Laboratories, Inc. http://www.bangslabs.com/support/index.php

(180) Lytton-Jean, A. K. R.; Mirkin, C. A. *J. Am. Chem. Soc.* **2005**, *127*, 12754-12755.

(181) O'Donnell, M. J.; Tang, K.; Köster, H.; Smith, C. L.; Cantor, C. R. *Anal. Chem.* **1997**, *69*, 2438-2443.

(182) Keller, G. H.; Manak, M. M. *DNA probes*; Stockton: New York, 1989.

(183) Heller, D. P.; Greenstock, C. L. *Biophys. Chem.* **1994**, *50*, 305-312.

(184) Bronich, T. K.; Nguyen, H. K.; Eisenberg, A.; Kabanov, A. V. *J. Am. Chem. Soc.* **2000**, *122*, 8339-8343.

(185) Tse, W. C.; Boger, D. L. *Acc. Chem. Res.* **2004**, *37*, 61-69.

(186) Izumrudov, V. A.; Zhiryakova, M. V.; Goulko, A. A. *Langmuir* **2002**, *18*, 10348-10356.

(187) Henke, L.; Piunno, P. A. E.; McClure, A. C.; Krull, U. J. *Anal. Chim. Acta* **1997**, *344*, 201-213.

(188) Harris, H. H.; Pickering, I. J.; George, G. N. *Science* **2003**, *301*, 1203.

(189) Clarkson, T. W.; Magos, L.; Myers, G. J. *N. Engl. J. Med.* **2003**, *349*, 1731-1737.

(190) Liu, B.; Tian, H. *Chem. Commun.* **2005**, 3156-3158.

(191) Caballero, A.; Martinez, R.; Lloveras, V.; Ratera, I.; Vidal-Gancedo, J.; Wurst, K.; Tarraga, A.; Molina, P.; Veciana, J. *J. Am. Chem. Soc.* **2005**, *127*, 15666-15667.

(192) Song, K. C.; Kim, J. S.; Park, S. M.; Chung, K. C.; Ahn, S.; Chang, S. K. *Org. Lett.* **2006**, *8*, 3413-3416.

(193) Ha-Thi, M. H.; Penhoat, M.; Michelet, V.; Leray, I. *Org. Lett.* **2007**, *9*, 1133-1136.

(194) Nolan, E. M.; Lippard, S. J. *J. Am. Chem. Soc.* **2003**, *125*, 14270-14271.

(195) Nolan, E. M.; Lippard, S. J. *J. Am. Chem. Soc.* **2007**, *129*, 5910-5918.

(196) Ko, S. K.; Yang, Y. K.; Tae, J.; Shin, I. *J. Am. Chem. Soc.* **2006**, *128*, 14150-14155.

(197) Yang, Y. K.; Ko, S. K.; Shin, I.; Tae, J. *Nature Protocols* **2007**, *2*, 1740-1745.

(198) Huang, C. C.; Yang, Z.; Lee, K. H.; Chang, H. T. *Angew. Chem. Int. Ed.* **2007**, *46*, 6824-6828.

(199) Darbha, G. K.; Ray, A.; Ray, P. C. *ACS Nano* **2007**, *1*, 208-214.

(200) Vannela, R.; Adriaens, P. *Environmental Engineering Science* **2007**, *24*, 73-84.

(201) Hollenstein, M.; Hipolito, C.; Lam, C.; Dietrich, D.; Perrin, D. M. *Angew. Chem. Int. Ed.* **2008**, *47*, 4346-4350.

(202) Zhao, Y.; Zhong, Z. *J. Am. Chem. Soc.* **2006**, *128*, 9988-9989.

(203) Zhao, Y.; Zhong, Z. *Org. Lett.* **2006**, *8*, 4715-4717.

(204) Matsushita, M.; Meijler, M. M.; Wirsching, P.; Lerner, R. A.; Janda, K. D. *Org. Lett.* **2005**, *7*, 4943-4946.

(205) Wegner, S. V.; Okesli, A.; Chen, P.; He, C. *J. Am. Chem. Soc.* **2007**, *129*, 3474-3475.

(206) Ono, A.; Togashi, H. *Angew. Chem. Int. Ed.* **2004**, *43*, 4300-4302.

(207) Chiang, C. K.; Huang, C. C.; Liu, C. W.; Chang, H. T. *Anal. Chem.* **2008**, *80*, 3716-3721.

(208) Wang, J.; Liu, B. *Chem. Commun.* **2008**, 4759-4761.

(209) Liu, B. *Biosens. Bioelectron.* **2008**, *24*, 762-766.

(210) Miyake, Y.; Togashi, H.; Tashiro, M.; Yamaguchi, H.; Oda, S.; Kudo, M.; Tanaka, Y.; Kondo, Y.; Sawa, R.; Fujimoto, T.; Machinami, T.; Ono, A. *J. Am. Chem. Soc.* **2006**, *128*, 2172-2173.

(211) Tanaka, Y.; Oda, S.; Yamaguchi, H.; Kondo, Y.; Kojima, C.; Ono, A. *J. Am. Chem. Soc.* **2007**, *129*, 244-245.

(212) Clever, G. H.; Kaul, C.; Carell, T. *Angew. Chem. Int. Ed.* **2007**, *46*, 6226-6236.

(213) Lee, J. S.; Han, M. S.; Mirkin, C. A. *Angew. Chem. Int. Ed.* **2007**, *46*, 4093-4096.

(214) Xue, X.; Wang, F.; Liu, X. *J. Am. Chem. Soc.* **2008**, *130*, 3244-3245.

(215) Liu, J.; Lu, Y. *Angew. Chem. Int. Ed.* **2007**, *46*, 7587-7590.

(216) Li, D.; Wieckowska, A.; Willner, I. *Angew. Chem. Int. Ed.* **2008**, *47*, 3927-3931.

(217) Wang, S.; Gaylord, B. S.; Bazan, G. C. *Adv. Mater.* **2004**, *16*, 2127-2132.

(218) Wang, Y.; Liu, B. *Chem. Commun.* **2007**, 3553-3555.

(219) Wang, Y.; Liu, B. *Anal. Chem.* **2007**, *79*, 7214-7220.

(220) Okamoto, K.; Niki, I.; Shvartser, A.; Narukawa, Y.; Mukai, T.; Scherer, A. *Nature Materials* **2004**, *3*, 601-605.

(221) Pompa, P. P.; Martiradonna, L.; Torre, A. D.; Sala, F. D.; Manna, L.; De Vittorio, M.; Calabi, F.; Cingolani, R.; Rinaldi, R. *Nature Nanotechnology* **2006**, *1*, 126-130.

(222) Noginov, M. A.; Zhu, G.; Bahoura, M.; Small, C. E.; Davison, C.; Adegoke, J.; Drachev, V. P.; Nyga, P.; Shalaev, V. M. *Physical Review B - Condensed Matter and Materials Physics* **2006**, *74*.

(223) Cheng, D.; Xu, Q. H. *Chem. Commun.* **2007**, 248-250.

(224) Hayakawa, T.; Selvan, S. T.; Nogami, M. *Appl. Phys. Lett.* **1999**, *74*, 1513-1515.

(225) Lakowicz, J. R. *Anal. Biochem.* **2005**, *337*, 171-194.

(226) Tovmachenko, O. G.; Graf, C.; Van Den Heuvel, D. J.; Van Blaaderen, A.; Gerritsen, H. C. *Adv. Mater.* **2006**, *18*, 91-95.

(227) Fu, Y.; Zhang, J.; Lakowicz, J. R. *Chem. Commun.* **2009**, 313-315.

(228) Mackowski, S.; Wormke, S.; Maier, A. J.; Brotosudarmo, T. H. P.; Harutyunyan, H.; Hartschuh, A.; Govorov, A. O.; Scheer, H.; Brauchle, C. *Nano Lett.* **2008**, *8*, 558-564.

(229) Ray, K.; Badugu, R.; Lakowicz, J. R. *Chem. Mater.* **2007**, *19*, 5902-5909.

(230) Wang, Y.; Liu, B. *Macromol. Rapid Commun.* **2009**, *30*, 498-503.

(231) Park, H. J.; Vak, D.; Noh, Y. Y.; Lim, B.; Kim, D. Y. *Appl. Phys. Lett.* **2007**, *90*, 161107.

(232) Pu, K. Y.; Liu, B. *Adv. Funct. Mater.* **2009**, *19*, 277-284.

(233) Yu, D.; Zhang, Y.; Liu, B. *Macromolecules* **2008**, *41*, 4003-4011.

(234) Sun, C. J.; Gaylord, B. S.; Hong, J. W.; Liu, B.; Bazan, G. C. *Nature Protocols* **2007**, *2*, 2148-2151.

(235) Caruso, F.; Lichtenfeld, H.; Donath, E.; Mohwald, H. *Macromolecules* **1999**, *32*, 2317-2328.

(236) Chen, Y.; Munechika, K.; Jen-La Plante, I.; Munro, A. M.; Skrabalak, S. E.; Xia, Y.; Ginger, D. S. *Appl. Phys. Lett.* **2008**, *93*, 053106.

(237) Lieberman, I.; Shemer, G.; Fried, T.; Kosower, E. M.; Markovich, G. *Angew. Chem. Int. Ed.* **2008**, *47*, 4855-4857.

(238) Nooney, R. I.; Stranik, O.; McDonagh, C.; MacCraith, B. D. *Langmuir* **2008**, *24*, 11261-11267.

(239) Zhang, J.; Fu, Y.; Lakowicz, J. R. *J. Phys. Chem. C* **2007**, *111*, 50-56.

(240) Gryczynski, I.; Malicka, J.; Gryczynski, Z.; Lakowicz, J. R.; Geddes, C. D. *Journal of Fluorescence* **2002**, *12*, 131-133.

(241) Xie, F.; Baker, M. S.; Goldys, E. M. *Chem. Mater.* **2008**, *20*, 1788-1797.

(242) Heeger, P. S.; Heeger, A. J. *Proc. Natl. Acad. Sci. U. S. A.* **1999**, *96*, 12219-12221.

(243) Meek, T. D.; Dreyer, G. B. *Ann. N.Y. Acad. Sci.* **1990**, *616*, 41-53.

(244) Enzyme. http://en.wikipedia.org/wiki/Enzyme

(245) An, L.; Tang, Y.; Feng, F.; He, F.; Wang, S. *J. Mater. Chem.* **2007**, *17*, 4147-4152.

(246) An, L.; Wang, S.; Zhu, D. *Chemistry - An Asian Journal* **2008**, *3*, 1601-1606.

(247) Lakowicz, J. R. Principles of Fluorescence Spectroscopy; 2nd ed.; Kluwer Academic/Plenum, 1999.

APPENDIX I

LIST OF PUBLICATIONS

Journal Publications:

1. **Wang, Y.**; Liu, B.; Mikhailovsky, A.; Bazan, G. C. Conjugated polyelectrolyte-metal nanoparticle platforms for optically amplified DNA detection. *Advanced Materials*, 2010, 22 (5), 656-659.

2. **Wang, Y.**; Liu, B. Amplified fluorescence turn-on assay for mercury(II) detection and quantification based on conjugated polymer and silica nanoparticles. *Macromolecular Rapid Communications*, 2009, 30 (7), 498-503.

3. Wang, Y.; **Wang, Y.**; Liu, B. Fluorescent detection of ATP based on signaling DNA aptamer attached silica nanoparticles. *Nanotechnology*, 2008, 19, 415605.

4. **Wang, Y.**; Liu, B. Label-free single-nucleotide polymorphism detection using a cationic tetrahedralfluorene and silica nanoparticles. *Analytical Chemistry*, 2007, 79, 7214-7220.

5. **Wang, Y.**; Liu, B. Silica nanoparticle assisted DNA assays for optical signal amplification of conjugated polymer based fluorescent sensors. *Chemical Communications*, 2007, 34, 3553-3555.

Conference Proceeding:

1. **Wang, Y.**; Liu, B. *Materials Research Society (MRS) Proceedings*, Fall Meeting 2008, Boston, MA, USA, December 2008, DOI: 10.1557/PROC-1134-BB05-01.